KERNFORSCHUNGSZENTRUM

KARLSRUHE

Dezember 1971 KFK 1539

Institut für Neutronenphysik und Reaktortechnik
Projekt Schneller Brüter

Investigation of Reactor Physics Properties of the SNEAK 3 A – 2 Core in the Fast Thermal Reactor STARK, Assembly 6

H. Meister

GESELLSCHAFT FÜR KERNFORSCHUNG M. B. H.
KARLSRUHE

GESELLSCHAFT FÜR KERNFORSCHUNG M.B.H.
KARLSRUHE

KERNFORSCHUNGSZENTRUM KARLSRUHE

Institut für Neutronenphysik und Reaktortechnik

Dezember 1971 KFK 1539

Projekt Schneller Brüter

Investigation of Reactor Physics Properties of the SNEAK 3A-2 Core in the Fast Thermal Reactor STARK, Assembly 6

Compiled by

H. Meister

With contributions from

U. Bicking, H. Bluhm, Chr. Brückner, K. Burkart, G. Fieg, R. Kalckbrenner, G. Kußmaul, M. Müller, H. Werle, J. Wolff

Gesellschaft für Kernforschung mbH., Karlsruhe

Abstract

Some of the reactor physics investigations carried out in the fast critical facility SNEAK, assembly 3A-2, were repeated in the coupled fast-thermal reactor STARK whose central fast zone was loaded with the same core composition. The experimental program comprised measurements of differential neutron spectra, reaction rate ratios, reactivity worths of material samples and Doppler sample measurements at core center. For some reaction rates the fine structure within the lattice cell as well as macroscopic traverses have been determined.

The experimental data are compared with the SNEAK 3A-2 results and discussed on the basis of multigroup calculations with different cross section sets. The results of this comparison show that most of the SNEAK 3A-2 data obtained at core center are reproduced with reasonable accuracy in the STARK experiment.

Zusammenfassung

Einige der an der schnellen kritischen Anordnung SNEAK 3A-2 durchgeführten reaktorphysikalischen Untersuchungen wurden im gekoppelten schnell-thermischen Reaktor STARK wiederholt, dessen zentrale schnelle Zone mit der gleichen Core-Zusammensetzung beladen war. Das experimentelle Programm umfasste Messungen des differentiellen Neutronenspektrums, von Reaktionsratenverhältnissen, Reaktivitätswerten von Materialproben sowie Doppler-Probenmessungen im Corezentrum. Für einige Reaktionsraten wurden die Feinstruktur innerhalb der Gitterzelle sowie makroskopische Traversen bestimmt.

Die Messdaten werden mit den Ergebnissen von SNEAK 3A-2 verglichen und auf der Grundlage von Multigruppenrechnungen mit verschiedenen Querschnittsätzen diskutiert. Die Ergebnisse des Vergleichs zeigen, daß die meisten der im Corezentrum von SNEAK 3A-2 erhaltenen Daten im STARK-Experiment mit ausreichender Genauigkeit reproduziert werden.

1. Introduction

The main objective of the present investigations was to repeat in the coupled fast-thermal reactor STARK [1] some of the integral experiments performed previously in the fast critical assembly SNEAK 3A-2 [2] by adopting a fast-core composition virtually identical to that of the SNEAK core. In this way, empirical information should be gained on how well the real and adjoint spectra of an all-fast system are reproduced in a fast-thermal assembly with a rather small test zone. In particular, the question should be answered as to which experiments can be advantageously carried out in the STARK facility without introducing substantial systematic errors. This question is of practical interest since STARK requires only 1/5 to 1/10 of the fuel inventory necessary for the corresponding all-fast system, its operation costs are much lower and loading changes can be made in a shorter time. Furthermore, it was intended to give some general assessment concerning the accuracy of predictions made with standard multigroup methods.

The composition of SNEAK 3A-2, a 510 l uranium-fueled core with polythene admixture to simulate a steam coolant, has been chosen for this investigation since its fuel concentration is typical for a fast breeder and because this system has been studied both experimentally and theoretically in much detail. In addition, some remaining discrepancies of the SNEAK 3A-2 experiment should be cleared up.

The dimensions of the SNEAK 3A-2 core, 44.7 cm radius and 80.5 cm height, are large enough that real and adjoint spectra in its central region closely approach the equilibrium spectrum, whereas larger deviations are expected in the smaller core of STARK 6. In the present experiment, however, it was not intended to improve the spectrum match by a possible optimization of the buffer region.

2. Description of the Assembly

The STARK facility has been described in detail in previous papers [1,3]. In principle, it consists of a central fast core (37.2 cm diameter) which is surrounded by a 5.6 cm - thick natural uranium buffer, a light water moderated driver and an outer graphite reflector as shown in Fig. 1.

In the present experiment the 5.1 x 5.1 cm^2 stainless steel tubes of the fast zone were filled with 3.14 cm - thick platelets of 20% enriched uranium metal, Al_2O_3, aluminum frames (25% of normal density) and stainless steel frames with 0.5 mm - thick polythene foils according to the loading pattern of Fig.2 which is identical to that of SNEAK 3A-2. However, due to the somewhat smaller repetition length of the tube lattice (5.40 cm instead of 5.44 cm in SNEAK), the homogenized fast zone of STARK contained about 1.5% more core material per unit volume (cf. Tab.1).

Adjacent to the 60.5 cm-high core region (≙48 unit cells) 8.4 cm - thick axial reflector zones were arranged which contained blocks and platelets of natural uranium metal. As in earlier assemblies, the height of the fast core was chosen in a manner to obtain the same axial buckling as in the driver, such that one-dimensional calculation methods can be applied to the entire system. The total fuel mass of the fast zone was 57.36 kg U^{235}, 19.86% enriched; the H/U-ratio was 0.177.

The thermal driver contained Al-clad fuel plates with 20.83 g U^{235}, 20% enriched; they were arranged with a 6.2 mm spacing inside the inner part of the annular light water tank, while its outer part was filled with graphite. The fuel mass needed for the driver to make the entire system critical was 5.987 kg U^{235} at the normal operating temperature of 80°C.

3. Multigroup Calculations

The multigroup calculations used as a basis for discussion of the experimental results were carried out with the Karlsruhe nuclear code system NUSYS [4]. To describe the entire assembly, standard one-dimensional 26-group diffusion calculations were performed in which the reactor was treated as a system of homogeneous cylindrical zones equal in area to the actual zones of the reactor. Composition and geometry of this model are given in Tab.1. In the axial direction a zone-and group-independent buckling, $B_z^2 = 13.99 \cdot 10^{-4}$ cm^{-2}, was assumed which corresponds to an effective core height $H_{eff} = 84$ cm, in accordance with fission chamber traverse measurements (cf. Sec. 4.2). In these calculations the system was made critical by variation of the outer radius of the thermal zone.

The following cross section sets were used in the computations:

1. The Russian cross section set of ABAGJAN et al. [5], referred to as ABN set, which is based on a 1/E-weighting spectrum.

2. The KFK-SNEAK set prepared in Karlsruhe [6] and referred to as SNEAK set. This set is based on a re-evaluation of cross sections for a number of materials and is weighted with a smoothed collision density spectrum of SNEAK 3A-2. Other materials are taken unchanged from the ABN set.

3. The H2ØPMB set [7] which differs from the SNEAK set in two respects: First, U^{238} capture data in the energy region from 1o to 8OO keV (groups 6 to 11) have been slightly decreased according to measurements of PÖNITZ et al. [8] and, secondly, U^{235} capture and fission data in the region from 21.5 to 4OO keV (groups 7 to 1O) have been slightly decreased leaving $\alpha = \sigma_c/\sigma_f$ unchanged.

4. The MØXTØT set [9] where the U^{238} capture data of MOXON et al. [10] are used in the energy region from 0.5 to 1OO keV.

5. The KFKINR set [11] which is an improved version of the MØXTØT set with reduced inelastic scattering cross sections of U^{238}. In our calculations the earlier version (26-GR.LALINR) based

on the SNEAK 3A-2 weighting spectrum has been used. The energy group structure of all sets is identical to that of the ABN set and is shown, for example, in Fig. 3. For the thermal zones (No. 2 to 7) always the ABN data were used in the thermal group.

In succeeding evaluation and perturbation calculations reaction rates and reactivity worths of dilute material samples were computed (cf. Sec. 8). Also the power contribution of zone m

$$\gamma_m = \frac{\int_{\text{zone m}} \sum_{i=1}^{26} \Sigma_{fi} \phi_i(r)\, dV}{\int_{\text{reactor}} \sum_{i=1}^{26} \Sigma_{fi} \phi_i(r)\, dV} \quad , \tag{3.1}$$

its relative importance

$$\alpha_m = F_m / F \, , \quad F_m = \int_{\text{zone m}} \sum_{i,j=1}^{26} \phi_i^+ \chi_i \nu \Sigma_{fj} \phi_j \, dV \, , \quad F = \sum_{\text{all zones}} F_m \quad , \tag{3.2}$$

the overall neutron generation time

$$\Lambda = \frac{1}{F} \int_{\text{reactor}} \sum_{i=1}^{26} \phi_i^+ \frac{1}{V_i} \phi_i \, dV \quad , \tag{3.3}$$

and the partial effective delayed neutron fractions of fissionable isotope M ($M = U^{235}, U^{238}$)

$$\beta_{i,\text{eff}}^M = \frac{\beta_i^M}{F} \int_{\text{reactor}} \sum_{k,j=1}^{26} \phi_k^+ \chi_{ki}^M \nu \Sigma_{fj}^M \phi_j \, dV \tag{3.4}$$

(χ_{ki}^M = spectrum of delayed group i, Σ_{fj}^M = fission cross section of M) were calculated by these codes. The symbols used in Eqs. (3.1) to (3.4) have the conventional meaning.

Some results of these calculations are given in Tab.2 and in Fig.3 to 6 where real and adjoint spectra are shown at various

radial positions. Tab.3 gives the kinetic parameters $\beta_{i_{eff}}^{M}$, λ_i and Λ used for the evaluation of reactivity measurements.

In addition to the first-order perturbation calculations, the dependence of the reactivity worth on sample size was derived from a special code [12] based on a collision probability formalism. It allows to calculate the reactivity worth of a finite sample in a surrounding homogeneous medium, considering resonance self-shielding within the sample (cf. Sec. 8).

To investigate the fine structure of reaction rates in the fast zone (Sec.7), various cell calculations were made with the one-dimensional heterogeneity program ZERA [13] which also employs the collision probability method. This code calculates spectra and reaction rates in the individual zones of the cell and produces cell-averaged cross sections that can be used for further homogeneous reactor calculations.

Finally, a zero-dimensional P_1-calculation was run with the Karlsruhe 208-group cross section set [14] to facilitate a direct comparison with differential neutron spectrum measurements in the center of the fast zone (Sec.5). In all calculations, unless otherwise noted, the system was made critical by radius or buckling variation so as to avoid systematic spectrum changes that would arise from an adjustment of ν, the number of fission neutrons, in normal static k_{eff}-calculations.

4. Start-Up Experiments

4.1. Approach to Critical

As in earlier assemblies [15-18], the approach to critical started from a configuration where the thermal zone was filled with moderator and about 80 percent of the estimated critical fuel mass, while the fast zone contained no fuel. The loading process continued by first introducing fuel elements into the fast zone until it was completely loaded and then filling up the thermal zone until criticality was reached. Thus, the cadmium safety plates acting upon the thermal zone (Fig.1) were kept fully effective during the entire loading process and the increase in multiplication could easily be watched in a 1/M-experiment using BF_3-counters on top of the driver zone.

Criticality was reached with 287.4 fuel plates at the normal moderator temperature of 80°C. This corresponds to a critical mass of 5.987 kg U^{235} in the thermal driver.

4.2. Power Distribution

To study the macroscopic power distribution, fission rates of U^{235} and U^{238} were measured with small cylindrical fission chambers (Sec. 6.2) that were inserted into a fuel element provided with a vertical channel, or into channel V (Fig.1) of the natural uranium zone. The chambers had been calibrated against parallel-plate absolute fission chambers in the central position of the reactor (Sec. 6.1). In this way, axial and radial traverses have been obtained throughout the fast core and the natural uranium zone (Fig. 7 and 8).

In the driver zone the thermal and epithermal neutron fluxes were measured in radial direction by irradiating pairs of gold and copper foils as described in [18]. From the flux traverses the U^{235} fission rate has been evaluated on the basis of known thermal and epithermal fission cross sections [18];

the resulting data are included in Fig.7.

The axial U^{235} fission rate traverse in the driver (Fig.9) was measured with a miniature fission chamber (FC-08, 20th Century Electronics) which was inserted into the water gap between the fuel plates. This chamber was also used to normalize the Au+Cu-foil data to the fission chamber measurement in the center of the fast zone.

The following effective core heights were found by fitting cosine functions to the unperturbed central parts of the axial fission rate traverses:

U^{235} fission in fast zone (r = o):	$H_{eff}=85\pm2$ cm,
U^{238} fission in fast zone (r = o):	$H_{eff}=84\pm2$ cm,
U^{235} fission in thermal zone (r=34.8 cm):	$H_{eff}=86\pm2$ cm.

Within experimental error the results agree with those of the earlier STARK assemblies [16,17,18].

By spatial integration of the axial and radial fission rate traverses the total reactor power and the power fractions γ_m of the individual zones have been derived; they are listed in Tab.2 for comparison with the values calculated from Eq.(3.1).

The ratio of the power density in the fast core fuel platelets relative to that in the matrix of the thermal fuel plates was found to be

$$s_1/s_4 = 0.35,$$

which is substantially below the maximum permissible value $w_1/w_4 = 1.16$ at 70°C stated in the safety report [3].

4.3. Temperature Coefficient

The temperature coefficient of reactivity for the thermal zone was measured by continuously raising the moderator temperature at a rate of 4°C per hour in the range from 50 to 75°C. The resulting reactivity change $\Delta\rho$ was counterbalanced by control plates R_2 and R_3 (Fig.1) such as to keep the reactor at a given power level. Reactivity calibration of the control units was accomplished in the course of the experiment by stepwise withdrawal of the plate and measurement of the asymptotic period.

By normalizing the resulting $\Delta\rho$ vs. ϑ-curve to an earlier measurement on STARK 2 [16], which extends over a much wider temperature range, the reactivity gain due to a temperature drop from 80 to 20°C was inferred:

$$\Delta\rho \ (80 \rightarrow 20^{\circ}C) = 1.04 \pm 0.015\,\$ = 0.776 \pm 0.010\ \%k.$$

The temperature coefficient around 80°C was found to be

$$\frac{\Delta\rho}{\Delta\vartheta} = 2.2\,¢/^{\circ}C = 0.016\ \%\ k/^{\circ}C.$$

4.4. Calibration of Control and Safety Units

The integral reactivity worths of the three control plates (R_1, R_2, R_3), various groups of safety plates (S_1, S_2, S_3) and the fuel-poison safety rod S_4 (Fig.1) were measured by the rod drop method. The neutron signal from a B-ionization chamber was converted to reactivity by a digital inverse kinetics code as described in an earlier paper [18] using the kinetic parameters of Tab. 3.

Since the deviation from point reactor behaviour is rather strong in STARK, a special correction procedure was employed [19] which rejects the information contained in the prompt jump and renders reactivity values nearly independent of detector position. The reactivity data of Tab.4 show some mutual

shadowing when all plates are dropped simultaneously. The total shut-down reactivity was found to be -4.5% k.

Differential calibration curves of various control plates were measured by the continuous run method [18]. Results for plate R_3 are shown in Fig. 10 where also a comparison with the other methods is made.

4.5. Comparison with Multigroup Calculations

In Tab.2 a comparison is made between experimental reactor parameters and one-dimensional diffusion calculations.

For the power contribution of the fast zone a satisfactory agreement with the calculation is found, while the power contribution of the buffer is underestimated in accordance with observations in previous assemblies [15,18]. Among the various calculations, that with the KFKINR set comes closest to the experimental data. In general, criticality is over-estimated by the calculations; a better agreement can hardly be expected with the simplifications made in reactor geometry (homogenization of air gaps etc.).

As a check of the one-dimensional model, a comparison was made with a two-dimensional diffusion calculation which gave a very good agreement in k_{eff} (within 0.04% k). Also the shape of the fission source distribution in the reactor midplane was found to agree well with the one-dimensional calculation.

5. Differential Neutron Spectrum

The neutron spectrum in the center of the fast zone has been investigated by three experimental methods:

1. Proton recoil spectrometry using hydrogen-filled proportional counters for the energy range from 10 keV to 1.4 MeV,
2. He^3 coincidence spectrometry for the energy range above 0.1 MeV,
3. the sandwich activation method for some resonance energies in the eV- and keV-region.

The experimental data are compared with calculated spectra derived from 26- and 208-group cross section sets.

5.1. Proton Recoil Measurements

Spectrum measurements in the energy range from 10 to 700 keV were made with spherical proportional counters (3.94 cm diameter) filled with 1, 2 and 4 atm H_2, respectively, while a similar counter with 3 atm CH_4 was used for energies from 400 to 1400 keV. The counters were placed in a 5 x 5 x 16 cm^3 void zone at the center of the fast core.

Below 60 keV the γ-n pulse shape discrimination technique [20] was employed which allows an almost complete separation of neutron- and γ-induced events. For the small fraction of unseparable events a correction was made on the basis of measurements with a pure γ-source. Fig.11 shows a schematic block diagram of the electronic system.

The proton recoil distributions were converted to neutron spectra by an unfolding process using calculated response functions as described in [21]; the energy calibration was accomplished by means of a monoenergetic Pu^{239} α-source. The resulting differential neutron spectrum is shown in Fig. 12 and 13.

5.2. Measurements with a He^3-Spectrometer

To investigate the high energy part of the spectrum from 0.1 to 5.5 MeV a He^3 sandwich spectrometer was used which allows discrimination against γ-background and an exact correction for the energy loss of protons and tritons in the He^3 gas volume. A description of the method is given in [22].

The spectrometer consists of two surface barrier detectors (450 mm^2 sensitive area, 400 μ depletion depth). The 10 mm-wide gap between the detectors together with a 40 μ-thick anode wire serves as a proportional counter to measure the ionization in the He^3 gas. The system is enclosed in a 1 mm-thick steel cylinder and filled with 2 atm He^3 and 10 Torr CH_4.

The energy calibration of the solid state detectors was carried out with a U^{233} α-source placed in the evacuated spectrometer. In a second step the amplification of the proportional counter circuit was adjusted such that the thermal peak of the He^3-reaction (764 keV) appears at the correct position.

The spectrum measurements were again made in a void volume in the central element. To eliminate the background due to (n,α)- and (n,p)-reactions within the detectors a second measurement was run where the spectrometer was filled with He^4.

5.3. Measurements with Sandwich Detectors

For spectrum measurements in the low energy region the sandwich activation technique was employed, using the same substances as in SNEAK 3A-2 [23]. The sandwich foils were irradiated between the platelets inside the central element and their γ-activities were measured with NaJ scintillation counters. The observed activity differences (outer minus inner foil), which are a measure for the capture rate at the main resonance, were converted to neutron flux on the basis of known resonance parameters and an absolute calibration of γ-detectors as described in [23]. The experimental results are shown in Fig. 14.

5.4. Spectrum Calculations

The general behaviour of the neutron spectrum in STARK 6 is illustrated in Fig. 3 and 4, where 26-group real and adjoint fluxes from a one-dimensional diffusion calculation are shown for some radial positions r. The general space dependence is very similar to that of the STARK assemblies discussed in earlier reports [15,18].

Fig.5 shows the relative deviation of the STARK spectrum at r = 0 from the equilibrium spectrum calculated for a one-zone fast system of the same core composition with the same cross section set. In the whole energy range above 10 eV, deviations stay within ± 3 to 5 percent, depending to some extent on the cross section set used. Below 10 eV appears a 15% excess of slow neutrons coming from the thermal driver which, however, do not measurably contribute to the reaction rates at core center. The deficit of high energy neutrons ($E \gtrsim 0.5$ MeV) is due to the lower fission source in the buffer and could be compensated for, in principle, by adding a certain amount of U^{235} fuel to the edge of the fast core.

A similar diagram for the adjoint flux ϕ_i^+ is shown in Fig. 6. Here deviations are found of the order of ± 6% that turn out to be almost independent of the cross section set used. The more pronounced minimum of the adjoint in STARK is due to the presence of excess U^{238} in the buffer and the influence of its fission threshold as discussed in [17]. In general, spectrum and adjoint match are not so good as in the previous assemblies STARK 4 and 5 [17,18].

To check the influence of heterogeneity on the neutron spectrum a calculation was made with the cell program ZERA (cf. Sec. 7.2). The results are discussed in Fig.15 which shows the relative flux deviation, $(\phi_i^{het} - \phi_i^{hom})/\phi_i^{hom}$, from a corresponding homogeneous calculation for a one-zone system of the same overall composition.

It turns out that for energies $E \gtrsim 100$ eV the spatially averaged cell spectrum agrees within ± 2 percent with the homogeneous

calculation; at lower energies, however, heterogeneity leads to a strong spatial variation of ϕ_i^{het} and to an average cell spectrum softer than that of the homogeneous model.

For the following discussion of proton recoil and He^3-spectrum measurements in the energy range from 0.01 to 5 MeV the influence of heterogeneity can be completely neglected. In Fig.12 the measured differential spectra are compared with a zero-dimensional P_1-calculation using the Karlsruhe 208-group cross section set; pairs of two neighboring groups of the calculation have been collapsed to obtain a group width comparable to the energy resolution of the experiment.

The He^3 data are seen to follow closely the calculated spectrum, especially for energies above 0.5 MeV. Also for the proton recoil measurement a satisfactory agreement is found within the ± 10 percent experimental error. Thus, for STARK 6 a much better agreement is obtained than for the previous assemblies STARK 4 and 5 ⟨18⟩ which contained larger amounts of U^{238}; there the experimental spectrum above 0.5 MeV showed a more pronounced slope than the 208-group calculation.

In Fig.13 both the experimental data and the 208-group spectrum have been condensed to 26 groups for comparison with one-dimensional STARK calculations using various 26-group cross section sets. Differences as high as 20 percent occur between the ABN set on one hand and the improved sets (SNEAK, MØXTØT, KFKINR) which are mainly due to the influence of the weighting spectrum on the elastic removal cross section ⟨18⟩ as illustrated in Fig. 16. The calculations with the improved sets yield similar spectra while, in general, the 208-group spectrum and the experiment lie between these and the ABN calculation. Fig.13 shows that the experimental data agree better with the condensed 208-group spectrum than with any of the original 26-group calculations.

A substantial deviation between the ABN calculation and those with the improved 26-group sets appears in group 6 ($0.4 \leq E \leq 0.8$ MeV), which includes the large oxygen resonance at 442 keV.

While in the ABN set a simple 1/E-weighting spectrum is used, in the improved sets a variation of the weighting spectrum $\varphi(E)$ for the SNEAK 3A-2 core according to

$$\varphi(E) = \frac{\psi(E)}{\Sigma_{tot}(E)} \qquad (\psi(E) \approx \text{const.}), \tag{5.1}$$

is adopted, assuming the collision density $\psi(E)$ to vary smoothly with energy. As shown in Fig. 13 and 16, the 208-group calculation as well as the experimental data in groups 6 and 7 do not confirm the improved weighting according to Eq. (5.1). This is due to the fact that the assumption $\psi(E) \approx$ const. is not justified for the relatively wide oxygen resonance, as shown by the detailed 208-group calculation.

This situation does not change very much when the iterative REMØ correction /9/ is applied to the elastic removal cross sections of the 26-group sets, since it is also based on a smoothed $\psi(E)$. Instead of this procedure, it was attempted to improve the 26-group calculation by replacing the transfer cross sections $\Sigma_{i \to i+1}$ with values derived from the 208-group spectrum by usual condensation (Fig.16). The application of this concept to a calculation with the 26-group SNEAK set yields a spectrum that comes quite close to the result of the 208-group calculation (Fig.17).

In the low-energy region ($E \lesssim 1$ keV) heterogeneity effects cannot be neglected (Fig.15). A comparison of the sandwich foil activation data with homogeneous and heterogeneous calculations with the KFKINR set is made in Fig.14. The experimental data are seen to agree well with the cell-averaged spectrum of the heterogeneous calculation.

5.5. Comparison with SNEAK 3A-2

In Fig.18 a comparison is made between the differential neutron spectra measured at the center of STARK 6 and SNEAK 3A-2. For this comparison the SNEAK 3A-2 proton recoil data have been reevaluated employing the unfolding method now in use.

For the proton recoil measurement in the energy range from 20 to 800 keV the ratio of group fluxes in both assemblies turns out to be constant within ± 10 percent, i.e. the same spectra are observed within experimental error.

Also the sandwich foil data at low energies show a good agreement with the SNEAK 3A-2 experiment. Thus, no difference of central neutron spectra in both assemblies can be seen by present experimental techniques.

6. Reaction Rates and Spectral Indices

Reaction rates were studied mainly for two reasons:

1. To obtain absolute reaction rates in the center of the fast zone for comparison with calculated spectral indices and for calibration of other experiments.
2. To get some information on the spatial variation of the neutron spectrum within the fast zone on the basis of measured reaction rate traverses.

6.1. Absolute Fission Chamber Measurements

The absolute fission rate measurements in the central position of the fast zone were performed with KIRN-type parallel-plate fission chambers. The chambers (2.5 cm diameter, 0.4 cm plate distance) had 0.3 mm-thick aluminum walls and were operated as flow counters with an argon-methane mixture. The layer of fissionable material, about 200 µg/cm^2 thick, was prepared by electrodeposition on a 0.2 mm-thick stainless steel disk [24]. The amount of fissionable material deposited is known within ± 1 to 2 percent from the concentration of the stock solution and has been checked by low geometry α-counting and also, on

the basis of known thermal cross sections, by intercomparison of chambers in the thermal column of STARK.

For the fission ratio measurement two parallel-plate chambers containing different isotopes were arranged back-to-back inside a 10 x 5 x 5 cm^3 void volume spared out in the central element. Thus, the sensitive areas of both counters were exposed to the same neutron spectrum at the center of the cavity, which is supposed to be close to the spatially averaged spectrum of the heterogeneous core structure (cf. Sec. 7.2).

A comparison of experimental results with 26-group calculations is made in Tab.5.

6.2. Spatial Variation of Fission Rates

To study the spatial dependence of the neutron spectrum inside the fast zone, fission rates and their ratios were measured for the isotopes U^{235}, U^{238}, Np^{237}, and Pu^{239} using cylindrical fission chambers of 6 mm diameter (FC-4, 20^{th} Century Electronics) which contained about 500 µg/cm^2 of fissionable material. Some of these chambers have been calibrated by comparison with the KIRN-chambers in the center of the fast zone.

The chambers were introduced into a special fuel element with an axial channel obtained by filling it with platelets provided with 12 mm-wide central holes. Axial traverses were measured by moving the chamber with an automatic driving mechanism, radial traverses by changing the position of the special element within the fast core.

6.3. Comparison with Multigroup Calculations

Fig.7 shows the radial variation of some measured fission rates per atom, $n_f^x(r)$, compared with calculated values which have been derived from the 26-group fluxes $\phi_i(r)$ (i=1,..26) of the onedimensional diffusion calculation:

$$n_f^x(r) = \sum_{i=1}^{26} f_i^x \sigma_{fi}^x \phi_i(r) \qquad (6.1)$$

where

σ_{fi}^{x} = infinite dilute fission cross section } for material x,
f_i^{x} = self shielding correction factor } energy group i.

The calculated curves are normalized such that the U^{235} fission rate n_f^{25} agrees with the experimental data in the thermal driver.

The U^{235} fission rate in Fig.7 shows, as a result of the strong absorption of low energy neutrons, a steep gradient in the buffer zone and at the edge of the fast core, which goes over into a relatively flat curve in its central region. The experimental data agree well with the calculation for $r \lesssim 10$ cm, but in the outer region they are definitely higher. A similar deviation was found in previous STARK assemblies and was explained by the fact that eV-neutrons penetrate deeper into the fast core than given by the diffusion calculation [15,18].

For the threshold substances relatively flat fission rate traverses were found which are consistent with the calculations and extend well into the buffer region.

To discuss spectrum changes in the fast zone the radial variation of fission ratios

$$\sigma_f^{x}/\sigma_f^{y} = n_f^{x}/n_f^{y} \qquad (6.2)$$

relative to U^{235} and U^{238} is shown in Fig.19 and 20, normalized to unity at core center. In addition to the experimental data, calculated curves obtained from four different cross section sets are plotted which show a common shape inside the fast zone but characteristic differences near its edge and in the buffer zone.

The fission ratios of threshold substances relative to U^{235} (Fig.19) follow closely the calculations with the KFKINR and the SNEAK set in the interior of the fast zone ($r \lesssim 15$ cm), while deviations occur in the buffer that are due to the U^{235}-discrepancy mentioned above. The fission ratios near the center show a slight curvature indicating that the spectrum hardens somewhat towards the center and that some deviation from the

equilibrium spectrum remains even at r = o. This is expected from the calculated STARK spectra, Fig.5, which show a characteristic 3 to 5 % neutron deficit at high energies (groups 1 to 6).

The Np^{237}/U^{238} fission ratio follows a flat shape with a slight increase towards the buffer as expected from the calculation.

As a spectral index sensitive to the low energy region, the fission ratio Pu^{239}/U^{235} is plotted in Fig.20. Similar to earlier STARK assemblies, the calculated curves show a characteristic maximum in the buffer zone. This behaviour can be explained by the fact that thermal neutrons are more strongly absorbed in the natural uranium than the eV neutrons that cause fission in the lower Pu-resonances [15,18]. Towards the interior of the fast core also the eV neutrons die out and the fission ratio goes over into a constant value characteristic of the fast spectrum. The experimental data in Fig.20 agree well with the calculation within the region $r \lesssim 15$ cm, while in the buffer zone $\sigma_f^{49}/\sigma_f^{25}$ is higher than calculated [18].

The axial dependence of fission ratios, Fig.21, shows constant values in the interior of the fast zone ($|z| \lesssim 20$ cm) with typical changes near the edge caused by the presence of the natural uranium reflectors.

The fission ratios measured with absolute chambers at core center are compared in Tab.5 with homogeneous 26-group calculations using different cross section sets. The use of the homogeneous model is justified by the heterogeneity calculation, Fig.15, which shows that, at least for this assembly, the cell-averaged spectrum is very similar to the homogeneous spectrum within the important energy range $E \gtrsim 500$ eV. In the following discussion we further assume that the fission cross sections and the fission chamber calibration are not affected by systematic errors.

The experimental fission ratio U^{233}/U^{235} appears to be consistent with the SNEAK, MØXTØT and KFKINR calculations, while the ABN set underestimates this quantity considerably. The ratios of threshold substances relative to U^{235} come out too high with the ABN set and too low with the MØXTØT set, while the other sets show a much better agreement. Hence one may conclude that the overall shape of the spectrum (ratio of the high energy part $E \gtrsim 1$ MeV to total) is best represented by the SNEAK and KFKINR calculations.

The fission ratios between two threshold substances, U^{234}/U^{238} and U^{236}/U^{238}, are sensitive to the slope of the spectrum at high energies, $E \gtrsim 0.5$ MeV. The experimental data are found to be 4 to 6 percent higher than the values calculated with the improved sets, but agree well with the ABN calculation. Considering the group contributions to the fission rate, $\phi_i \Sigma_{fi}$, shown in Fig.22 and excluding systematic errors, one is led to conclude that the slope at the high energy end of the spectrum must be steeper than given by the improved 26-group sets.

This general observation is consistent with the results of the differential spectrum measurements and the 208-group calculation discussed in Sec.5.4. To obtain a more quantitative information, the fission rates of Fig.20 have been reevaluated on the basis of a 26-group KFKINR calculation in which the group transfer cross sections $\Sigma_{i \to i+1}$ were replaced by values derived from the 208-group weighting spectrum as discussed in Sec.5.4. The resulting fission ratios, which are included in Tab.5, are found to be in satisfactory agreement with the experimental data.

6.4. Comparison of Fission Ratios with the SNEAK Results

A comparison between fission ratios measured in STARK 6 and SNEAK 3A-2 is made in Tab.6. The STARK 6 data have been corrected for two effects:

1. difference in the fast core composition of the two assemblies (correction factor F_1 in Tab.6),
2. deviation of the STARK 6 spectrum from the equilibrium spectrum (correction factor F_2).

F_1 has been derived from 26-group diffusion calculations carried out for two systems, namely STARK 6 and a modified system with the exact composition of SNEAK 3A-2 in the fast zone. Similarly, F_2 was found by comparison of reaction rates in STARK 6 with those in an all-fast system of the same composition. The resulting values F_1 and F_2 turned out to be nearly independent of the cross section set used such that the uncertainty of the total correction ($\approx$ 0.2%) appears to be much smaller than the experimental error.

The comparison in Tab.6 shows remarkable differences between the fission ratios measured in STARK 6 and in SNEAK 3A-2, namely +6% for the U^{233}/U^{235}-ratio and -10% for the U^{238}/U^{235}-ratio, which are both beyond the estimated experimental error. Considering the good agreement in the measured experimental spectra (Sec.5.5) and the results of the multigroup calculations, this discrepancy can only be explained by the fact that different sets of fission samples, which might disagree in the absolute calibration, were used in the two experiments.

Therefore the fission ratio measurements in STARK 6 were repeated with the old set of fission standards used in SNEAK 3A-2. The resulting U^{238}/U^{235} - and U^{233}/U^{235} -ratios were now found to be consistent with the SNEAK 3A-2 values (Tab.6). By direct comparison between the two sets an 11 percent discrepancy between the old and new U^{238} standards was found while the other samples are in better agreement. Since the calibration of the new standards is confirmed within $\pm$ 1.5 percent by additional checks (comparison of U^{238}/U_{nat} in a fast spectrum

and of U_{nat}/U^{235} in the thermal column), we have to assume that the calibration of the old sample was in error.

7. Heterogeneity Studies

7.1. Reaction Rate Measurements

The fine structure of U^{235} and U^{238} fission rates and of the U^{238} capture rate was studied in the normal lattice cell of the fast zone as well as in two bunched configurations, Fig.23 to 25, each comprising a central region of 21 fuel elements. To facilitate a comparison the same experimental technique as in SNEAK 3A-2 [25] was employed.

Pairs of uranium metal foils of ≈ 0.1 mm thickness, 25 mm diameter, with different enrichment (0.2 and 20% U^{235}) were placed between the platelets of the two central cells.

For measurements inside the U(20%) fuel a special uranium platelet provided with a 25 mm diameter hole was filled with detector foils and 1.4 mm-thick disks of 20% enriched uranium metal.

The foils were counted on an automatic sample changer [26] with two NaJ scintillation detectors. The induced fission product γ-activity above 660 keV served as a measure of the relative fission rate in the foil, from which isotopic values were derived by unfolding the data of different foil enrichments. The U^{238} capture rate was measured by γ-X-ray coincidence counting at 106 keV as described in [26].

For an absolute calibration of fission rates one pair of foils was irradiated in the same run between the sensitive areas of two parallel-plate fission chambers coated with U^{235} and U^{238}, which were located in an outer fast-core position.

The U^{238} capture rate has been calibrated by irradiating a 0.2% depleted uranium foil, that was attached to an absolute U^{235} fission chamber, inside the thermal column of STARK and

using the known ratio of thermal cross sections as a basis for calibration.

As in the SNEAK experiment, the γ-peak near 100 keV was used to stabilize the gain of the counting equipment, although it was found that this technique may lead to systematic errors in the measurement of the U^{238} fission rate. By evaluating the reaction rate traverses at different times after the irradiation within a period of about two days, it was found that the relative variation of the U^{238} fission rate traverse increased systematically with decaying γ-intensity, while no time dependence could be seen for the U^{238} capture and U^{235} fission rates. This effect is explained as follows:

In the measurement of the natural activity of the 0.2% depleted uranium foil, which has to be subtracted as a background, the peak stabilization centers on the 95 keV X-ray line, as it is the case also for the enriched uranium foils. For strongly activated 0.2% uranium foils, however, the stabilization centers on the γ- and X-ray lines near 106 keV coming from the Np^{239} decay; this leads to an increase of the integral discriminator threshold for the fission γ measurement and a corresponding reduction in counting efficiency. The variation of efficiency has been determined experimentally and was found to be -15 percent.

To eliminate this threshold variation, a correction was applied to the integral counting rates of the depleted uranium foils, assuming the counting efficiency ε to vary linearly with the mean energy of the γ-peaks in the window at 100 keV:

$$\varepsilon = \frac{N_\gamma^o + aN_\gamma^{37}}{N_\gamma^o + N_\gamma^{37}}$$

where

N_γ^o = natural γ-activity near 100 keV,

N_γ^{37} = γ-activity near 100 keV due to the Np^{237} decay.

Using this correction with a = 0.83, a time independent shape of the U^{238} fission rate traverses was obtained and the

originally decreasing U^{238}/U^{235} activity ratio became constant within experimental error.

Although it seems possible to correct for the sensitivity variation by the above procedure, even at low counting rates ($N_\gamma^{37} \approx N_\gamma^{o}$), for high-precision measurements one would prefer to avoid these difficulties by using an external γ-source of sufficiently high energy for stabilization.

7.2. Comparison with Cell Calculations

The fine structure of reaction rates was calculated by the cell program ZERA [13] which employs a collision probability method to solve the multigroup transport equation in a one-dimensional periodical lattice structure, assuming a constant transversal buckling.

A comparison with experimental data is complicated by two major problems:

1. The real fast core structure shows a two-dimensional lateral heterogeneity which arises from the fact that the platelet dimensions (5.07 x 5.07 cm^2) are considerably smaller than the lateral cell dimensions (5.4 x 5.4 cm^2) given by the repetition length of the matrix (Fig.2). This geometrical structure has to be approximated by a one-dimensional slab lattice extending in axial direction.

   In our ZERA calculations two concepts were employed (Tab.7): First, the material of the core platelets was homogenized in lateral directions to form slabs of the actual thickness with reduced atom densities (case I), second, slabs with atom densities of the actual platelets were used (case II). In both cases, the stainless steel of the element tubes was distributed uniformly over the entire lattice. Thus, in the first case the overall composition, in the second case the optical thickness on the cell axis is conserved.
   It exists the possibility to conserve both overall composition and optical thickness by adopting case I and increasing the linear cell dimensions by a factor of $(5.4)^2 / (5.07)^2$, as

done in the calculations with cell-averaged cross sections, Tab.8 and 9.

One expects that case I is more adequate to describe the overall neutron balance (e.g. k_{eff}) while concept II appears to be more appropriate for a description of the reaction rate fine structure on the cell axis.

2. The uranium of the relatively thick detector foils ($\approx$ 140 mg/cm^2) cannot be neglected against the amount of fuel contained in a normal lattice cell, such that changes in the neutron spectrum and self shielding are expected. For a comparison with reaction rate traverses this effect has been taken into account by considering the detector foils as an integral part of the lattice by adopting the real atom densities on the cell axis for the entire slab (case III); the resulting change in multiplication was compensated by a buckling variation to obtain $k_{eff} = 1$.

In Fig.26 to 28 the experimental cell traverses inside the fuel are compared with a ZERA calculation using the SNEAK set. The detector foils were treated as integral parts of the cell (case III) by introducing special zones with the actual foil thickness and composition from which the individual reaction rates in the foils have been derived.

Normalizing these calculated traverses to the experimental data in the interior of the fuel region, a good agreement in shape is observed (± 0.2 percent) for the three cell configurations, except for some deviations at the edge of the fuel zone.

Using the KFKINR set instead of the SNEAK set, almost no change in the shape of the traverses can be found. However, larger deviations are observed when the atom densities of case II (unperturbed cell) are used; calculations with the atom densities of case I (not shown) largely underestimate the variation of reaction rates.

From the normalized cell traverses, Fig.24 to 26, the mean reaction rate in the fuel plate of thickness a,

$$\bar{n}_f^x = \frac{1}{a}\int_0^a n_f^x(z)\,dz, \quad \bar{n}_c^x = \frac{1}{a}\int_0^a n_c^x(z)\,dz \qquad (7.1)$$

is derived, assuming the calculated shape as a basis for interpolation between experimental points. From these integral quantities average reaction rate ratios, $\bar{\sigma}_f^{28}/\bar{\sigma}_f^{25}$ and $\bar{\sigma}_c^{28}/\bar{\sigma}_f^{25}$, have been obtained that are plotted in Fig.29 as a function of the thickness of the unit cell. These results are compared with the experimental data of SNEAK 3A-2 and with ZERA calculations using the SNEAK, MØXTØT, and KFKINR sets and the atom densities of case II and III.

The fission ratio $\bar{\sigma}_f^{28}/\bar{\sigma}_f^{25}$ increases with the degree of bunching due to the rising self-multiplication. The dependence of the experimental fission ratios on the degree of bunching is well represented by the calculation with the atom densities of the perturbed cell (case III), while the calculation with the normal atom densities (case II) underestimates the slope, due to the difference in average fuel enrichment. Although the experimental results of STARK 6 are about 18% lower than the original SNEAK 3A-2 data, they are still a few percent above the various calculations.

The calculated capture-to-fission ratio $\bar{\sigma}_c^{28}/\bar{\sigma}_f^{25}$ decreases with the degree of bunching and shows, in contrast to the fission ratio, almost no dependence on the particle density concept used. The experimental data of STARK 6 are in excellent agreement with the KFKINR calculation and show less scattering than the original SNEAK 3A-2 data.

The measured reaction rate traverses throughout the entire cell are shown in Fig.23 to 25. For all lattice configurations the experimental data in the regions outside the fuel show a more pronounced spatial variation than the ZERA calculation.

7.3. Comparison with SNEAK 3A-2

In Fig. 23 to 25 a comparison is made between the shapes of the reaction rate traverses measured in STARK 6 and SNEAK 3A-2 by the same method. Considering first the reaction rates n_f^{25} and n_c^{28}, one finds similar cell traverses in both experiments. Except for some data at the surface of the fuel, where the strong gradient may affect the measurement, a standard deviation of $\pm$ 0.7% is found for n_f^{25} and $\pm$ 2.5% for n_c^{28}, which corresponds to the estimated experimental error if one considers the strong influence of self-shielding on n_c^{28}. In general, the STARK 6 data in the fuel show less statistical scattering around the calculation than the earlier experiment.

For the U^{238} fission rate a satisfactory agreement is found in the normal and the double bunched cell, while for the bunched cell the SNEAK data show a somewhat stronger spatial variation.

Comparing the average reaction rate ratios in the fuel, Fig.29, one finds that $\bar{\sigma}_f^{28}/\bar{\sigma}_f^{25}$ in STARK 6 is about 18 percent below the original SNEAK 3A-2 data. This discrepancy is largely due to the difference in absolute calibration of fission standards (cf. Tab.6), as shown by the reevaluation of the SNEAK 3A-2 data (Fig.29) on the basis of the present absolute fission standards.

The average capture to fission ratios, $\bar{\sigma}_c^{28}/\bar{\sigma}_f^{25}$, measured in STARK 6 are about 8 percent lower than the SNEAK 3A-2 data, while only a 0.3 percent difference is expected from the calculation (cf. Tab.6). This large discrepancy can only be understood by the different calibration methods used for the two experiments:
In SNEAK 3A-2 the U^{238} capture rate was calibrated by comparison with an absolute Am^{243} standard and corrections were made for the γ-self absorption in the detector foils [27], whereas in STARK 6 a calibration against the U^{235} fission rate has been made in the thermal column (Sec.7.1). The latter method was preferred since the Am^{243} calibration was found to be dependent on the differential discriminator setting used in the counting equipment.

7.4. Reactivity Effect of Bunching

The reactivity change caused by bunching the cell structure in certain regions of the fast core was measured by counter-balancing with a calibrated control plate. For small changes the measured reactivity variation $\Delta\rho$ of the multizone system is linked to the static reactivity change $(\Delta k/k)_b$ due to bunching of the infinite lattice by means of the equation

$$\Delta\rho = \alpha_b \left(\frac{\Delta k}{k}\right)_b \quad , \quad \alpha_b = \frac{\int_{\text{bunched zone}} \sum_{i,j} \phi_i^+ \chi_i \nu\Sigma_{fj} \phi_j \, dV}{\int_{\text{reactor}} \sum_{i,j} \phi_i^+ \chi_i \nu\Sigma_{fj} \phi_j \, dV} \tag{7.2}$$

which is based on the concept of reactivity partition. The reactivity fraction α_b of the bunched zone can easily be derived from a 26-group perturbation calculation (cf.Sec.2).

Tab.9 gives a comparison of the observed $\Delta\rho$ and the resulting $(\Delta\, k/k)_b$ with various ZERA calculations. One finds that a usual static ZERA calculation with a constant geometrical buckling chosen to make the normal lattice critical, underestimates the measured effect by an order of magnitude. The same occurs if a homogeneous calculation is performed with cell-averaged cross sections derived from a previous ZERA calculation.

As demonstrated in Fig.29, the gain in neutron balance with bunching due to the increase of n_f^{28}/n_f^{25} and the decrease of n_c^{28}/n_f^{25} is properly described by ZERA. Thus, to arrive at the calculated reactivity values one has to assume that this gain must be nearly compensated in ZERA by an increase in radial leakage with bunching which is much larger than in reality. This may be due to the fact that the leakage cross section DB^2 of the diffusion approximation is used in the ZERA code.

In addition to the previous calculations, the reactivity effect of bunching $(\Delta\, k/k)_b$ was estimated, assuming a radial leakage independent of the degree of bunching. The calculation was made with cell-averaged cross sections, but replacing the diffusion constant D_i for all lattice configurations by that

of the homogeneous mixture. The results are seen to agree much better with the experiment than those of the normal ZERA calculation.

8. Material Worth Measurements

The reactivity worths of some typical material samples have been determined in the center of STARK 6 using a square-wave pile oscillator technique. In most cases, measurements were done for two or more sample thicknesses in order to allow an extrapolation to zero sample size such that a comparison can be made with first-order perturbation theory. To study the influence of the local environment, the samples were placed in a void volume and also at two characteristic positions directly between the platelets of the normal cell structure.

8.1. Experiments

The oscillator equipment described in [18] consists of a 1.45 m-long stainless steel tube filled with 4.66 x 4.66 cm^2 platelets of the fast core materials according to Fig.1 into which two aluminum containers were embedded, one for the sample and the other used as a dummy. This oscillator rod was driven by a pneumatic device in a square-wave manner such that the sample was oscillated between the center of the fast core and a position outside the blanket (z = 42.5 cm). The usual oscillation period was 2T = 64 sec.

The neutron signal caused by the sample oscillation was measured by a B-ionization chamber in the graphite reflector and was stored as a two-period train in a multiscaler analyzer. Conversion to reactivity was accomplished by a computer program using Fourier analysis and the inverse kinetics method with the parameters of Tab.3. As shown in a previous paper [28] this evaluation technique allows to eliminate transient effects due to neutron scattering and the motion of fuel contained in the oscillator which acts as a time-dependent delayed neutron source. The standard deviation of Δ k obtained in a typical run (20 min

at 10 Watts reactor power) was $\approx 3 \cdot 10^{-7}$k which is close to the theoretical value [29] determined by reactor noise.

As discussed in [18], the experimental reactivity change $\Delta\rho$ represents the difference of the sample worth at core center, $\rho(o)$, minus the residual worth ρ^* in the out-position at $z = 42.5$ cm and one has

$$\rho(o) = \Delta\rho + \rho^* \qquad (8.1)$$

Because of the limited stroke of the oscillator equipment, the residual worth ρ^* is negligibly small only for the fissile and predominantly absorbing materials, while it is of the order of 10 percent of $\Delta\rho$ for typical scattering materials. A correction for ρ^* has been made on the basis of the semi-empirical model described in [18], using experimental data together with calculated reactivity worth ratios obtained by first-order perturbation theory.

8.2. Results

Tab.10 gives the masses of the various samples and their reactivity worths per gram measured at core center. Usually the samples were platelets or foils of 4.6 x 4.6 cm^2 outer dimension, except for B, Eu and Pu, which were enclosed in aluminum containers of the same size. The data of Tab.10 are average values of at least two independent runs; the data of B, Eu and Pu have been corrected for the effects of the Al-container, the U-data for the nickel coating of the platelets or foils.

In general, sample worths were studied in two environments (Fig.30):

1. Void environment:
   The sample was placed vertically inside the empty container (4.6 x 4.6 x 4.6 cm^3) such that it was exposed to the spatially averaged cell spectrum filtered through the 1 mm stainless steel walls and the aluminum walls of the container.

2. Cell environment:
   The sample container and the dummy were filled with platelets according to the normal or a slightly modified cell structure (Fig.30); the sample replaced the Al-frame at a position either adjacent to the U(20%) (pos.1) or the CH_2 foil (pos.2) without changing the arrangement of the other platelets.

Comparing the sample worths in the two cell positions (Tab.10), no spatial dependence was found for the majority of materials; the exceptions are:

1. The worth of depleted uranium is 4% more negative when the sample is placed adjacent to the CH_2 foil, probably due to a reduction of resonance self-shielding.
2. The worth of Pu is 4% higher at the CH_2-position; a similar effect for U^{235} was not observed.
3. The worth of CH_2 is 4% higher at the CH_2-position, which can be understood on the basis of the experimental sample size dependence of Fig. 34.

In general, the cell measurements show 3 to 5% higher reactivity worths than the measurement in the void environment. This is to be expected since the neutron flux and the adjoint show a slight spatial depression in the voided region due to the missing fuel and excess stainless steel. Larger deviations are found for Pu where the cell data are 6.6 or 11% higher, respectively, and for U(0.4%), where the void data are about 10% more negative than the cell data. The latter effect can be explained by a reduction in resonance self-shielding caused by scattering in the container walls. A similar effect was found in the SNEAK 3A-2 measurements [2], cf. Tab. 12.

For a comparison with first-order perturbation calculations it is necessary to correct the experimental data for the effect of finite sample size, i.e. the influence of self-shielding and self-multiplication. This has been done for the measurements in the void region by extrapolating the reactivity worth per gram to zero sample mass (Fig. 31 to 34), using the calculated

sample size dependence as obtained with the collision probability code described in [12].

The extrapolated reactivity worths per gram were converted to isotopic values, in case of U by combining the data of enriched and depleted uranium, in case of B^{10} by correcting for the small effect of B^{11} on the basis of the multigroup calculation. The resulting isotopic reactivity worths are given in Tab.11, which also includes data relative to U^{235} as a reference substance.

8.3. Comparison with Multigroup Calculations

In Fig. 31 to 33 the experimental data are compared with integral transport calculations [12] on the basis of the KFKINR set; the calculated curves have been normalized by a common factor to the U(93%) measurement. The comparison shows that the experimental sample size dependence is quite well represented by the calculation, although some deviations in absolute value occur, especially for CH_2 and Fe.

The influence of heterogeneity on the calculated sample worth was found to be important only in the case of the strongly absorbing materials (B, Eu, Ta), where the softer heterogeneous spectrum leads to a more pronounced sample size dependence.

In Tab.11 the extrapolated sample worths are compared with first-order perturbation data obtained from 26-group diffusion calculations with different cross section sets. In these calculations, a small amount of sample material (10^{19} atoms per cm^3) was added to the homogeneous core mixture within the perturbed zone at core center [18].

To be independent of the normalization integral F of perturbation theory (cf. Eq.(3.2)), which is largely dependent on the critical mass of the particular system, primarily the reactivity worths relative to U^{235}, ρ^x/ρ^{25}, are discussed. These quantities may be considered as indices characteristic of the spectrum and adjoint behaviour at the sample position.

A comparison among the calculated values of Tab.11 shows quite strong variations with the cross section set used. The deviation from experiment is largest for the ABN set. In general, the discrepancies are greatly reduced when using the improved sets, although deviations remain for some of the scattering materials. The best overall agreement with experiment is found for the H2ØPMB and the KFKINR sets, in accordance with observations in STARK 5 [18].

In the following, a short description of some individual results will be given:

1. B^{10}, Eu, Mo, Ta:

For these predominantly absorbing materials a strong sample size dependence is observed which agrees reasonably well with the heterogeneous calculation (Fig.32 and 33). The extrapolated values for B^{10}, Mo and Ta agree within a few percent with the KFKINR calculation, while the Eu-worth was found to be 10 percent higher than calculated.

2. Fissionable materials:

The measured Pu-worth is consistent with calculations on the basis of the improved 26-group cross section sets. The U^{238}-worth in the void region was found to be 15 percent more negative than the KFKINR calculation; this discrepancy reduces to 8 percent for the measurement inside the cell.

3. Hydrogen:

The measured hydrogen worth is underestimated by all cross section sets; the calculation with the KFKINR set comes closest to the experimental value.

4. Scattering materials:

For the group of scattering materials, whose reactivity worths depend strongly on the slope of the adjoint flux, deviations of 10 to 20 percent are typical. Normally, the measured worth is higher in absolute value than the calculated one. This indicates that the slope of $\phi^+(E)$ at both sides of its minimum is greater than given by the calculation [17].

8.4. Comparison with the SNEAK 3A-2 Measurements

Tab.12 gives a comparison of reactivity worths measured in STARK 6 and SNEAK 3A-2 for samples of the same mass. In the case of CH_2 the STARK 6 data were taken from the measured sample size dependence, Fig.34.

To discuss the question whether reactivity worths in SNEAK can be predicted from a STARK experiment, in Tab.12 the ratio of reactivity worths in both assemblies, $\rho^{STARK}/\rho^{SNEAK}$, is considered, a quantity which would be a constant if spectrum and adjoint had the same energy dependence.

For a group of materials (B^{10}, Ta, Pu, U^{238}), where scattering effects are of minor importance, the ratio $\rho^{STARK}/\rho^{SNEAK}$ turned out to be 0.49 ± 0.02. For the group of scattering materials, however, ratios are found that are usually higher (0.56 for CH_2 and 0.62 for Fe). In these materials neutron moderation gives positive as well as negative group contributions, depending on the slope of the adjoint, such that in case of Al and C, compensation leads to a rather small net effect.

As shown in Fig.4, the energy dependence of ϕ^+ in STARK has a more pronounced minimum than in SNEAK 3A-2 which is caused by the presence of the natural uranium buffer as discussed in Sec.5.4. Hence, moderation effects in STARK are expected to be higher in absolute value, in accordance with most experimental data of Tab.12.

It may be concluded that for fissile as well as predominantly absorbing materials the reactivity worths in an all-fast system can be predicted from a STARK experiment with reasonable accuracy, whereas for the group of scattering materials such predictions can only be made with corrections based on reactor theory.

9. Doppler Effect

9.1. Measurements

The temperature effect on reactivity for samples of 0.4% depleted uranium oxide and of plutonium oxide has been determined in the center of STARK 6 using the same square-wave pile oscillator technique as in Sec.8. The sample and an equivalent dummy were embedded in the oscillator element whose empty regions were again filled with core material to reduce spectral disturbances.

The Doppler samples are identical to those used in the SNEAK 3A-2 experiment. They can be heated electrically to about 1000 ^{o}K and the temperature distribution can be monitored by a set of thermocouples. A detailed description of the samples is given in [30].

The observed variation of reactivity with temperature is shown in Fig.35 for the UO_2 sample, in Fig.36 for the PuO_2 sample. For plutonium an additional measurement was made within a boron-loaded environment comprising a region of the eight surrounding elements, similar to the experiment described in [31].
Within this zone the U^{235} has been replaced by an amount of boron that has about the same neutron absorption at Doppler energies. Thus, this substitution leads to a depression of the adjoint flux at low energies around the sample such that the Doppler effect arising from absorption is reduced without changing the spectrum in the sample. The experimental data for Pu, Fig.36, show a negative Doppler effect in the normal core that changes to a small positive effect in the boron environment.
Tab.13 gives the measured Doppler reactivities for a temperature change from 300 to 1000 ^{o}K as well as the ratios of the STARK 6 data relative to those of SNEAK 3A-2. Comparing these ratios with the ratios of the U^{235} and Pu worth measurements one finds that the U^{238} Doppler effect normalized to U^{235} is 20% greater than in the SNEAK 3A-2 experiment; for Pu a deviation of +45% is found.

This discrepancy cannot be explained by spectral effects since both spectra agree very well in the low keV region as shown in Fig.14. It is rather thought that the deviation is caused by the imperfect experimental conditions in STARK: due to its large axial extension part of the Doppler sample in its out-position occupies a region where the scattering contribution to the reactivity worth cannot be neglected. Axial expansion with rising temperature thus leads to an increase in the reactivity difference for the two sample positions. To avoid this systematic error it would be necessary to increase the stroke of the oscillator equipment by at least 10 cm.

10. Conclusions

From the comparison of the STARK 6 and SNEAK 3A-2 experiments the following principal results are summarized:

1. The differential neutron spectrum measurements at core center of both assemblies give the same results. The calculated deviation of spectra ($\pm$ 4% for $E \gtrsim 10$ eV) is too small to be detected by present experimental techniques. The spectrum above 30 keV is in good agreement with the 208-group calculation, while all 26-group sets show certain deviations due to the influence of the weighting spectrum on the elastic removal cross section.

2. For the spectral indices at core center deviations up to 3% are expected from multigroup calculations, in accordance with fission chamber measurements performed with the same set of samples. A comparison between the present fission standards and the old ones used in SNEAK 3A-2 showed an 11 percent discrepancy in the calibration of the U^{238} samples. The original difference between the measured and calculated U^{238}/U^{235} ratios in SNEAK 3A-2 is substantially reduced when using the new set of standards.

3. A satisfactory agreement is found for the measured shape of U^{235} fission and U^{238} capture rate traverses in the central lattice cell of both assemblies.
   The discrepancies between measured absolute reaction rates and the ZERA calculation in SNEAK 3A-2 are considerably reduced when the new fission samples are taken as standards. The present experiments are in good agreement with the ZERA calculation in the fuel, if the actual atom densities on the cell axis are used.

4. Material worth measurements for the fissile and the predominantly absorbing materials agree within $\pm$ 3 percent, except for a common normalization factor F. For most scattering materials, however, larger deviations are found that are explained by the $\pm$ 6 percent deviation in the energy dependence of the adjoint flux.

5. Doppler measurements could be made in the center of STARK 6 with sufficient statistical accuracy ($\approx 10^{-7}$k). The Doppler data for U^{238} normalized to the measured U^{235} worth deviate from the SNEAK results by 20 percent, while deviations of 45 percent occur for the Pu^{239} data. These discrepancies are explained by systematical errors due to the limited stroke of the oscillator in STARK.

6. Comparing the STARK 6 results with multigroup calculations one finds that for most quantities the influence of the cross section set used is much larger than the effect due to the deviation from the equilibrium spectrum. In general, the best agreement is found with the 26-group KFKINR set improved by introducing group transfer cross sections derived from a preceding 208-group spectrum calculation by usual condensation.

From this it may be concluded that, with the exception of the reactivity worths of the scatterers and the Doppler effect, all important quantities measured at the center of SNEAK 3A-2 can be predicted from the STARK experiment with systematic errors

smaller than the present experimental uncertainties.

Calculations have shown that the spectrum and adjoint match in this STARK assembly can be considerably improved by adding enriched uranium and some moderating material to the edge of the fast core without changing the natural uranium buffer zone.

The present comparison between STARK 6 and SNEAK 3A-2 can be considered as typical for a fast breeder core composition with the same fuel concentration (0.88 kg U^{235} per liter). For sodium and gas-cooled systems, the equilibrium spectrum will be considerably harder such that in STARK a larger excess of low energy neutrons ($E \lesssim 10$ keV) is expected, similar to the situation in the assemblies STARK 3 and 4 [17]. However, the contribution of these neutrons to the principal reaction rates at core center will only be in the order of 1 to 2 percent. Furthermore, there exists the possibility to reduce this low energy tail by adding boron to the buffer or to the edge of the fast zone.

References:

/1/ MEISTER, H., K.H. BECKURTS, W. HÄFELE, W.H. KÖHLER, and K. OTT: The Karlsruhe Fast-Thermal Argonaut-Reactor Concept, KFK-217, Kernforschungszentrum Karlsruhe (1964)

/2/ SCHRÖDER, R., et al.: Physics Investigations of Uranium-Fueled Fast Steam-Cooled Reactors in SNEAK, Assemblies 3A-0, 3A-2, 3A-3, KFK-847, Kernforschungszentrum Karlsruhe (1968)

/3/ MEISTER, H., et al.: Sicherheitsbericht für den gekoppelten schnell-thermischen Argonaut-Reaktor Karlsruhe (STARK), March 1964, unpublished

/4/ BACHMANN, H. et al.: The Karlsruhe Nuclear Code System NUSYS, unpublished

/5/ ABAGJAN, L.P. et al.: Gruppenkonstanten schneller und intermediärer Neutronen für die Berechnung von Kernreaktoren, KFK-tr-144, Kernforschungszentrum Karlsruhe (1964)

/6/ BACHMANN, H. et al.: The Cross-Section Set KFK-SNEAK Preparation and Results, KFK-628, Kernforschungszentrum Karlsruhe (1967)

/7/ HUSCHKE, H.: Gruppenkonstanten für dampf- und natriumgekühlte schnelle Reaktoren in einer 26-Gruppendarstellung; KFK-770, Kernforschungszentrum Karlsruhe (1968)

/8/ PÖNITZ, W.P.: Some New Measurements and Renormalizations of Neutron Capture Cross Section Data in the keV Energy Range, KFK-635, Kernforschungszentrum Karlsruhe (1967)

/9/ KIEFHABER, E. et al.: Evaluation of Fast Critical Experiments by Use of Recent Methods and Data, BNES Conf. on The Physics of Fast Reactor Operation and Design, London (1969)

/10/ MOXON, M.C.: UKAEA-Report AERE-R 6074 (1969)

/11/ KIEFHABER, E.:1. Vierteljahresbericht 1971, p. 122/14, KFK-1271/1 (1971)

/12/ FISCHER, E.A.: A Method to Calculate Reactivity Worth by Integral Transport Theory, KFK-995, Kernforschungszentrum Karlsruhe (1969)

/13/ WINTZER, D.: Heterogeneity Calculations Including Space Dependent Resonance Self-Shielding. KFK-633 (1967), and Fast Reactor Physics II, Vienna, p.237-255 (1968)

/14/ HUSCHKE, H.: Die Beschreibung der Datei GRUBA für 208 Energiegruppen, unpublished

/15/ BARLEON, L. et al.: Evaluation of Reactor Physics Experiments on the Coupled Fast-Thermal Argonaut Reactor STARK, KFK-482, Kernforschungszentrum Karlsruhe (1966) and ANL-7320

/16/ BARLEON, L. et al. (compiled by H. MEISTER): Untersuchungen an der Ladung 2 des Schnell-Thermischen Argonaut-Reaktors STARK, KFK-592, Kernforschungszentrum Karlsruhe (1967)

/17/ BARLEON, L. et al. (compiled by G. KUSSMAUL, and H. MEISTER): Untersuchungen an den Ladungen 3 und 4 des Schnell-Thermischen Argonaut-Reaktors STARK, KFK-668, Kernforschungszentrum Karlsruhe (1967) and EUR-3701d.

/18/ KUSSMAUL, G. and H. MEISTER: Investigation of Integral Parameters of the Fast-Thermal Reactor STARK, Assembly 5, KFK-1465, Kernforschungszentrum Karlsruhe (1971)

/19/ KUSSMAUL, G.: Prompt Jump Correction of Inverse Kinetics Rod Drop Measurements, Nucl.Sc.Eng.40, 494 (1970)

/20/ BENNETT, E.F.: Fast Neutron Spectroscopy by Proton-Recoil Proportional Counting, Nucl.Sc.Eng.27, 16-27 (1967)

/21/ WERLE, H.: Spektrumsmessungen radioaktiver Neutronenquellen im Energiebereich von 10 keV bis 10 MeV mit Protonenrückstoß-Proportionalzählrohren, KFK-Externer Bericht, INR-4/70-25, Kernforschungszentrum Karlsruhe (1970)

/22/ BLUHM, H.: 2. Vierteljahresbericht 1970 PSB, KFK 1270/2 p.121-1, Kernforschungszentrum Karlsruhe (1970)

/23/ MÜLLER, M.: Messung von Neutronenspektren im Energiebereich von 1 eV bis 10 keV mit Hilfe der Sandwichtechnik, KFK 1233, Kernforschungszentrum Karlsruhe (1970)

/24/ KUHN, D., unpublished

/25/ BÖHME, R., SEUFERT, H.: Uranium Reaction Rate Measurements in the Steam-Cooled Fast Reactor SNEAK, Assembly 3A-2, KFK-811, Kernforschungszentrum Karlsruhe (1968)

/26/ BLANK, K.H, and H. SEUFERT: An Automatic Sample Changer with a Special Changing Method for γ- and $\gamma\gamma$-Active Sources, Nucl.Instr.Meth.46, 86-96 (1966)

/27/ SEUFERT, H., and D. STEGEMANN: A Method for Absolute Determination of U^{238} Capture Rates in Fast Zero-Power Reactors, Nucl.Sci.Eng.28, 277-285 (1967)

/28/ KUSSMAUL, G., and H. MEISTER: Material Worth Measurements with a Fuel-Filled Pile Oscillator Rod, to be published Journal of Nucl. Energy 25, 373-387 (1971)

/29/ FRISCH, O.R., and LITTLER, D.J.: Pil.Mag.7, p.45 (1954)

/30/ BARLEON, L.: Messung des Dopplerkoeffizienten an verschiedenen Kernbrennstoffproben in einer schnellen und schnellthermischen Reaktoranordnung mit der Pileoszillatormethode, KFK-1350, Kernforschungszentrum Karlsruhe (1970)

/31/ BARLEON, L., and FISCHER, E.A.: Small-Sample Doppler Effect Measurements and their Interpretation in Fast Reactor Spectra, to be published.

Tab. 1 Atom densities ($10^{20}/cm^3$) of STARK 6 and SNEAK 3A-2 used for homogeneous calculations

Assembly	STARK 6							SNEAK 3A-2
Zone No.	1	2	3	4	5	6	7	-
Zone	Fast core	Natural uranium	Graphite + tank walls	Thermal core	Graphite	Graphite + tank walls	Graphite reflector	Central zone
Outer radius	18.60 cm	24.20 cm	30.50 cm	R [3]	46.00 cm	50.00 cm	86.00 cm	-
Al	130.96		92.643	130.07		72.60		129.10
C	9.60		492.25	169.31	852.55	428.9	852.55	9.32
Co [1]	0.21							0.19
Cr	36.50							34.53
Fe	126.52							121.85
H	18.76		3.680	360.80		5.267		17.92
Mg	0.71							0.64
Mn [2]	1.04							1.94
Mo+Nb	0.47							0.39
Ni	19.28							18.54
O	147.29			193.94				145.29
Si	1.88							1.88
Ti	0.44							0.40
U-235	20.625	3.437		1.0162				20.31
U-238	82.26	473.94		4.0592				81.04

1) Co was added to Fe
2) Mn was added to Cr

3) Values obtained from radius variation ($k_{eff} = 1$):
ABN : R = 41,019 cm MOXTOT: R = 40.155 cm
SNEAK : R = 40.356 cm KFKINR: R = 40.061 cm
H2ØPMB: R = 40.297 cm

Tab. 2 Experimental reactor parameters compared with 26-group diffusion calculations

	Measurement	ABN-set	SNEAK-set	H2ØPMB-set	MØXTØT-set	KFKINR-set	
Criticality data:							
Fuel mass, fast core	52.36	52.36	52.36	52.36	52.36	52.36	kg U^{235}
Fuel enrichment, fast core	19.86	19.86	19.86	19.86	19.86	19.86	atom%
Fuel mass, therm. core (20°C)	5.737±0.04	5.716	5.306	5.270	5.183	5.126	kg U^{235}
Fuel mass, therm. core (80°C)	5.987±0.02	-	-	-	-	-	kg U^{235}
Deviation of calc. k_{eff} from experiment	-	+0.06	+1.32	+1.43	+1.70	+1.88	%k
Power contributions:							
Fast core, γ_1	14.2 ±1.0	13.57	12.94	12.80	14.02	14.01	%
Uranium zone, γ_2	12.2 ±1.0	11.17	10.88	10.93	10.93	11.29	%
Thermal core, γ_4	73.6 ±1.5	75.26	76.18	76.27	75.05	74.70	%
Reactivity contributions:							
Fast core, α_1	-	14.88	13.48	13.37	15.11	15.02	%
Uranium zone, α_2	-	12.46	11.78	11.88	11.97	12.37	%
Reactivity worths, fast zone:							
Central element vs. void	+0.17±0.01	+0.17	-	-	-	-	%k
Worth of safety rod S_4	-0.66±0.01	-0.68	-	-	-	-	%k
Reactivity worths, therm. zone:							
Worth of outer fuel plate	-	0.064	-	-	-	-	%k
Worth of temp. change 80→20°C	-0.776±0.015	+0.67+)	-	-	-	-	%k
Worth of 1 control plate	-0.38±0.005	-0.40+)	-	-	-	-	%k
Worth of all 12 control plates	-4.5 ±0.5	-4.2 +)	-	-	-	-	%k
Kinetic parameters:							
Generation time	-	1.056	1.073	1.077	1.059	1.063	10^{-4} sec
$\beta^{25}_{eff}/\beta_{eff}$	-	0.8689	0.8844	0.8837	0.8828	0.8761	
β_{eff}/β_{eff}	-	0.1311	0.1156	0.1163	0.1172	0.1239	
β_{eff}	-	0.747	0.738	0.738	0.738	0.739	10^{-2}

+) Extrapolated from STARK 3 measurements.

Tab. 3 Kinetic parameters of STARK 6 used for the reactivity evaluations (diffusion calculation with ABN-set)

Isotope	k	λ_k [sec^{-1}]	$a_k = \beta_{effk}/\beta_{eff}$
U^{235}	1	0.0124	0.029297
	2	0.0305	0.191788
	3	0.111	0.169571
	4	0.301	0.344228
	5	1.13	0.099294
	6	3.00	0.036270
U^{238}	1	0.0132	0.001630
	2	0.0321	0.017747
	3	0.139	0.020450
	4	0.358	0.050858
	5	1.41	0.029150
	6	4.02	0.009717
U^{235}	$\sum_{k=1}^{6} a_k = 0.870448$		
U^{238}	$\sum_{k=1}^{6} a_k = 0.129552$		

Delayed neutron fraction:

$$\beta_{eff} = 0.7468 \cdot 10^{-2}$$

Prompt neutron generation time:

$$\Lambda = 1.0565 \cdot 10^{-4} \text{ sec.}$$

Tab. 4 Integral reactivity worth of control units

Plate, Rod	Rod drop ρ/β [¢]	Continous run ρ/β [¢]	Rod drop ρ/β [¢] per plate
R_1	- 50.9±0.4		- 50.9
R_2	- 45.8±0.4		- 45.8
R_3	- 55.7±0.4	- 57±1	- 55.7
$R_1+R_2+R_3$	-164 ±4		- 54.7
6 S	-345 ±12		- 57.5
3R+9S	-600±60		- 50
S_4	- 88 ± 2		

Tab. 5: Fission ratios σ_f^x / σ_f^y in the center of STARK 6

Isotope ratio	Absolute fission chamber	26-group diffusion calculation (...) = calc./exp.					KFKINR, $\Sigma_i \rightarrow i+1$ taken from 208 group calculat.
		ABN	SNEAK	H2ØPMB	MØXTØT	KFKINR	
Th^{232}/U^{235}	-	0.00568	0.00549	0.00550	0.00527	0.00558	0.00566
U^{233}/U^{235}	1.575±0.025	1.439 (0.914)	1.579 (1.002)	1.632 (1.036)	1.580 (1.003)	1.603 (1.018)	1.606 (1.020)
U^{234}/U^{235}	0.181±0.004	0.1975 (1.091)	0.1748 (0.966)	0.1757 (0.971)	0.1647 (0.910)	0.1732 (0.9569)	0.1884 (1.041)
U^{236}/U^{235}	0.0619±0.0015	0.0650 (1.050)	0.0596 (0.963)	0.0597 (0.965)	0.0561 (0.906)	0.0596 (0.963)	0.0619 (1.000)
U^{238}/U^{235}	0.0270±0.0005	0.02914 (1.079)	0.02765 (1.024)	0.02769 (1.026)	0.02613 (0.968)	0.02704 (1.002)	0.02738 (1.014)
Pu^{239}/U^{235}		0.9926	0.9647	0.9936	0.9553	0.9907	1.0036
Pu^{240}/U^{235}	-	0.2080	0.1848	0.1857	0.1842	0.1964	0.2093
U^{234}/U^{238}	6.70 ±0.14	6.778 (1.012)	6.325 (0.944)	6.345 (0.947)	6.304 (0.941)	6.405 (0.956)	6.881 (1.027)
U^{236}/U^{238}	2.29 ±0.05	2.230 (0,974)	2.156 (0,941)	2.157 (0,942)	2.145 (0,937	2.203 (0.962)	2.261 (0.987)

Tab. 6 Fission ratios σ_f^x/σ_f^y measured with absolute fission chambers in the center of STARK 6 compared to those of SNEAK 3A-2

Isotope ratio	STARK 6 x)		Correction factors		STARK 6 (corrected)		SNEAK 3A-2	STARK 6 / SNEAK 3A-2
	new fission standards	old fission standards	F_1 (composition)	F_2 (eq.spectrum)	new fission standards	old fission standards	old fission standards	old fission standards
Th^{232}/U^{235}	-	-	1.006	1.033±0.004	-	-	0.00655	-
U^{233}/U^{235}	1.575	(1.522)	1.000	0.997±0.001	1.570	1.517	1.48	1.025
U^{234}/U^{235}	0.181	-	(1.005)	1.022±0.003	0.186	-	-	-
U^{236}/U^{235}	0.0619	-	1.006	1.034±0.005	0.0644	-	-	-
U^{238}/U^{235}	0.0270	(0.0306)	1.006	1.036±0.004	0.0281	0.0317	0.0313	1.013
Pu^{239}/U^{235}		-	1.000	1.002±0.001		-	1.007	-
Th^{232}/U^{238}	-	-	1.000	0.997±0.002	-	-	0.209	-
U^{234}/U^{238}	6.70	-	1.000	0.986±0.003	6.61	-	-	-
U^{236}/U^{238}	2.29	-	1.000	0.998±0.002	2.29	-	-	-

Recalibration of old fission standards:

Sample:	New sample mass:	New / old mass:
A-123	273.5 µg U^{233}	0.951
A-322	322 µg U^{235}	0.984
A-522	426 µg U^{238}	1.117

x) Error limits cf. Tab. 5.

Tab. 7 Atom densities ($10^{20}/cm^3$) used for heterogeneity calculations

Material	laterally averaged densities (case I)					actual densities on cell axis (Case II)				
	$SS+CH_4$	SS	Al_2O_3	U20%	Al 25%	$SS+CH_2$	SS	Al_2O_3	U 20%	Al 25%
Al			394.16		132.92			447.49		150.90
C	75.096	0.503				85.257	0.572			
Cr	59.664	164.94	12.418	12.418	12.895	67.737	187.26	14.098	14.098	14.639
Fe	201.97	558.11	42.143	42.143	42.143	229.30	633.63	47.846	47.846	47.846
H	149.88					170.16				
Nb	0.654	1.542	0.255	0.255	0.255	0.742	1.750	0.290	0.290	0.290
Ni	27.542	75.109	6.195	13.343	6.195	31.268	85.272	7.033	15.149	7.033
O			590.49					670.39		
Si	2.661	7.641	0.426	0.426	0.1528	3.021	8.675	0.484	0.484	1.734
Ti	0.824	2.660				0.935	3.020			
U^{235}				82.240					93.368	
U^{238}				327.99					372.37	

Tab. 8 Reaction rate ratios in the normal cell of STARK 6 (calculations with SNEAK set)

	Uranium foil activation	Fission chamber	ZERA	Homogeneous, one-zone system	Homogeneous, cell-aver. STARK 6	Homogeneous STARK 6
fuel-averaged values:						
$\bar{n}_f^{28} / \bar{n}_f^{25}$	0.0278	-	0.02858	-	-	-
$\bar{n}_c^{28} / n_f^{25}$	0.125	-	0.1334	-	-	-
cell-averaged values:						
$\bar{n}_f^{28} / \bar{n}_f^{25}$	0.0273	0.0270±0.0005	0.02781	0.02864	0.2797	0.02765
$\bar{n}_c^{28} / \bar{n}_f^{25}$	(0.137)	-	0.1880	0.1383	-	0.1388
$\bar{n}_f^{24} / \bar{n}_f^{25}$	-	0.181 ±0.004	-	0.1786	-	0.1748
$\bar{n}_f^{26} / \bar{n}_f^{25}$	-	0.0619±0.0015	0.06055	0.0616	0.0593	0.0596
$\bar{n}_f^{40} / \bar{n}_f^{25}$	-	-	0.1866	0.1892	0.1847	0.1848

Tab. 9 Reactivity change due to bunching of a central zone in STARK 6

Bunched Zone	Reactivity change Δρ			Reactivity fraction α_b	$(\Delta k/k)_b$ for infinite lattice		
	Measurement	Hom., calc. with cell-av. cross section	Hom., calc. with cell av. cross sections (D=const.)		Measurement	ZERA static k_{eff}-calc.	ZERA with constant leakage (D=const.)
normal cell						0	0
single bunch: 9 central elements	3.4±0.7 ¢	-	2.36 ¢	0.03476	0.73±0.15%k	+ 0.0138%k	+ 0.51%k
single bunch: 21 central elements	6.3±1.0 ¢	1.20 ¢	4.81 ¢	0.0707	0.67±0.11%k		
double bunching: 9 central elements	7.0±0.7 ¢	-	6.17 ¢	0.03476	1.51±0.15%k	- 0.2012%k	+ 1.33%k
double bunching: 21 central elements	13.8±1.0 ¢	0.24 ¢	12.5 ¢	0.0707	1.47±0.11%k		

Tab.10 Reactivity worth of samples measured at the center of STARK 6

Material	Mass /g/	Experimental reactivity worth /$/g/ Void volume	Cell(1)	Cell(2)	cell(1)/void	cell(2)/void
Al	172.90	$-0.47 \cdot 10^{-5}$				
	43.25	$-0.62 \cdot 10^{-5}$				
B^{10}*)	2.807	$-0.565 \cdot 10^{-2}$				
	0.972	$-0.632 \cdot 10^{-2}$	$-0.647 \cdot 10^{-2}$	$-0.648 \cdot 10^{-2}$	1.024	1.025
	0.644	$-0.665 \cdot 10^{-2}$				
	0.327	$-0.712 \cdot 10^{-2}$				
B_4C	6.27	$-0.1076 \cdot 10^{-2}$				
C	36.38	$+0.229 \cdot 10^{-4}$				
	12.15	$+0.218 \cdot 10^{-4}$				
CH_2	6.293	$+0.1443 \cdot 10^{-2}$				
	4.413	$+0.1395 \cdot 10^{-2}$				
	1.955	$+0.1378 \cdot 10^{-2}$	$+0.1374 \cdot 10^{-2}$	$+0.1427 \cdot 10^{-2}$	0.997	1.036
Cr	92.55	$-0.693 \cdot 10^{-5}$				
	36.07	$-0.672 \cdot 10^{-5}$				
Eu	3.562	$-0.568 \cdot 10^{-3}$				
Fe	127.64	$-0.752 \cdot 10^{-5}$				
	51.11	$-0.861 \cdot 10^{-5}$				
Mo	102.27	$-0.321 \cdot 10^{-4}$				
	33.95	$-0.365 \cdot 10^{-4}$				
Ni	114.62	$-0.113 \cdot 10^{-4}$				
	57.31	$-0.124 \cdot 10^{-4}$	$-0.122 \cdot 10^{-4}$	$-0.122 \cdot 10^{-4}$	0.984	0.984
Ta	107.09	$-0.934 \cdot 10^{-4}$				
	53.74	$-1.063 \cdot 10^{-4}$	$-1.093 \cdot 10^{-4}$	$-1.097 \cdot 10^{-4}$	1.028	1.032
	18.51	$-1.298 \cdot 10^{-4}$				
Pu x)	4.926	$+0.244 \cdot 10^{-3}$	$+0.260 \cdot 10^{-3}$	$+0.271 \cdot 10^{-3}$	1.066	1.111
	2.470	$+0.237 \cdot 10^{-3}$				
U (93%)	17.675	$+0.1739 \cdot 10^{-3}$				
	7.181	$+0.175 \cdot 10^{-3}$	$+0.182 \cdot 10^{-3}$	$+0.182 \cdot 10^{-3}$	1.040	1.040
	3.630	$+0.175 \cdot 10^{-3}$				
U (20%)	125.12	$+0.252 \cdot 10^{-4}$				
U (0.4%)	248.10	$-0.145 \cdot 10^{-4}$				
	123.85	$-0.155 \cdot 10^{-4}$	$-0.137 \cdot 10^{-4}$	$-0.143 \cdot 10^{-4}$	0.884	0.923
	61.60	$-0.161 \cdot 10^{-4}$				

*) Composition of B^{10} sample: 92.15 at.% B^{10}, 7.85 at.% B^{11}

x) Composition of Pu sample: 91.48% Pu^{239}, 7.68% Pu^{240}, 0.80% Pu^{241}, 0.03% Pu^{242}

Tab.11 Reactivity worth ratio of samples (extrapolated to zero sample mass)

Material	Experimental values: Extrapolated Sample worth $\langle\bar{\Delta}k/10^7\ g\rangle$	Experimental values: Extrapolated Sample worth $\langle\bar{\Delta}k/10^{30}\ atoms\rangle$	Experimental values: ρ/ρ^{25}	Calculated worth ratio ρ/ρ^{25}: ABN	SNEAK	H2ØPMB	MØXTØT	KFKINR	KFKINR calc./exp.
Al	- 0.48	- 2.2	-0.0039	-0.00216	-0.00367	-0.00382	-0.00287	-0.00314	0.805
$B^{1)}$	- 597	- 1000	-	-	-	-	-	-	-
C	+ 1.6	+ 3.3	+0.0059	+0.00435	+0.00218	+0.00274	+0.00352	+0.00414	0.702
CH_2	+99.7	+ 232	+0.421	+0.270	+0.290	+0.319	+0.290	+0.355	0.843
Cr	- 0.49	- 4.26	-0.0077	-0.00936	-0.00846	-0.00876	-0.00785	-0.00823	1.068
Eu	-53.8	-1357	-2.463	-	-	-	-	$-2.236^{4)}$	0.908
Fe	- 0.71	- 6.57	-0.0119	-0.00828	-0.0110	-0.0116	-0.0101	-0.01065	0.895
Mo	- 3.72	-59.3	-0.1076	-0.0865	-0.0947	-0.0999	-0.0983	-0.1057	0.982
Ni	- 1.14	-11.1	-0.0201	-0.0177	-0.0192	-0.0195	-0.0189	-0.0192	0.955
Ta	-16.80	- 504	-0.916	-0.694	-0.789	-0.836	-0.838	$\{-0.890$ / $-0.926^{4)}$	0.972 / 1.011
$Pu^{2)}$	+17.3	+ 688	+1.248	+1.324	+1.204	+1.247	+1.216	+1.210	0.970
U (93%)	+13.07	-	-						
U (0.4%)	- 1.277 / - 1.165 3)	-	-						
U^{235}	+14.13	+ 551	+1.000	+1.000	+1.000	+1.000	+1.000	+1.000	1.000
U^{238}	- 1.339 / - 1.226 3)	-52.9 / -48.5 3)	-0.0961 / -0.0880 3)	-0.0710	-0.0861	-0.0866	-0.0757	-0.0798	0.830 / 0.907
H	-	+ 114	+0.208	+0.133	+0.144	+0.158	+0.143	+0.1753	0.843
B^{10}	-	-1085	-1.969	-1.491	-1.709	-1.809	-1.821	$\{-1.909$ / $-2.024^{4)}$	0.970 / 1.027
Worth of U^{235} $\langle\bar{\Delta}k/10^{30}\ atoms\rangle$:			+ 551	+609	+563	+549	+628	+616	1.118

1) Composition of B^{10} sample: 92.15% B^{10} 7.85% B^{11}
2) Composition of Pu sample: 91.48% Pu^{239}, 7.69% Pu^{240}, 0.80% Pu^{241}, 0.03% Pu^{242}
3) Cell measurement
4) Heterogeneous calculation

Tab.12 Comparison of sample worths measured in STARK 6 and SNEAK 3A-2

Sample	Sample mass [g]	Reactivity [10^{-6} \$/g] in void environment		Reactivity [10^{-6} \$/g] in cell environment		Ratio $\rho^{STARK} / \rho^{SNEAK}$			
		STARK 6	SNEAK 3A-2	STARK 6	SNEAK 3A-2	void environm.	cell environ.	calc. (SNEAKset)	calc. KFKINRs.
U^{235}	17.8	+187	+353	+195[1]	+411	0.529	0.474	0.500	0.500
U^{238}	62	-16.8	-32	-	-	0.525		0.530	0.534
	262	-15.2	-29.8	-	-26.0	0.510		0.530	0.534
	998	-	-27.1	-	-				
Pu[3]	8.5	+244[2]	+506	+266[2]	+532	0.482	0.500	0.491	0.492
B^{10}	0.3	-	-	-	-17300				
	1.0	-6910	-14850	-7080	-14680	0.465	0.482	0.488	0.488
	2.9	-6180	-	-	-12800				
Ta	53	-107	-228	-110	-223	0.469	0.493	0.490	0.491
Ni	114	-11.3	-22	-12.2	-	0.51		0.516	0.520
Fe	128	- 7.5	-12	-	-12	0.62		0.576	0.590
CH_2	2.5	+1380	-	+1410	+2520		0.560	0.613	0.586
	3.6	+1390	+2310	-	-	0.602		0.613	0.586
C	48	+23	+61.4	-	+72.4	0.37		0.377	0.426
Al	160	- 4.7	-1.2	-	-0.7	-		0.86	1.04

1) sample mass 7.18 g

2) sample mass 4.93 g Pu

3) (91.48% Pu^{239}, 7.69% Pu^{240}, 0.80% Pu^{241}, 0.03% Pu^{242})

Tab. 13 Comparison of Doppler Measurements in STARK 6 and SNEAK 3A-2

Sample	Doppler reactivity from 300 to 1000°K/10^{-6}k/		
	STARK 6	SNEAK 3A-2	STARK/SNEAK
UO_2 (0.4%)	- 10±0.6	- 16	0.62±0.04
PuO_2	-4.5±0.5	- 6.2	0.72±0.08
	Material worth measurement		
			STARK/SNEAK
U^{235}			0.50±0.02
U^{238}			0.55±0.01
Pu			0.49±0.01

Data of Doppler Samples:

UO_2 Sample: 854 g UO_2 (0.4% depleted)
length 9.0 cm, diameter 3.5 cm

PuO_2 Sample: 451.7 g PuO_2 + 360.5 g Al_2O_3
length 15.0 cm, diameter 3.5 cm

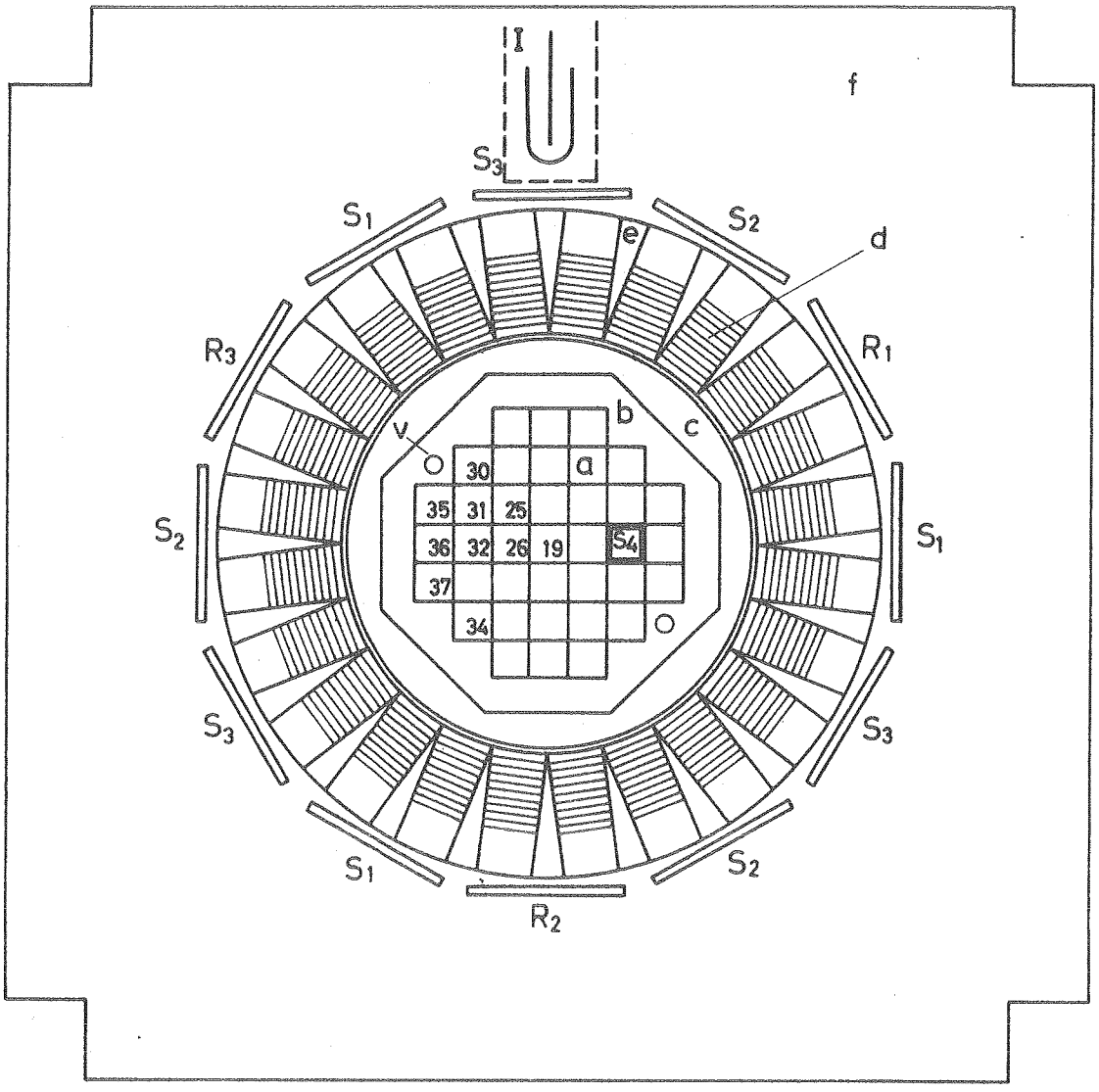

Fig. 1: Schematic cross section of STARK

a - fast core
b - natural uranium zone
c - graphite region
d - thermal core (fuel region)
e - thermal core (graphite pieces)
f - graphite reflector
v - vertical channel
19; 25; 26.... matrix positions for fission chamber and foil measurements
R_1, R_2, R_3 - control plates
S_1, S_2, S_3 - safety plates
S_4 - fuel-poison safety rod
I - boron-lined ionization chamber for kinetic measurements

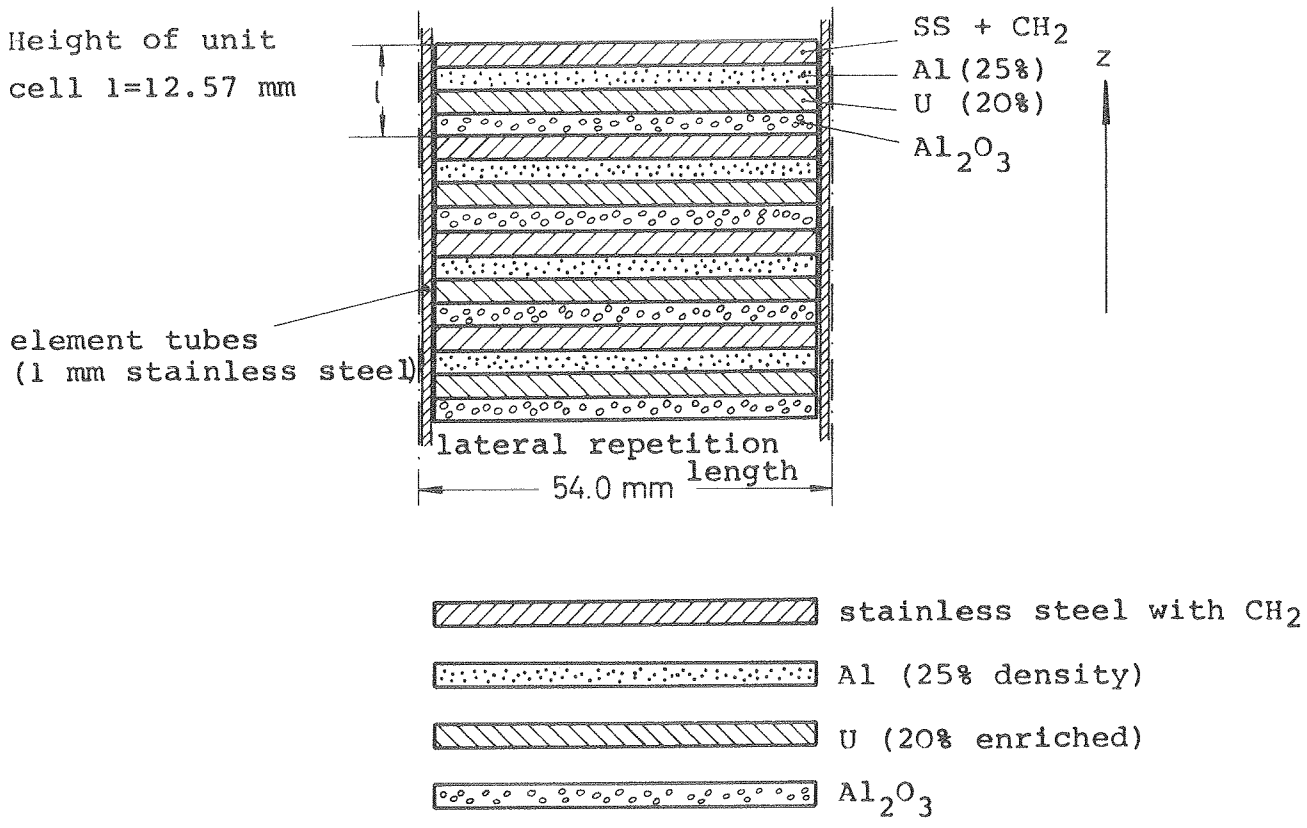

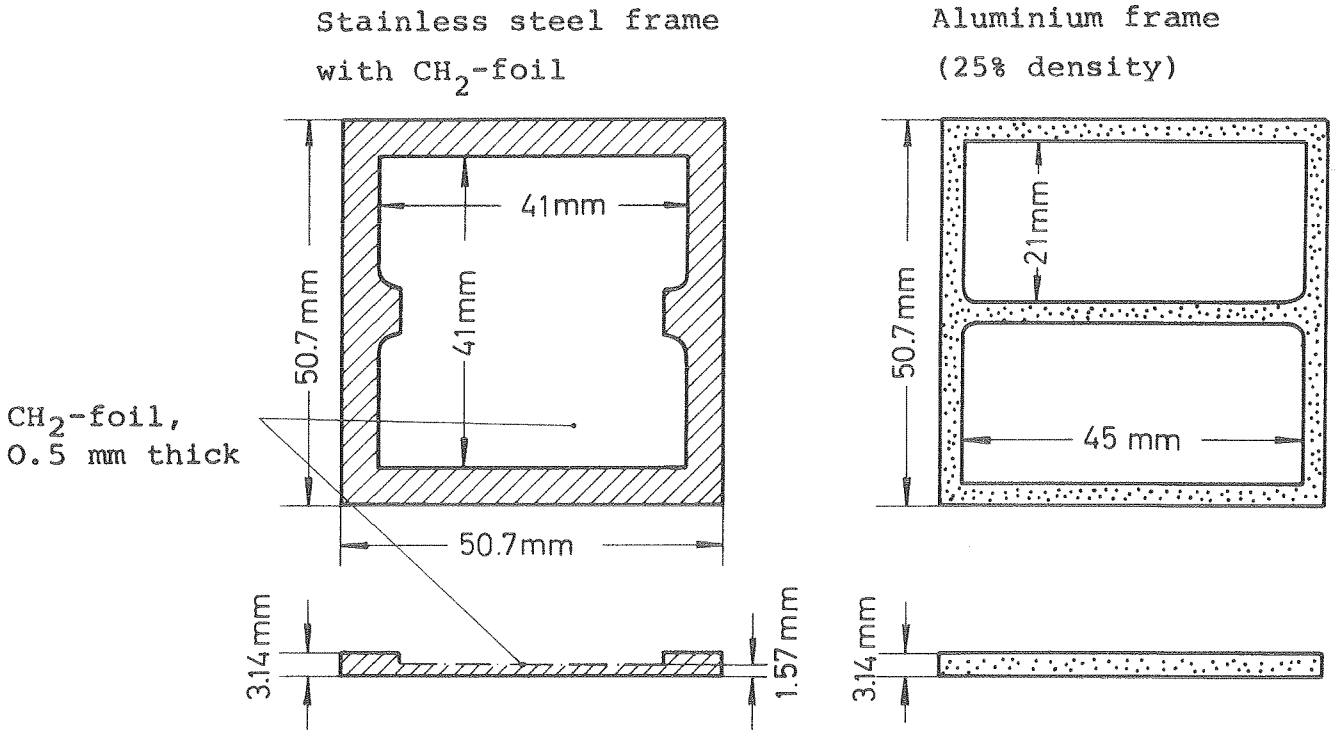

Fig. 2: Cell structure of the fast zone of STARK 6

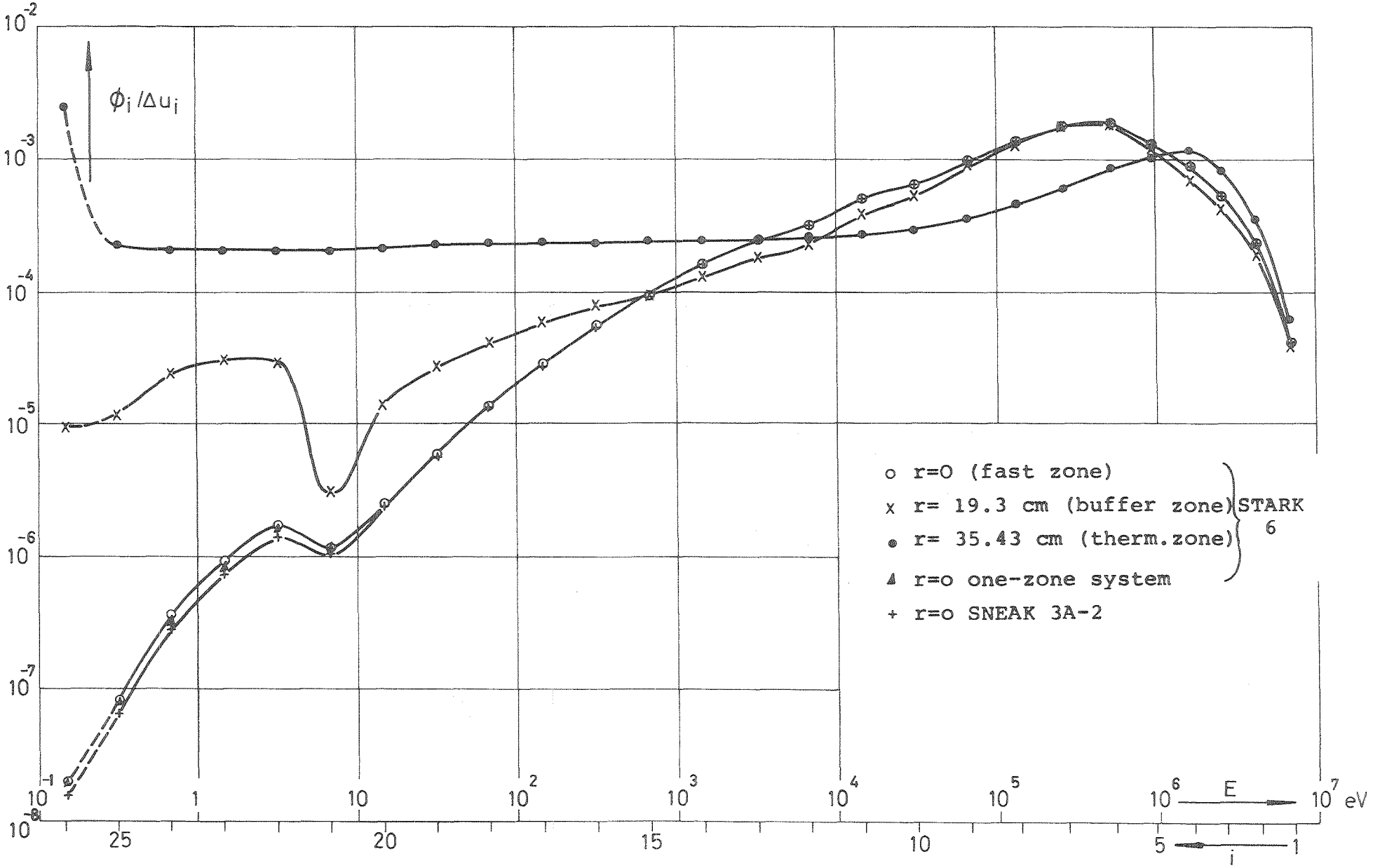

Fig. 3: Neutron spectrum $\phi_i/\Delta u_i$ at different radial positions in STARK 6, in the center of a one-zone system and in the center of SNEAK 3A-2 (one-dimensional diffusion calculation with 26-group ABN set)

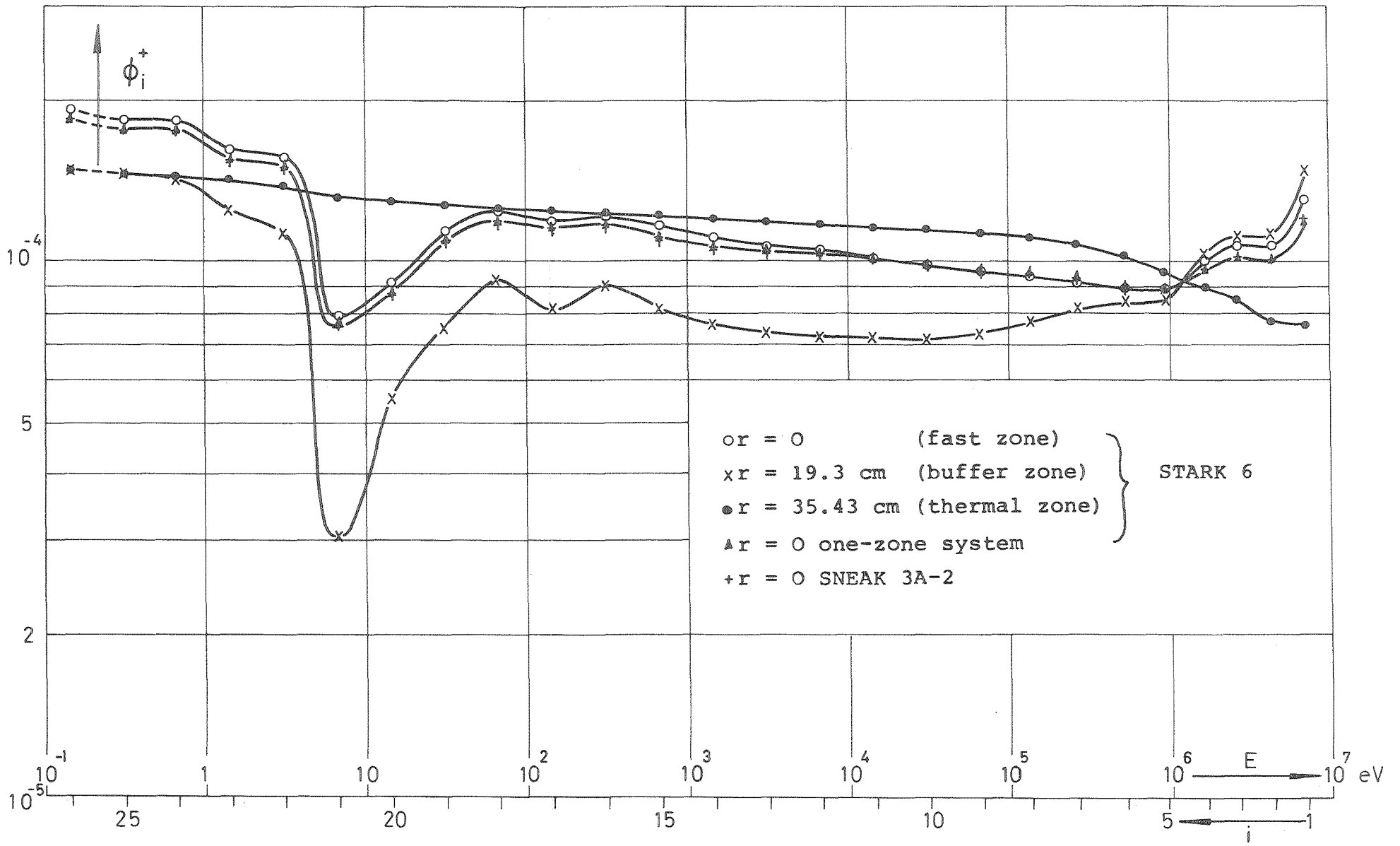

Fig. 4: Adjoint flux ϕ_i^+ at different radial positions in STARK 6, in the center of a one-zone system and in the center of SNEAK 3A-2 (one-dimensional diffusion calculation with 26-group ABN set)

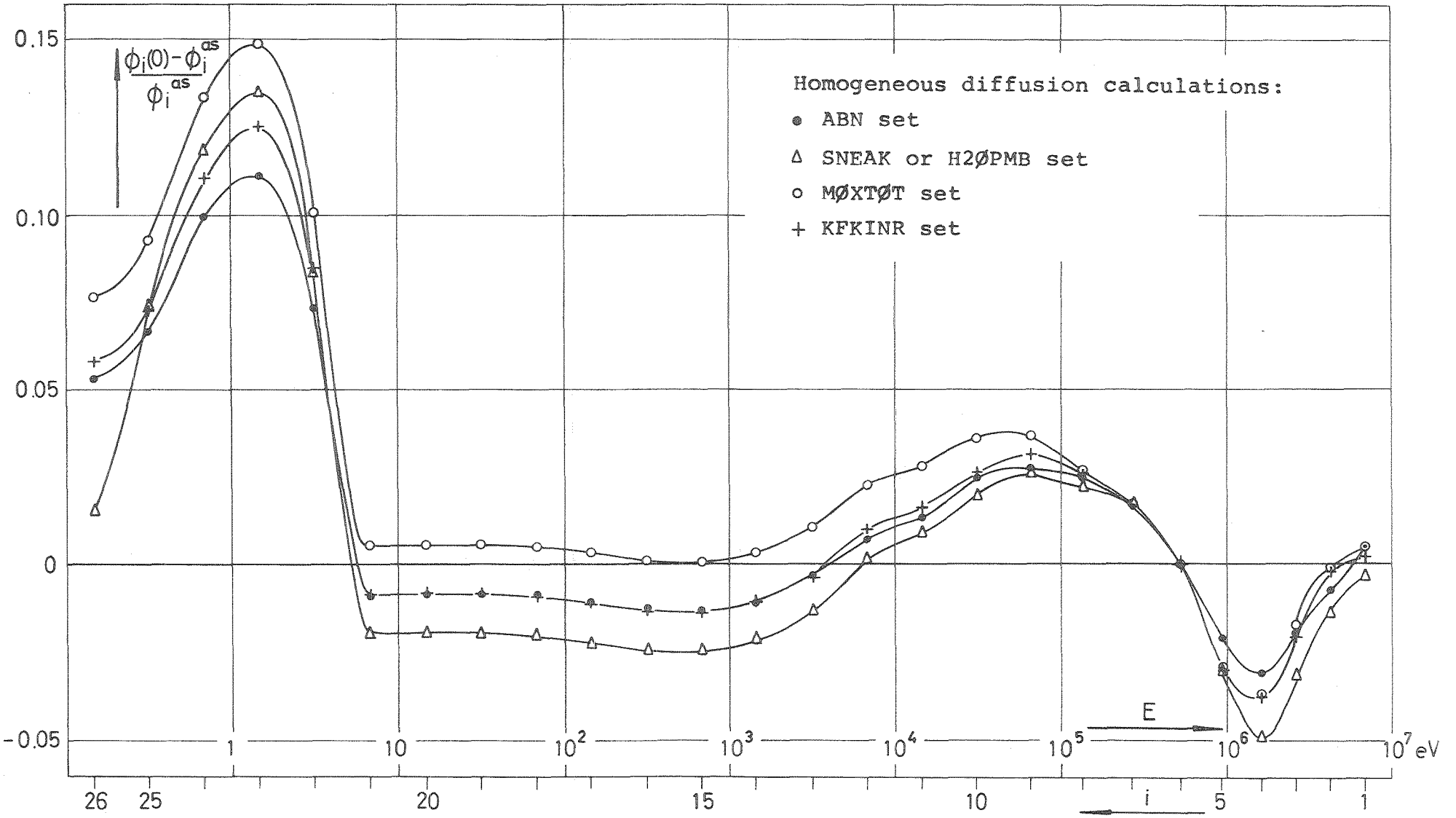

Fig. 5: Relative deviation of the neutron spectrum in the center of STARK 6, $\phi_i(0)$, from the equilibrium spectrum ϕ_i^{as} in a one-zone system (normalization in group i = 6)

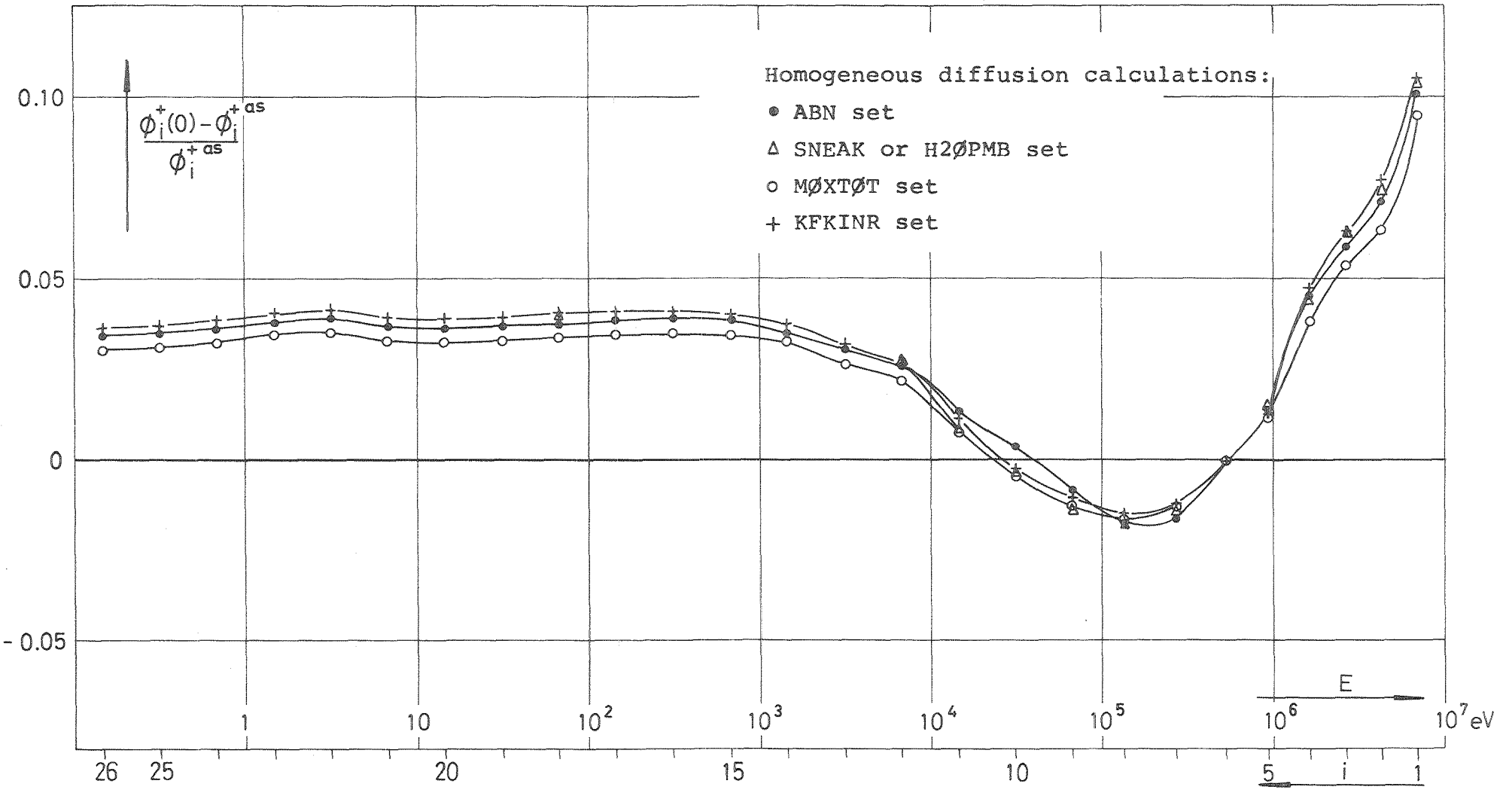

Fig. 6: Relative deviation of the adjoint flux in the center of STARK 6, $\phi_i^+(0)$, from the adjoint ϕ_i^{+as} in a one-zone system (normalization in group i = 6)

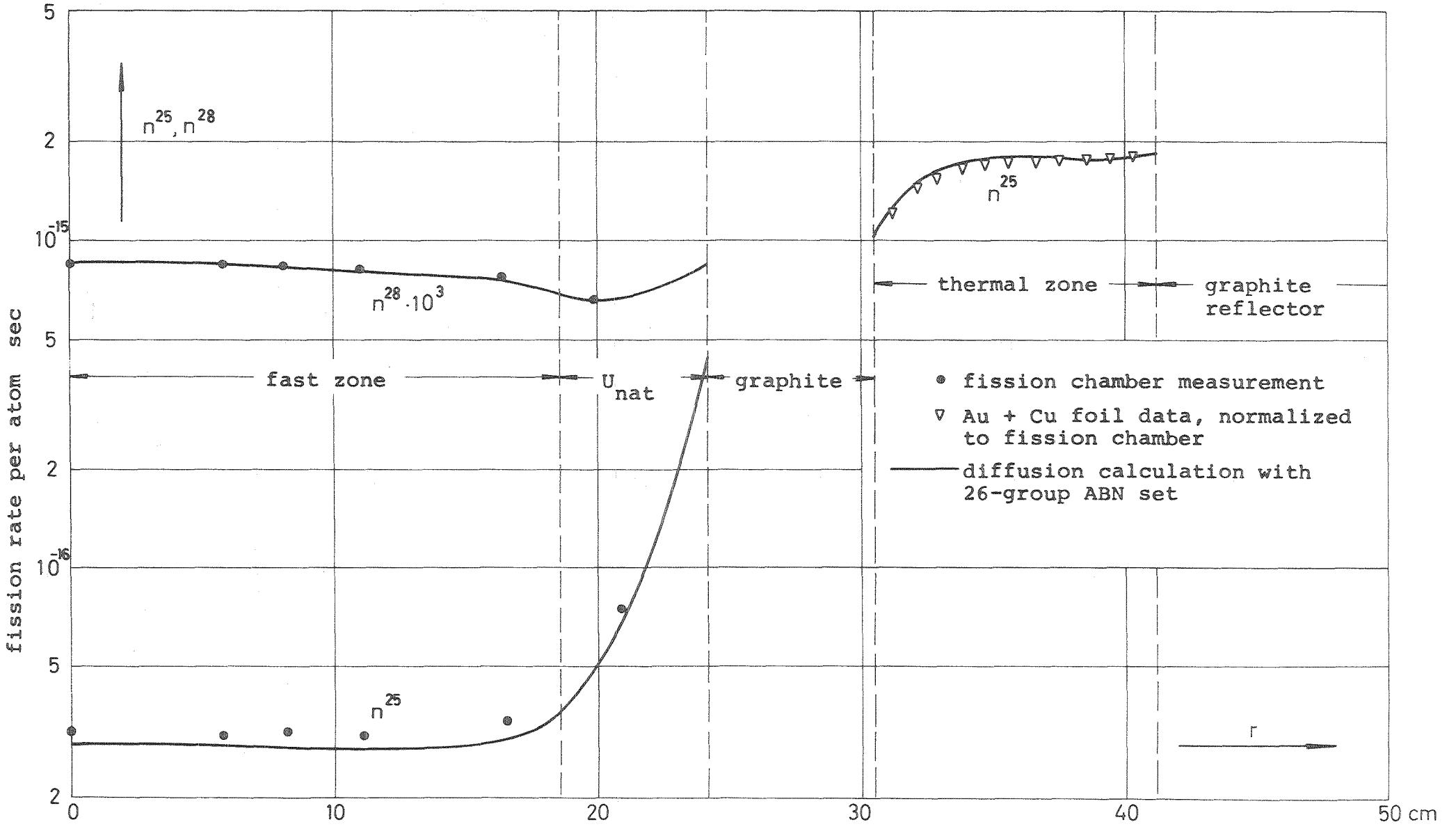

Fig. 7: Radial distribution of U^{235}- and U^{238}-fission rates per atom, n^{25} and n^{28}, in the midplane of STARK 6 at 1 Watt reactor power

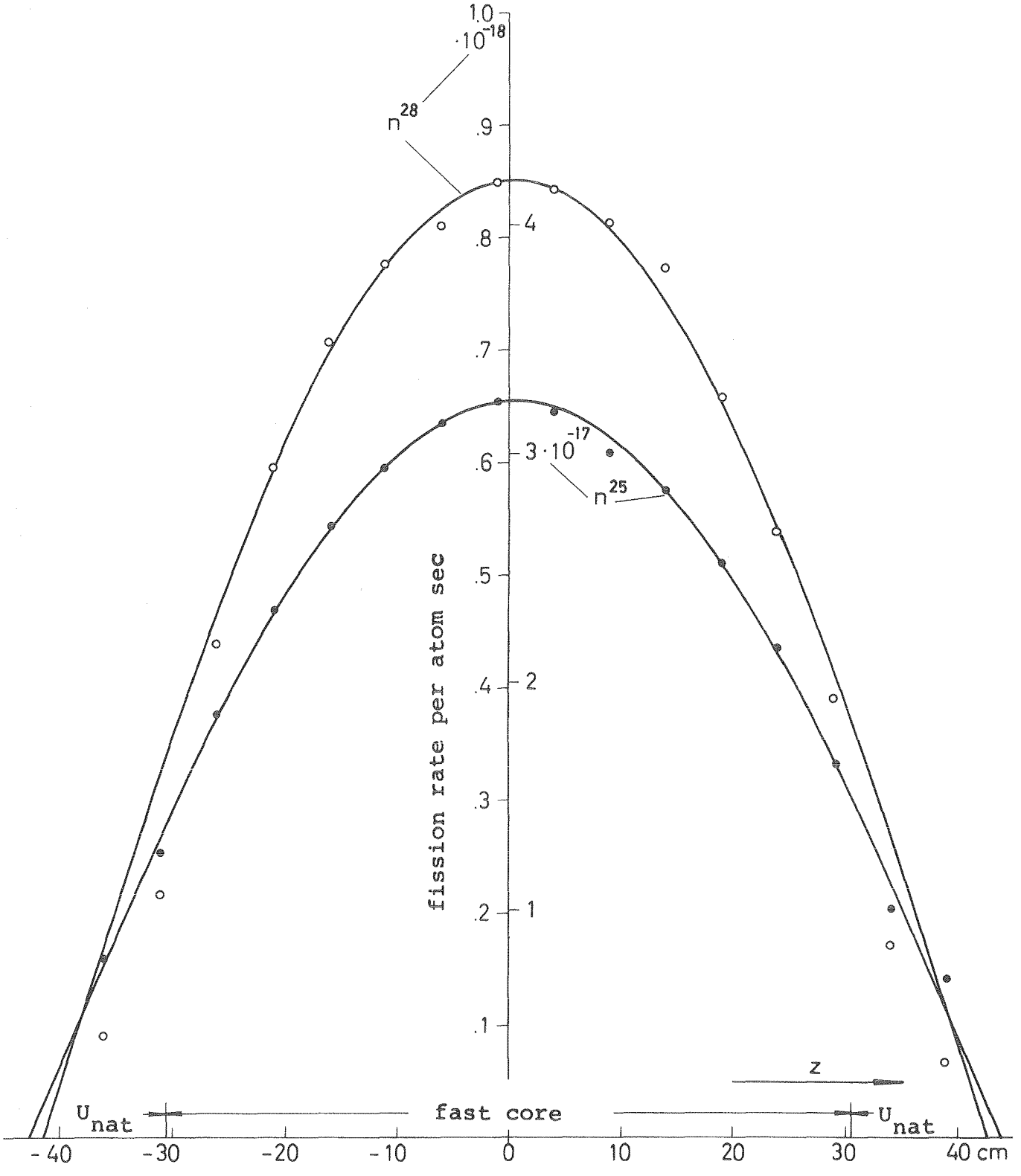

Fig. 8: Axial distribution of U^{235}- and U^{238}-fission rates per atom, n^{25} and n^{28}, in the central position of the fast zone at 1 Watt reactor power

- • U^{235} fission chamber traverse
- ○ U^{238} fission chamber traverse
- ——— $A \cdot \cos(z/H_{eff})$ fitted to experimental data

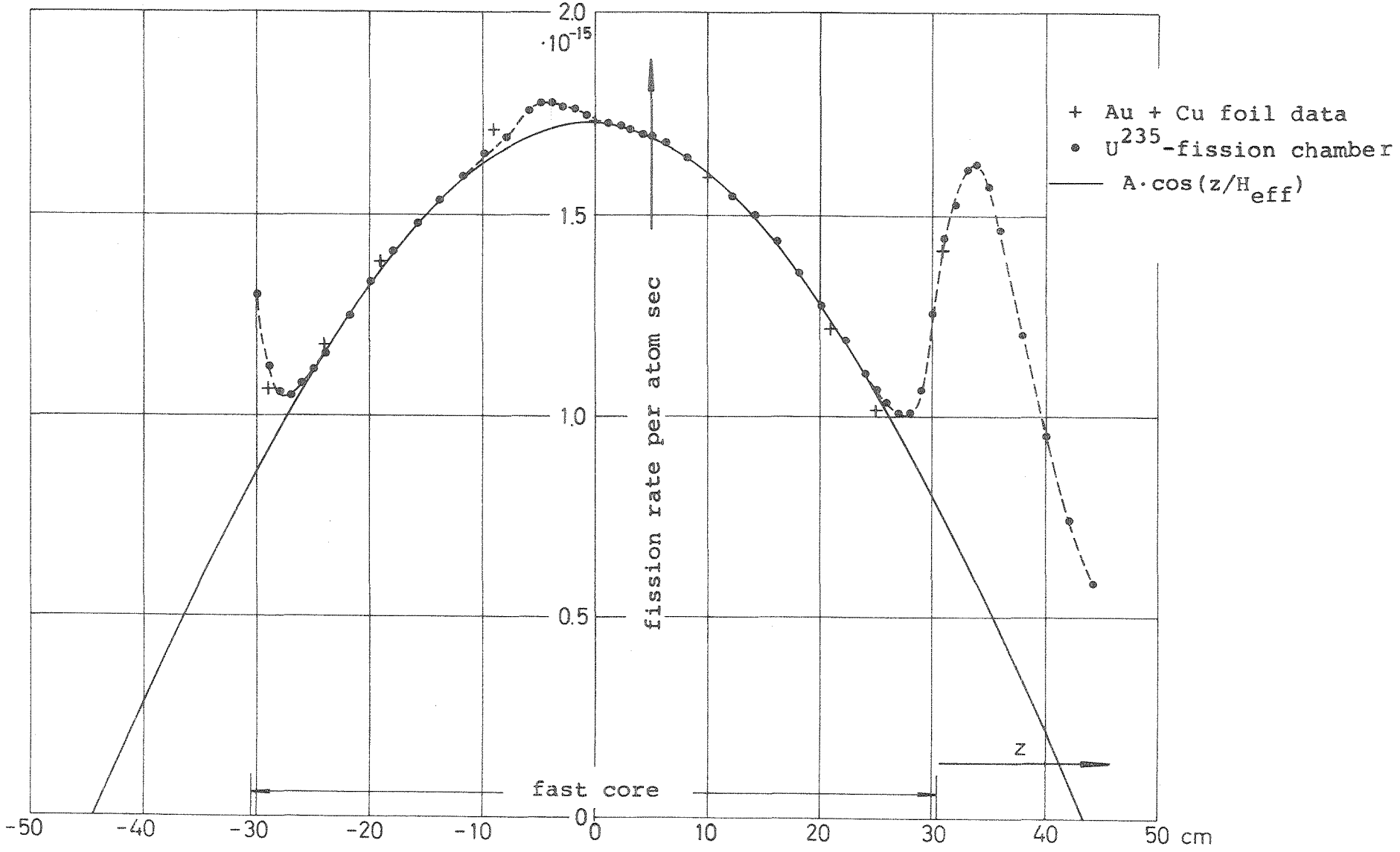

Fig. 9: Axial distribution of the U^{235}-fission rate in the thermal core (r = 34.8 cm) at 1 Watt reactor power

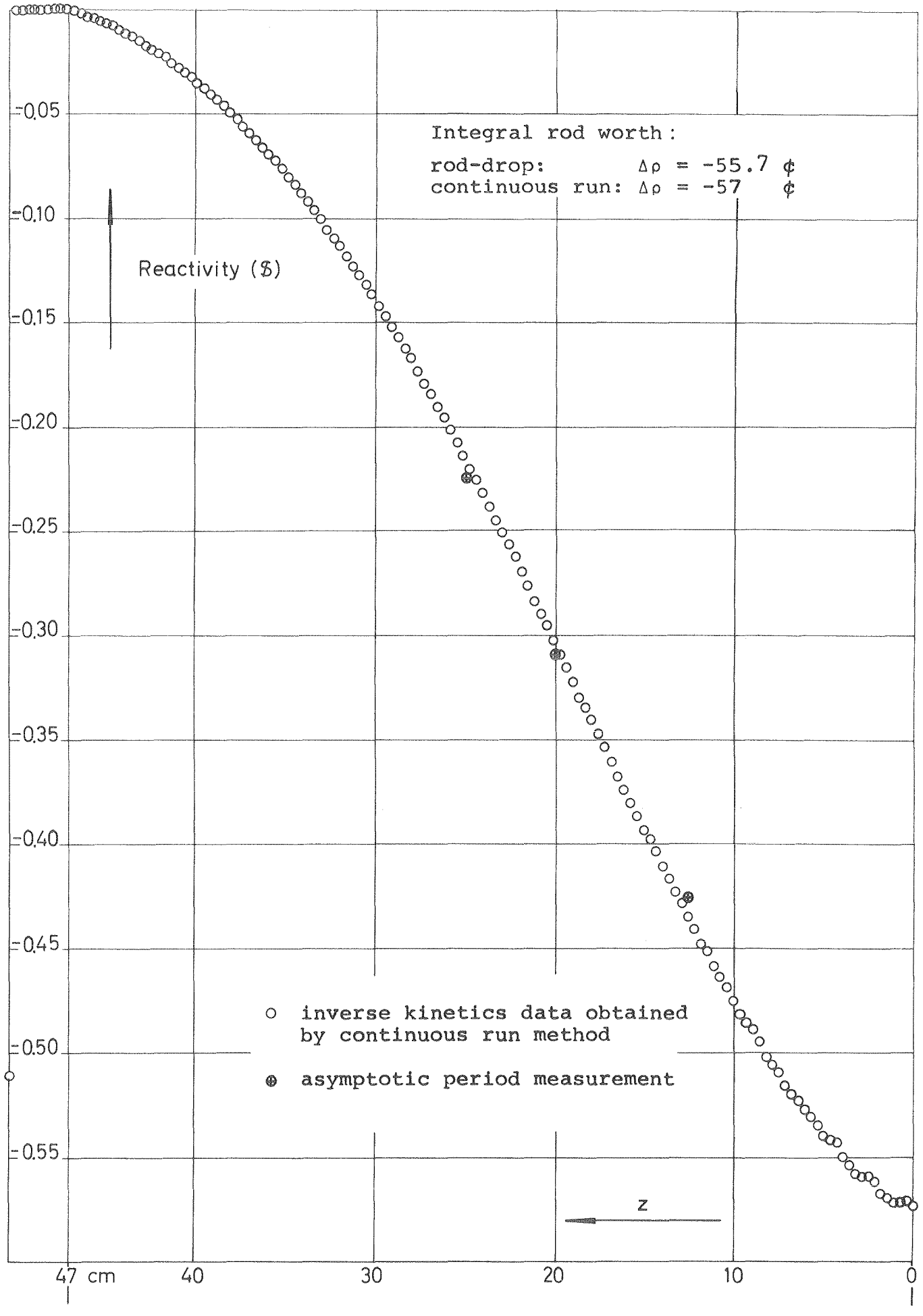

Fig. 10: Reactivity calibration of control plate R_3

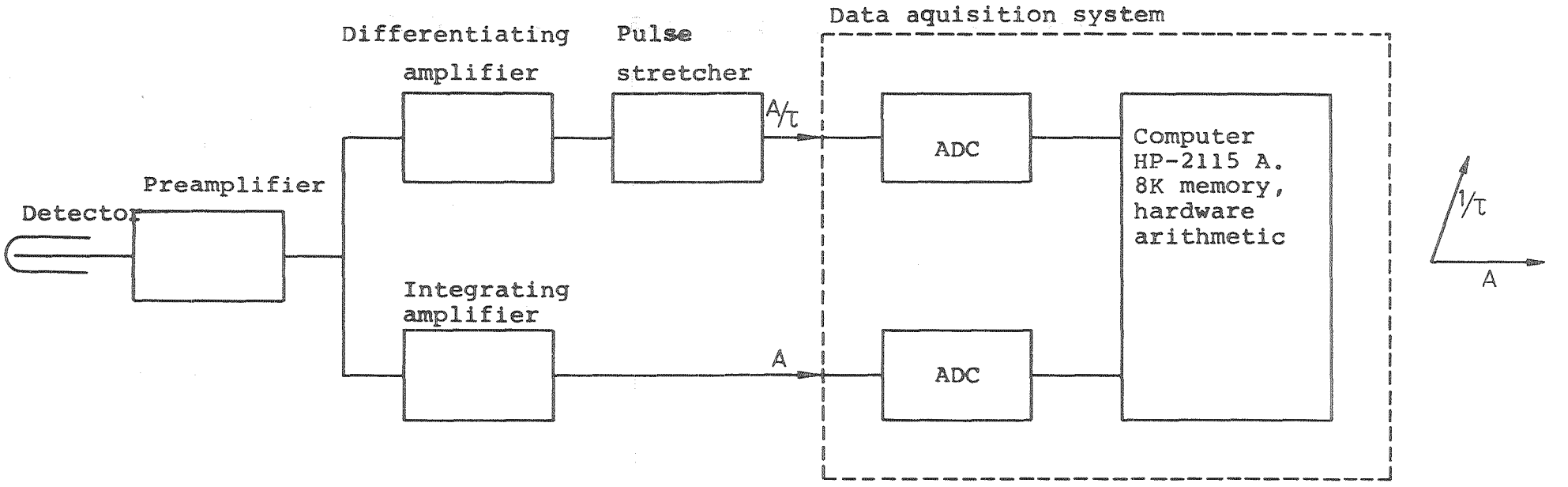

Fig. 11: Electronic system for γ-n-discrimination
(A = pulse height, τ = rise time)

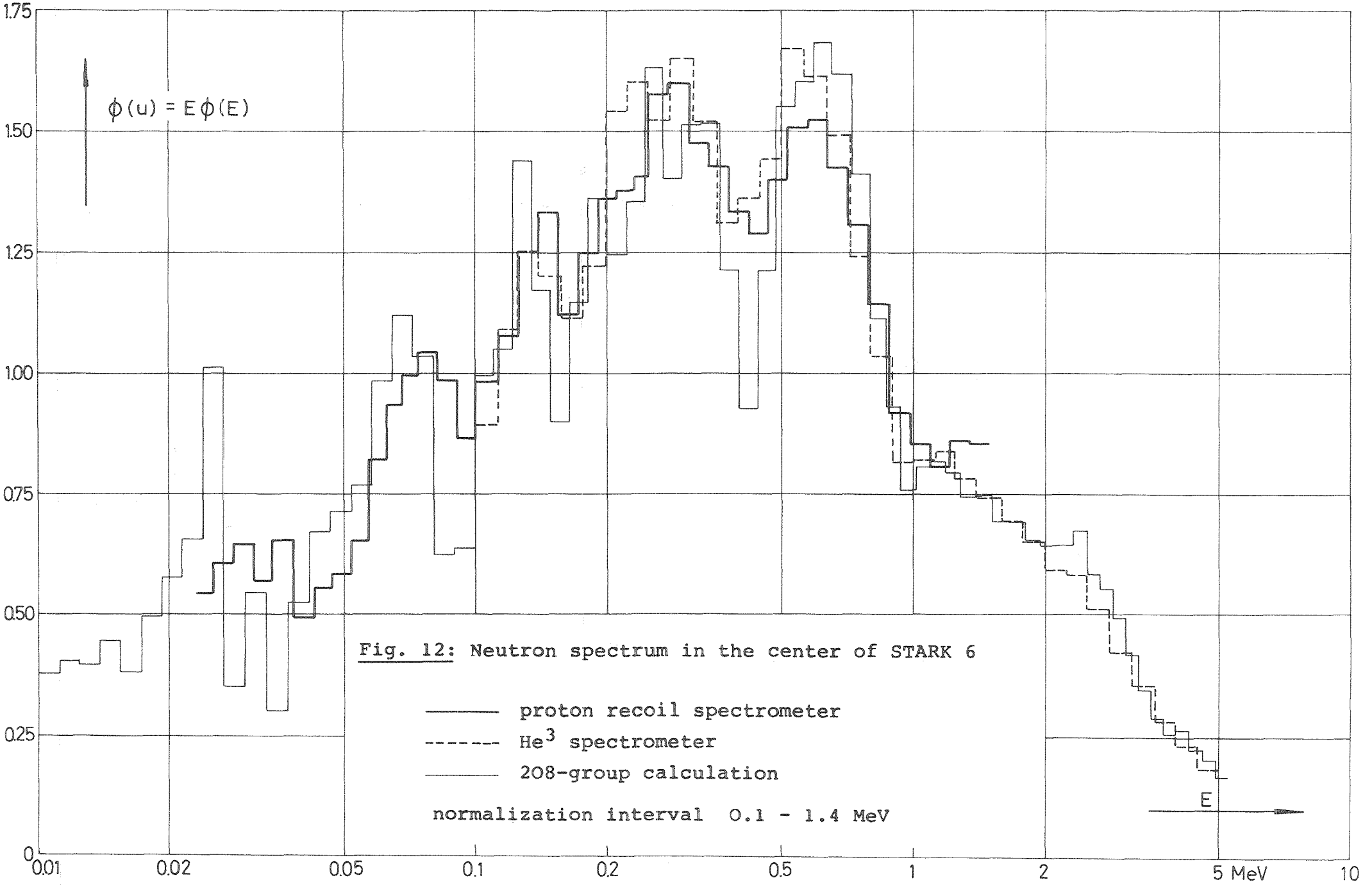

Fig. 12: Neutron spectrum in the center of STARK 6

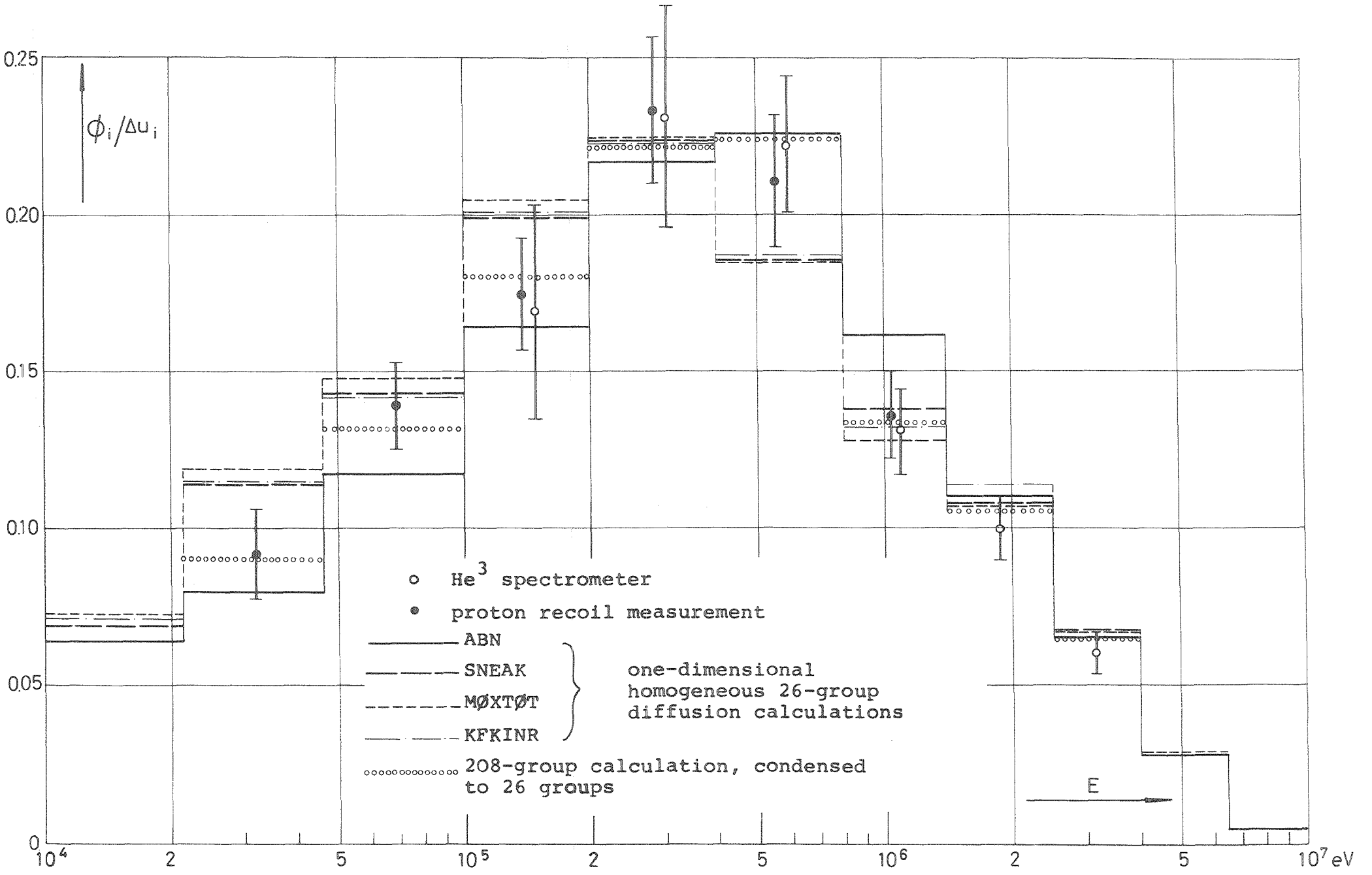

Fig. 13: Comparison of 26-group spectra for the center of STARK 6 (normalization interval 0.0465 to 2.5 MeV

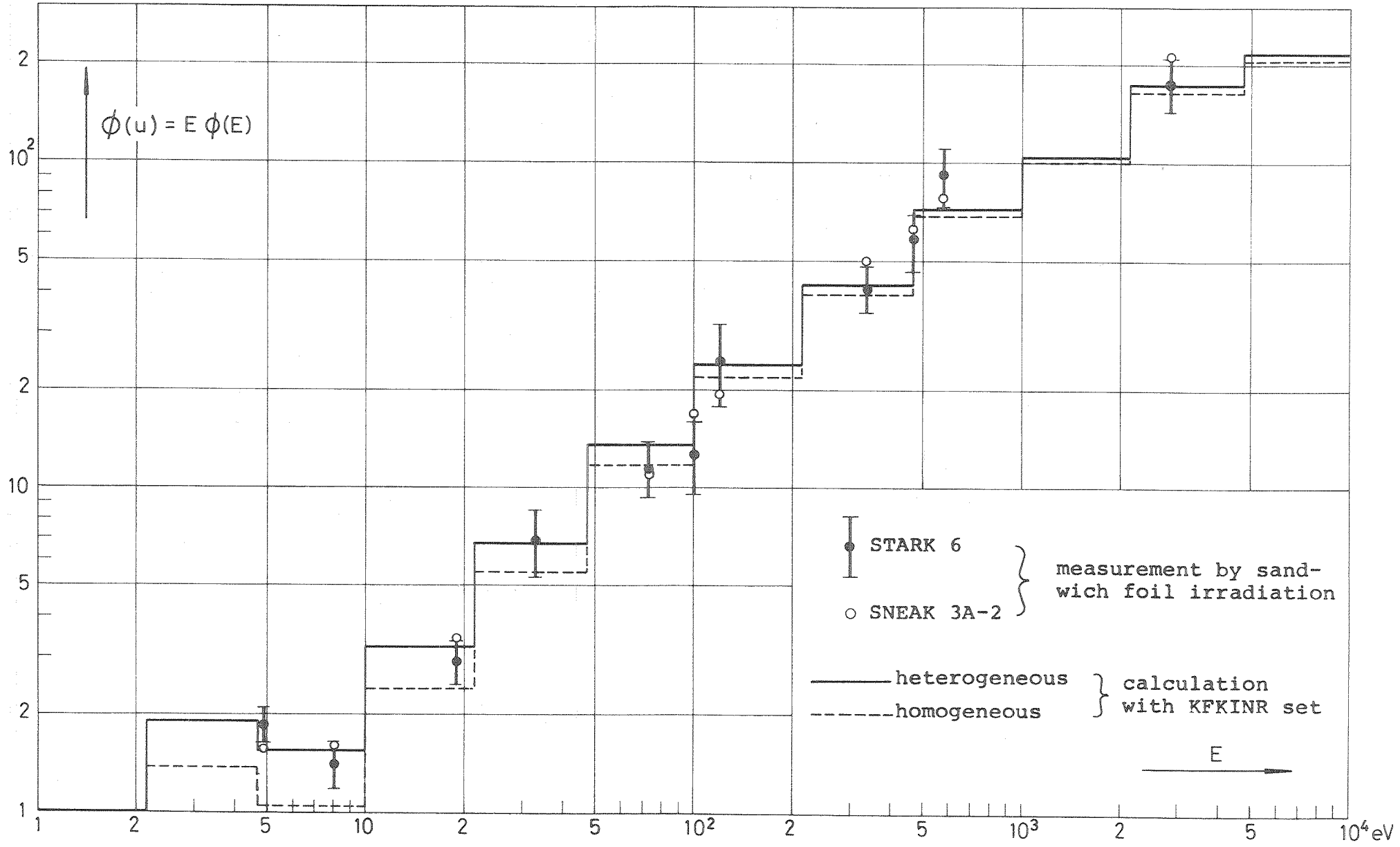

Fig. 14: Sandwich foil measurements in STARK 6 and SNEAK 3A-2

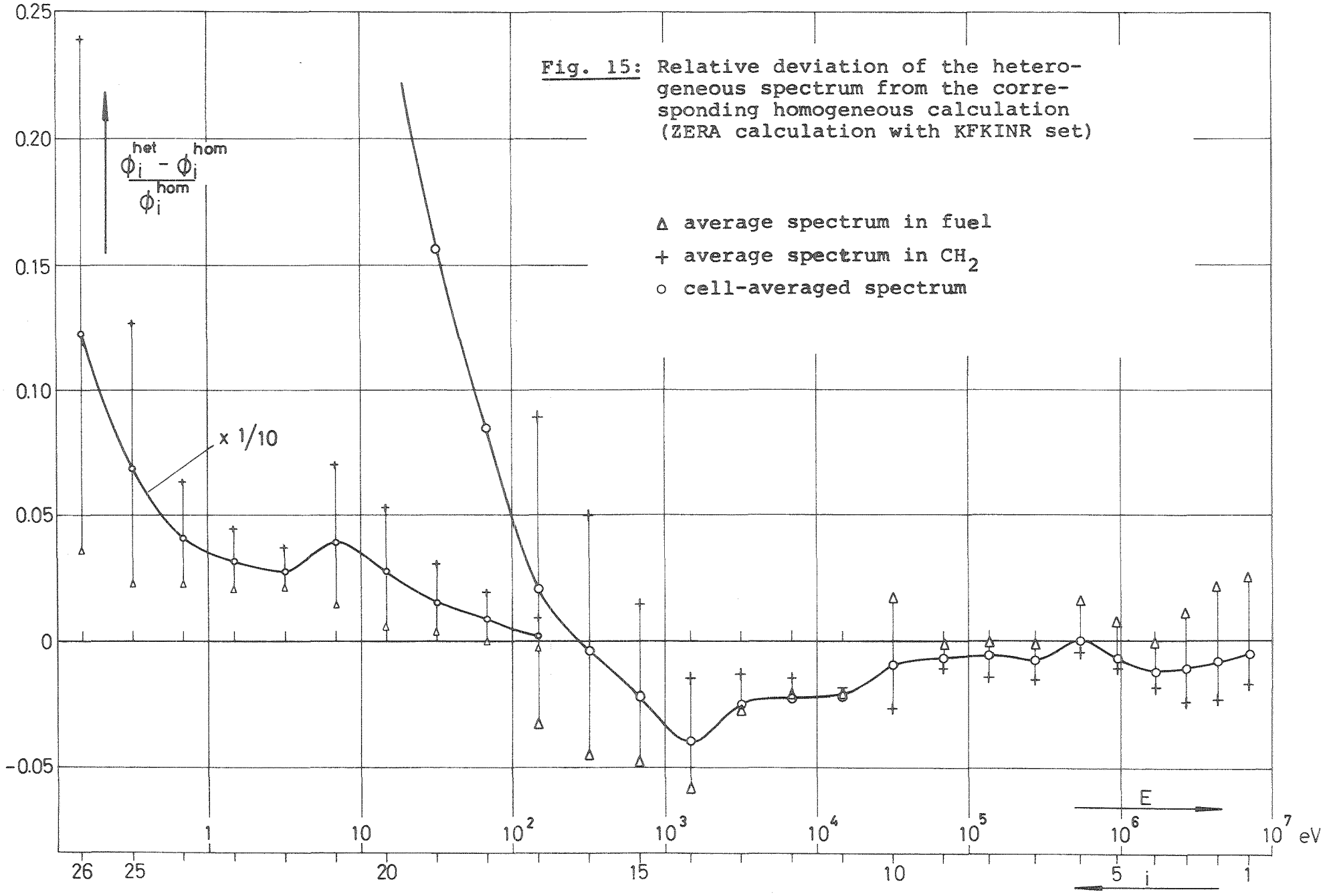

Fig. 15: Relative deviation of the heterogeneous spectrum from the corresponding homogeneous calculation (ZERA calculation with KFKINR set)

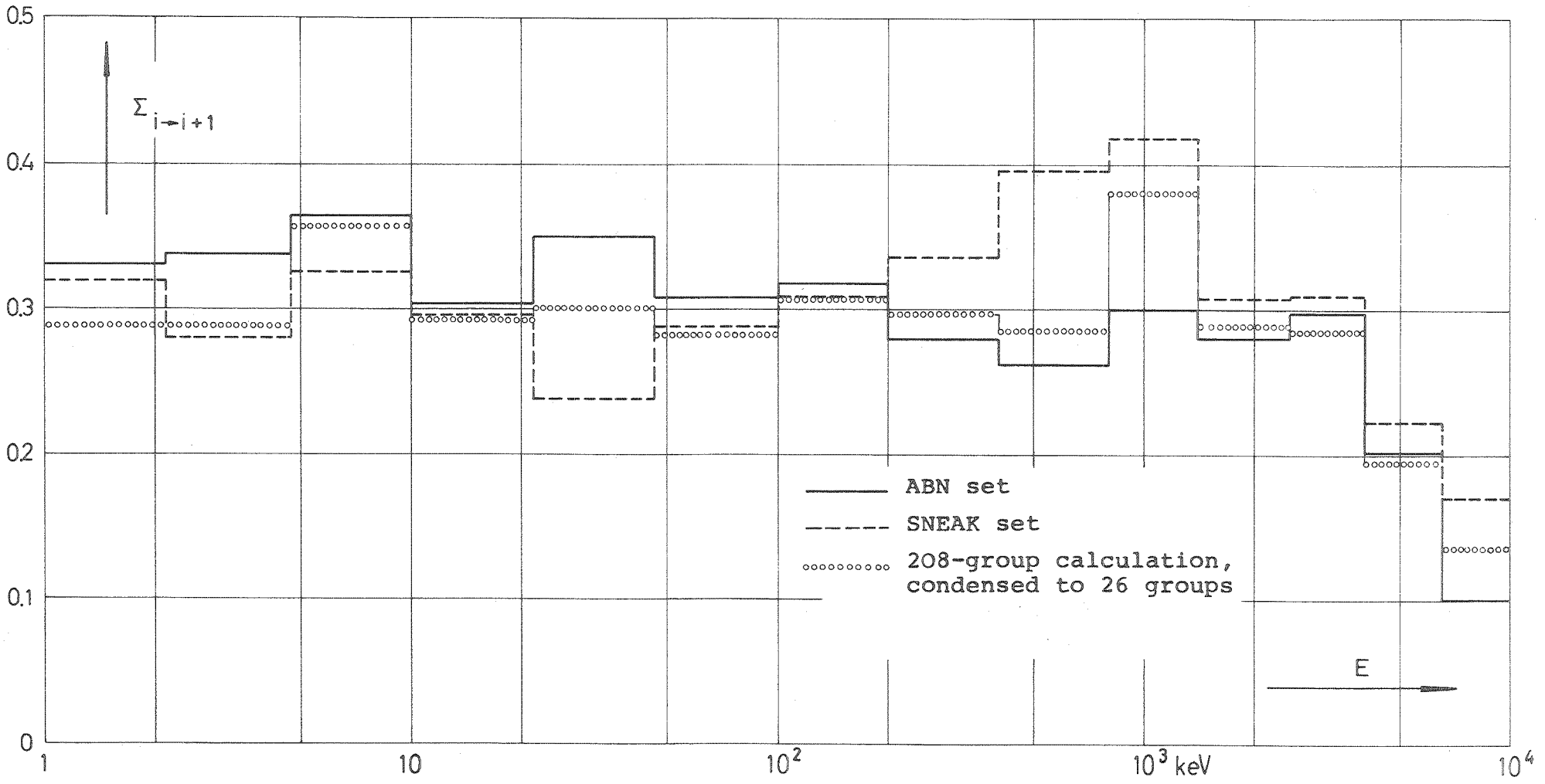

Fig. 16: Group transfer cross section $\Sigma_{i \to i+1}$ from 26-group sets and 208-group calculation

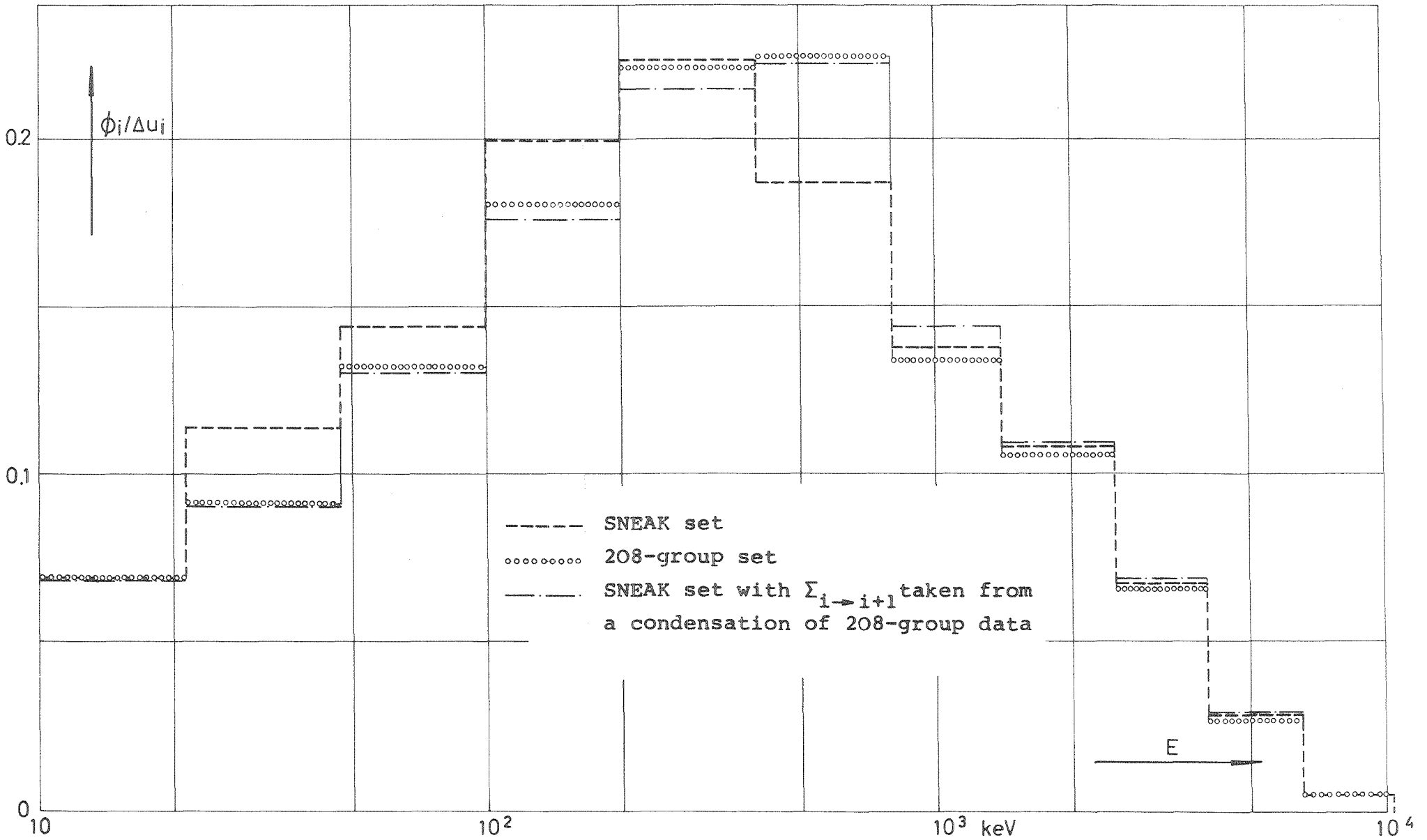

Fig. 17: 26 group spectra calculated for a one-zone system (O-dim. diffusion calculation)

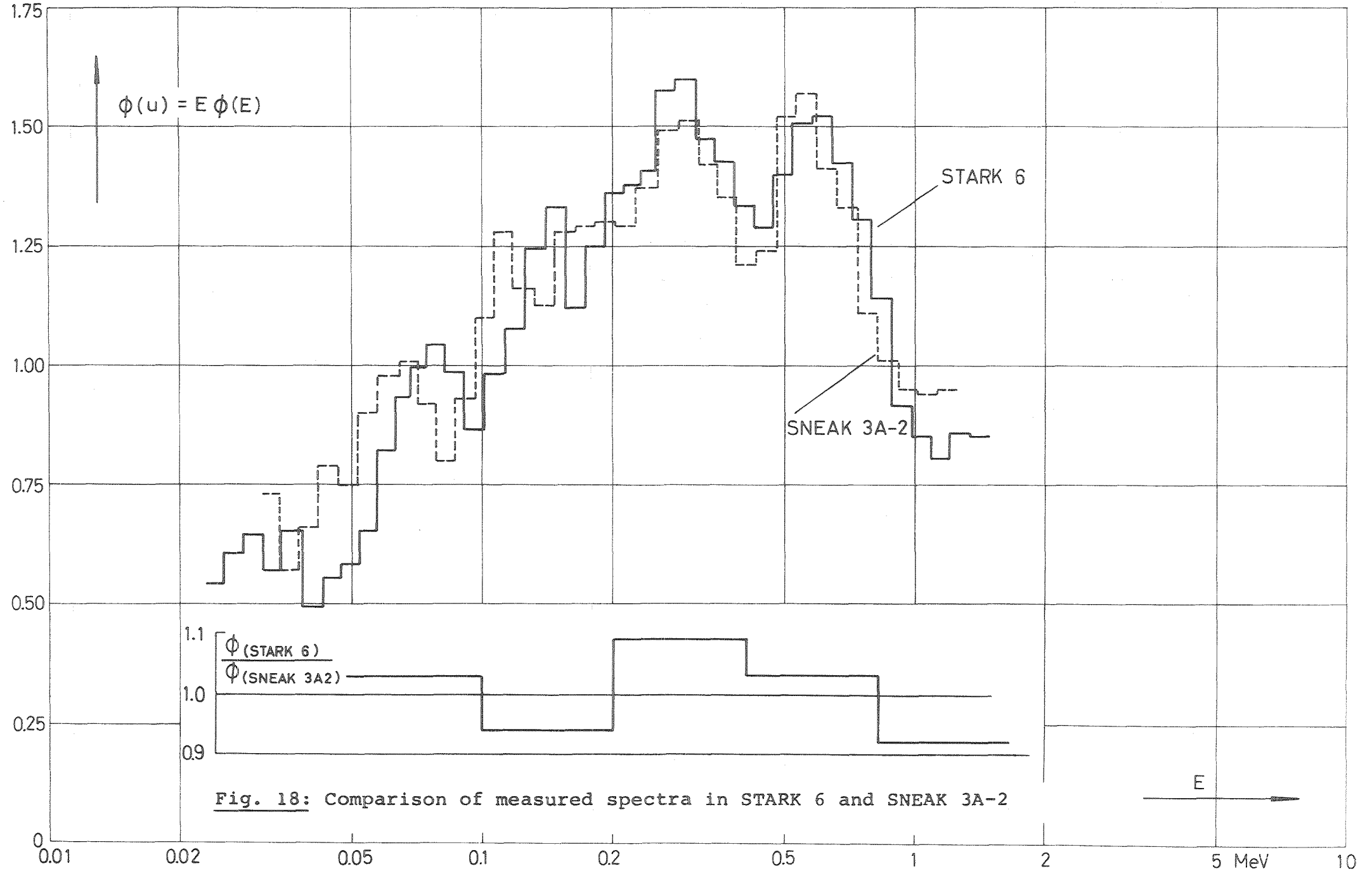

Fig. 18: Comparison of measured spectra in STARK 6 and SNEAK 3A-2

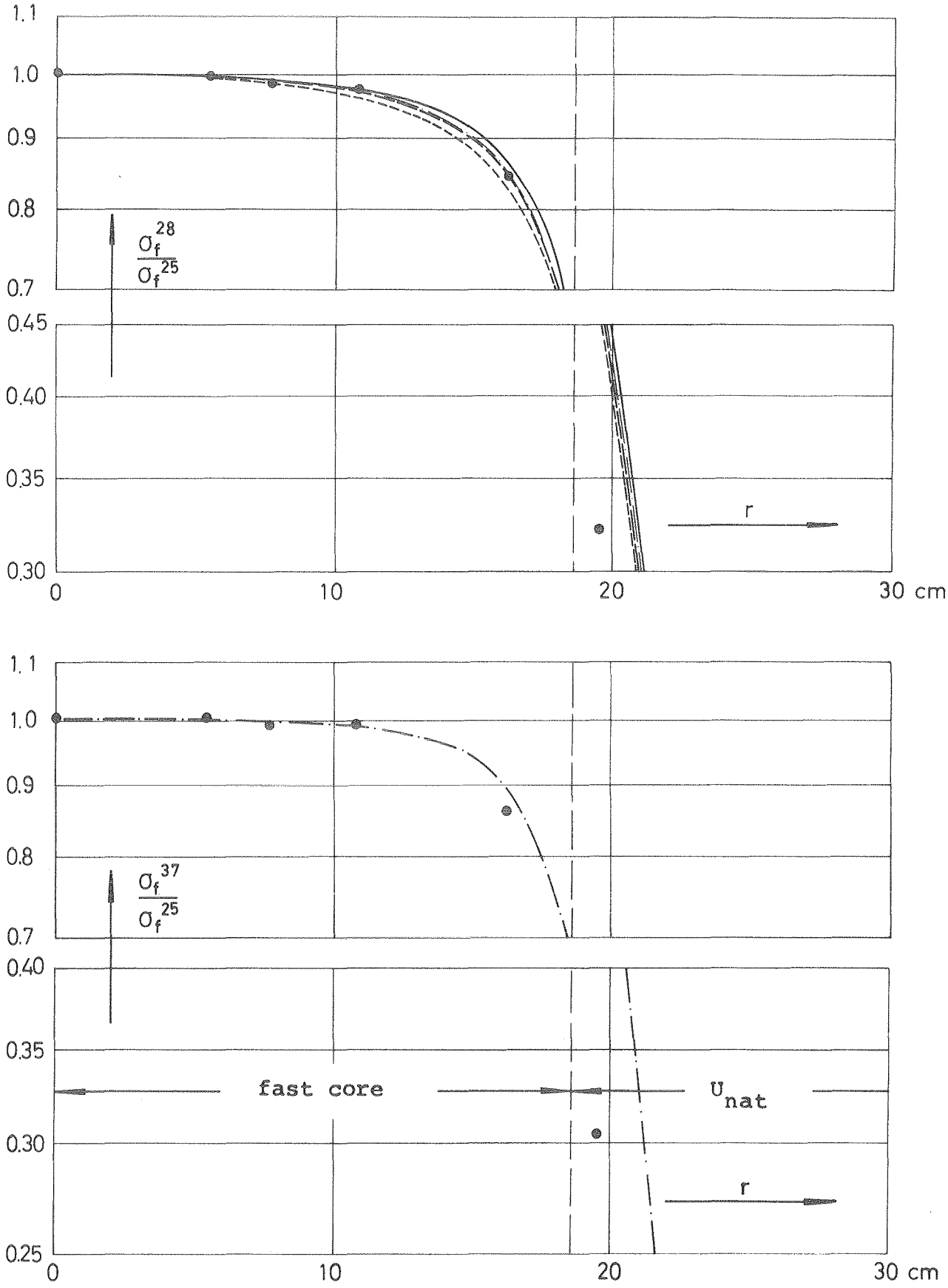

Fig. 19: Radial variation of fission ratios in the midplane of STARK 6 (the data are normalized to 1 at core center)

- fission chamber measurement

one-dimensional diffusion calculations:

——— ABN set

– – – – SNEAK set

— — — MØXTØT set

— · — · KFKINR set (= SNEAK set in fast core)

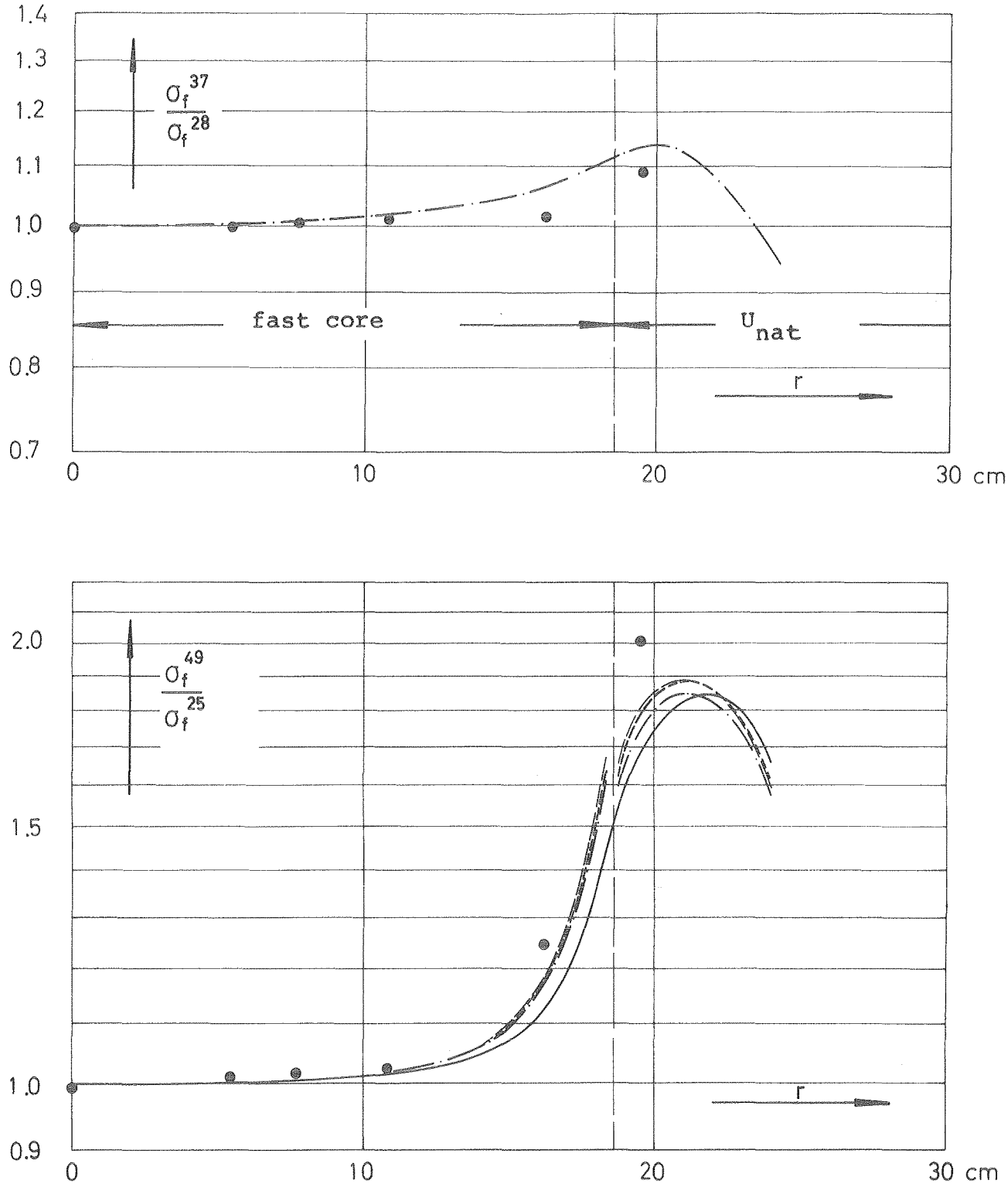

Fig. 20: Radial variation of fission ratios in the midplane of STARK 6 (the data are normalized to 1 at core center)

- fission chamber measurement

one-dimensional diffusion calculations:

——— ABN set

– – – – – MØXTØT set

— — — SNEAK set

— · — KFKINR set

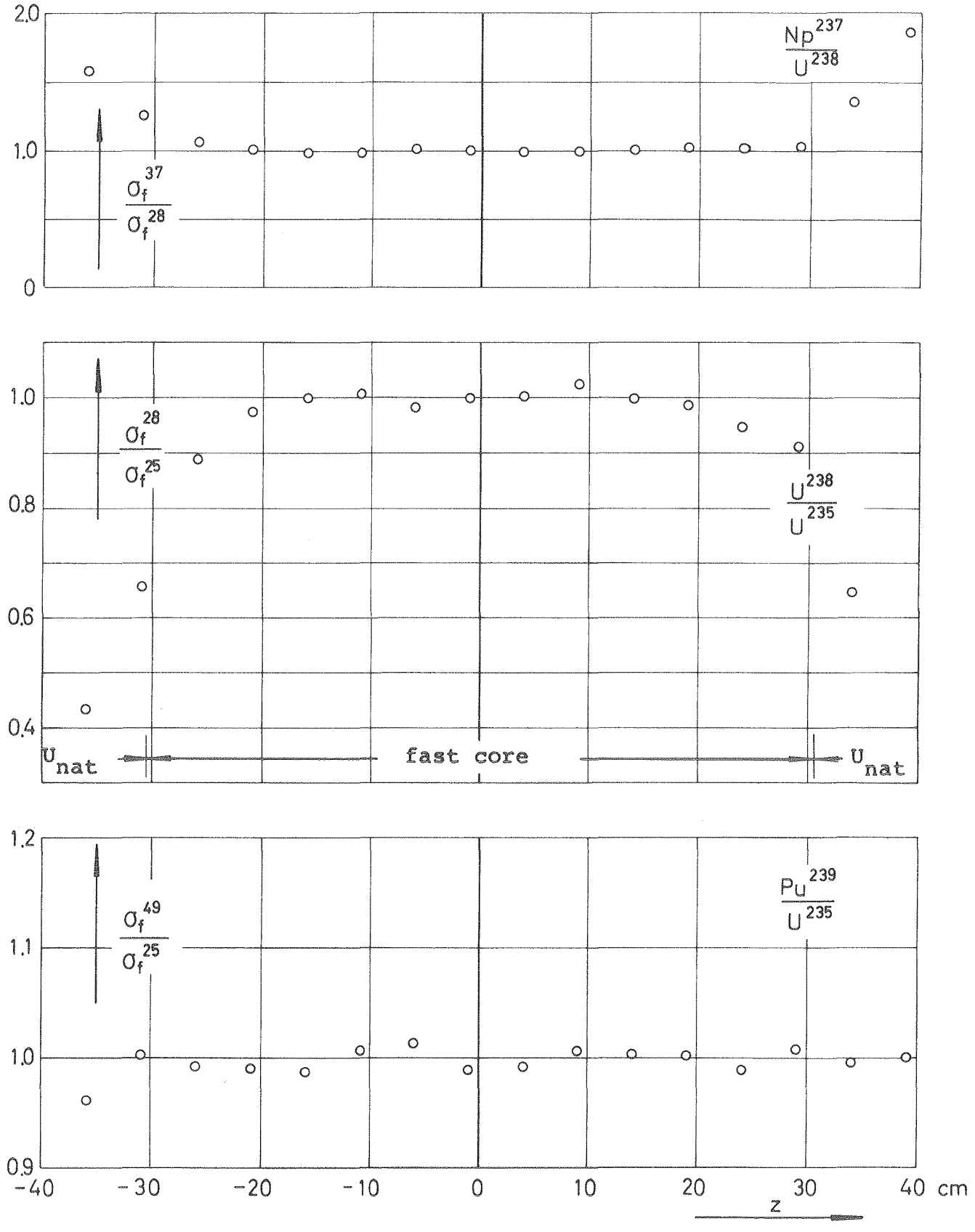

Fig. 21: Axial variation of fission ratios on the central axis (the data are normalized to 1 at core center)

o fission chamber measurement

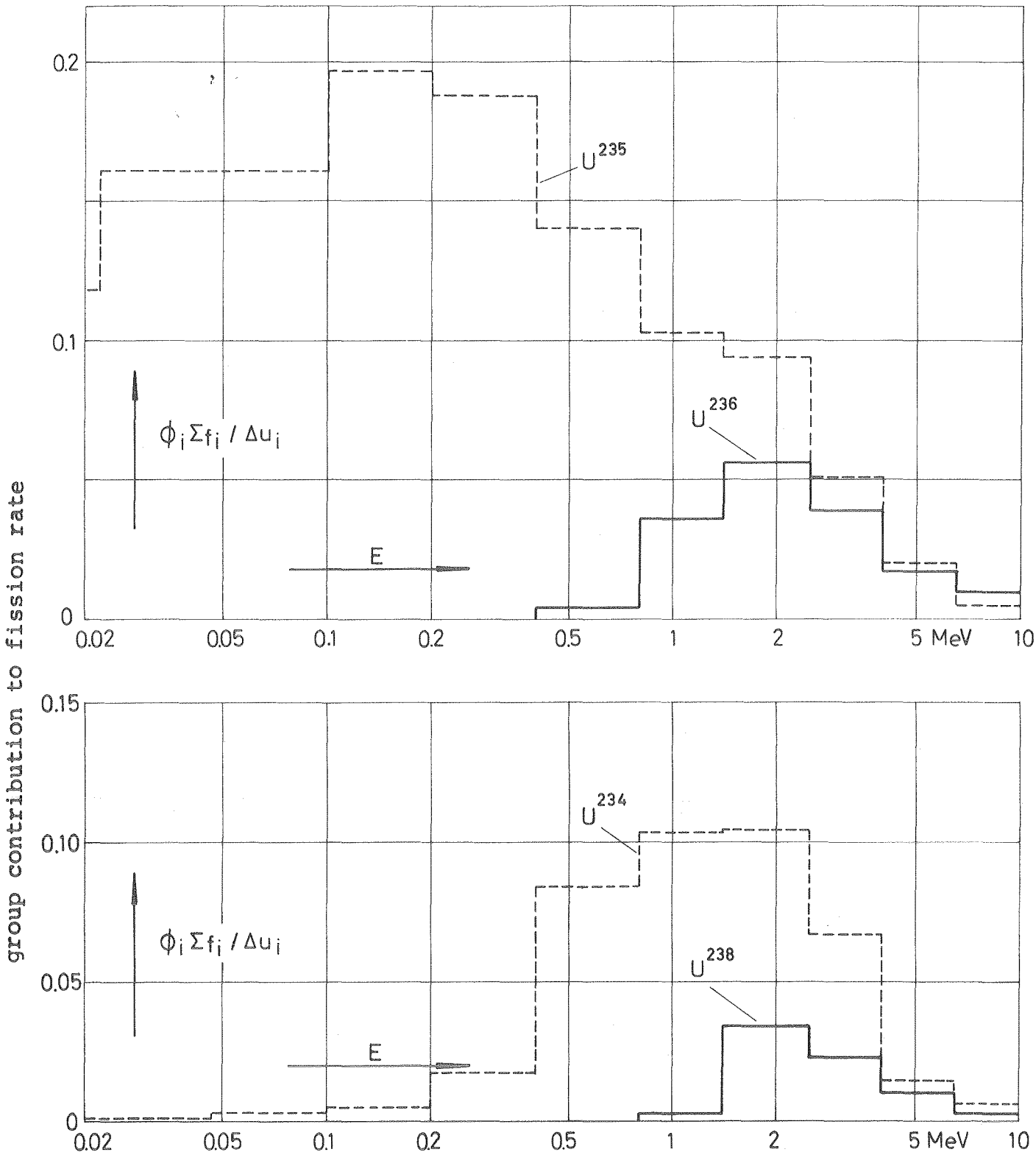

Fig. 22: Group contributions to the fission rate in the U isotopes

——— } homogeneous calculation with KFKINR set
- - - - - -

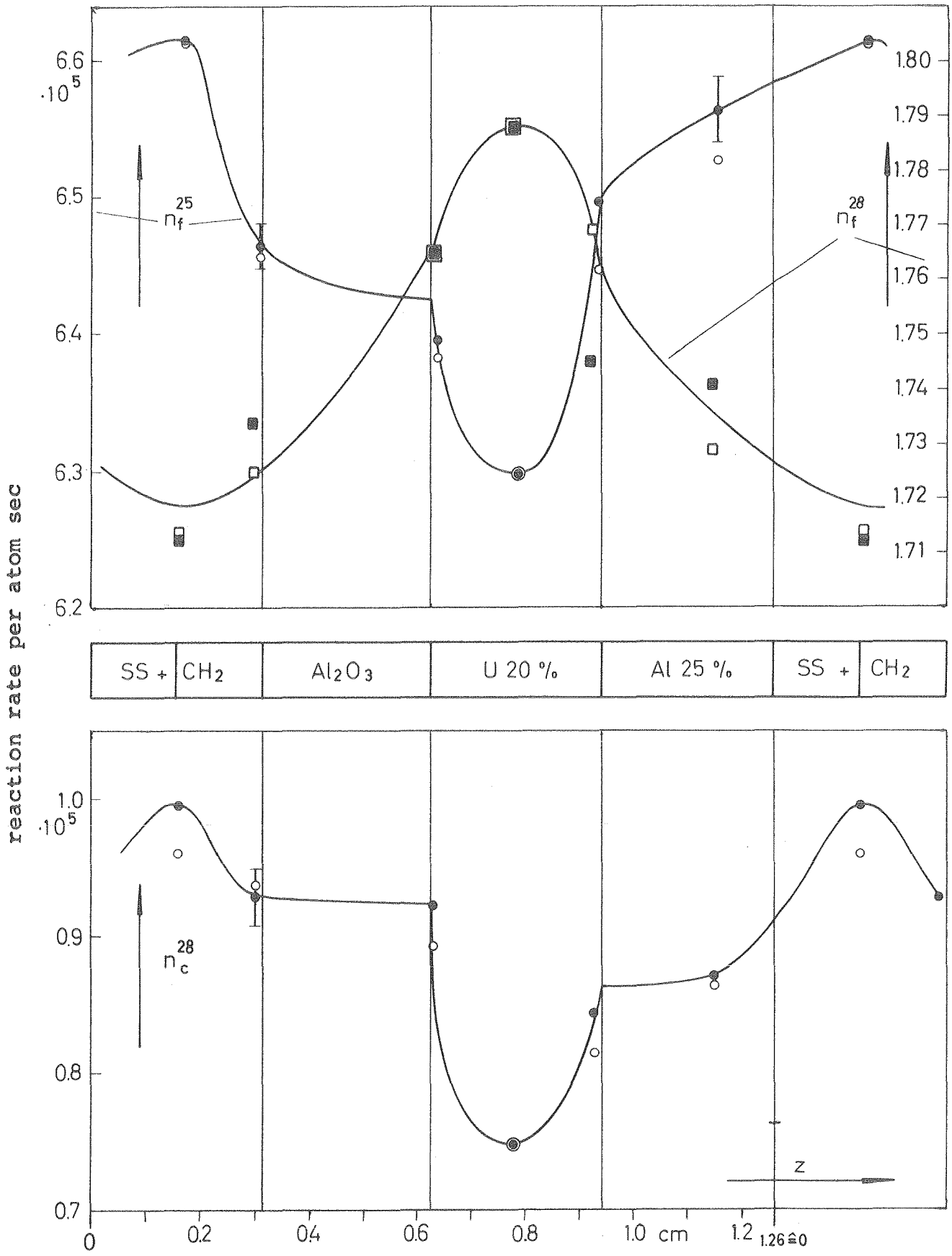

Fig. 23 Fine structure of reaction rates in the normal cell (l=1.257cm)

● ■ foil activation in STARK 6

○ □ foil activation in SNEAK 3A-2

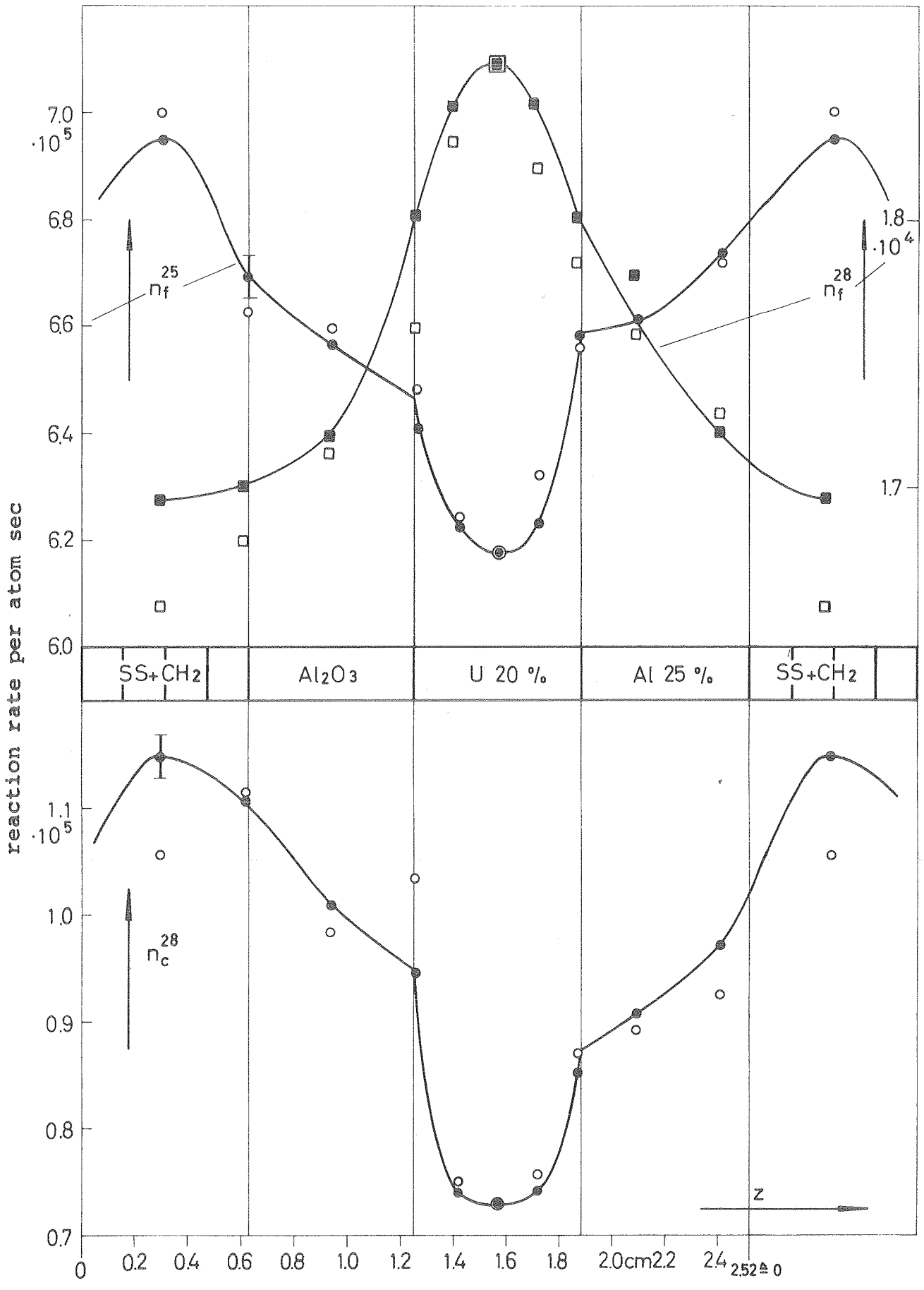

Fig. 24 Fine structure of reaction rates in the bunched cell (l = 2.514 cm)

● ■ foil activation in STARK 6

○ □ foil activation in SNEAK 3A-2

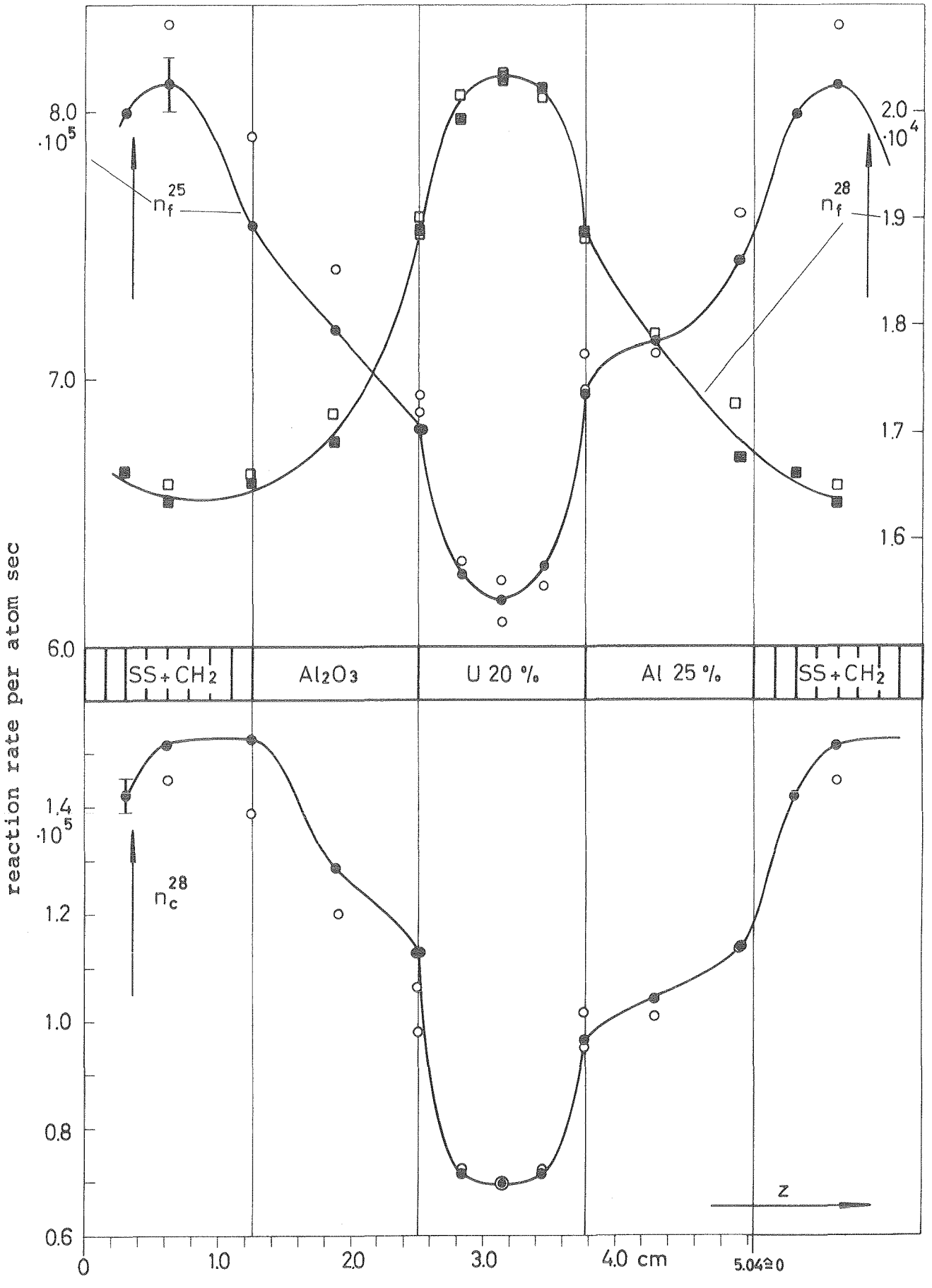

Fig. 25 Fine structure of reaction rates in the double bunched cell (l = 5.028 cm)

● ■ foil activation in STARK 6

○ □ foil activation in SNEAK 3A-2

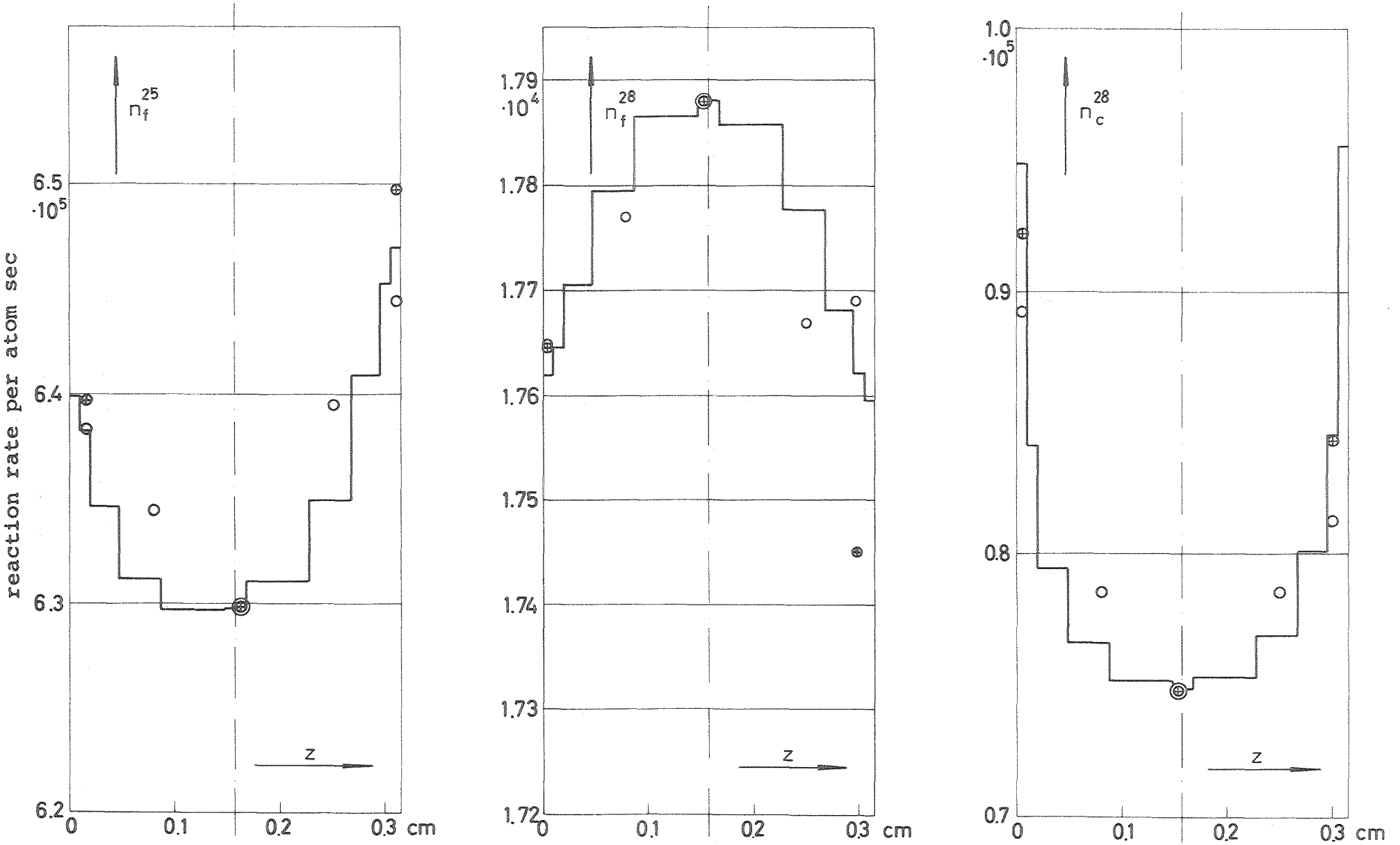

Fig. 26: Fine structure of reaction rates within the U(20%) platelet (normal cell, l = 1.257 cm)

⊕ foil measurement in STARK 6 o foil measurement in SNEAK 3A-2 (normalized)
—— ZERA calculation with SNEAK set (case III), normalized to STARK 6 experiment

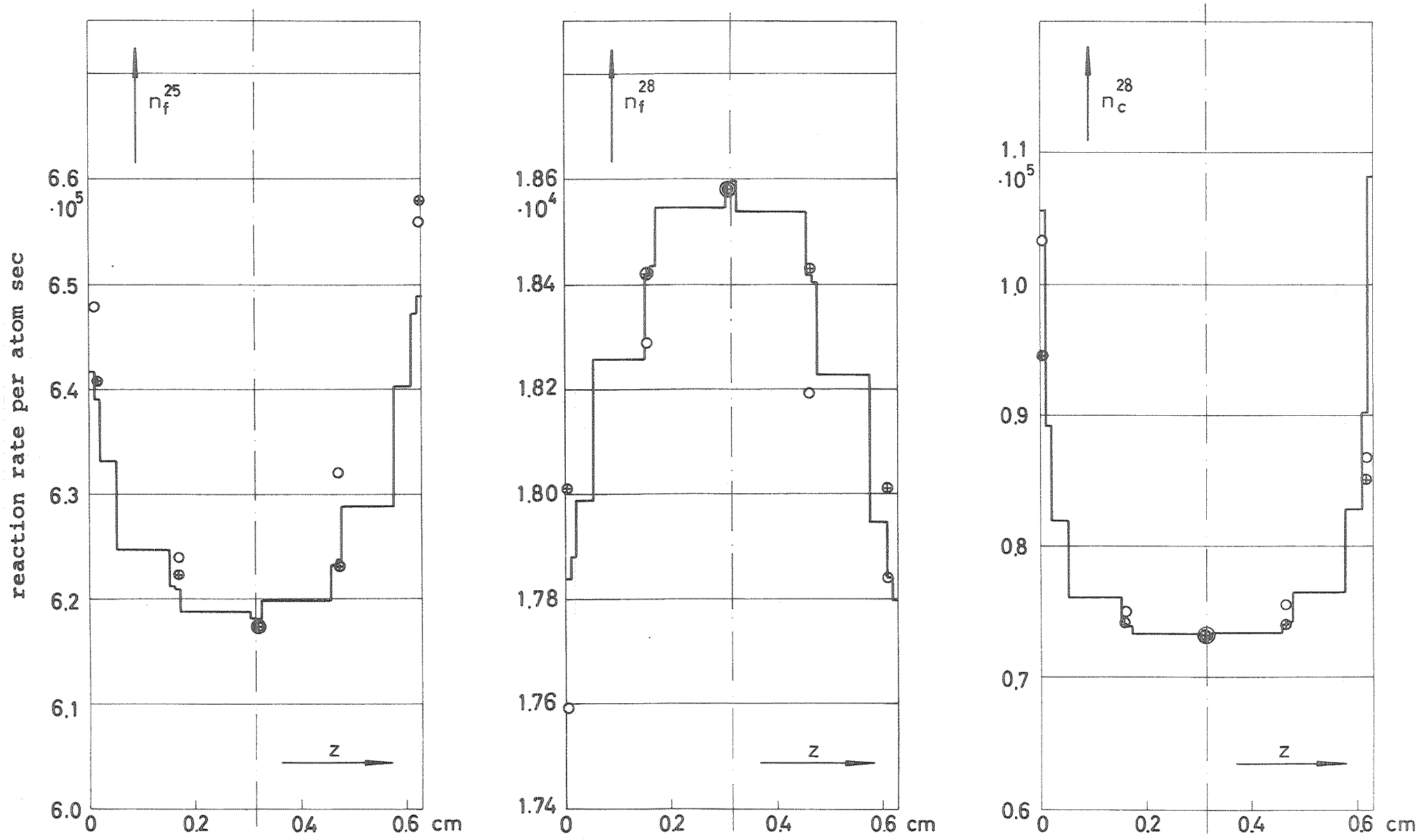

Fig. 27: Fine structure of reaction rates within the U(20%) platelets (bunched cell, l = 2.514 cm)

⊛ foil measurement in STARK 6 o foil measurement in SNEAK 3A-2 (normalized)
—— ZERA calculation with SNEAK set (case III), normalized to STARK 6 experiment

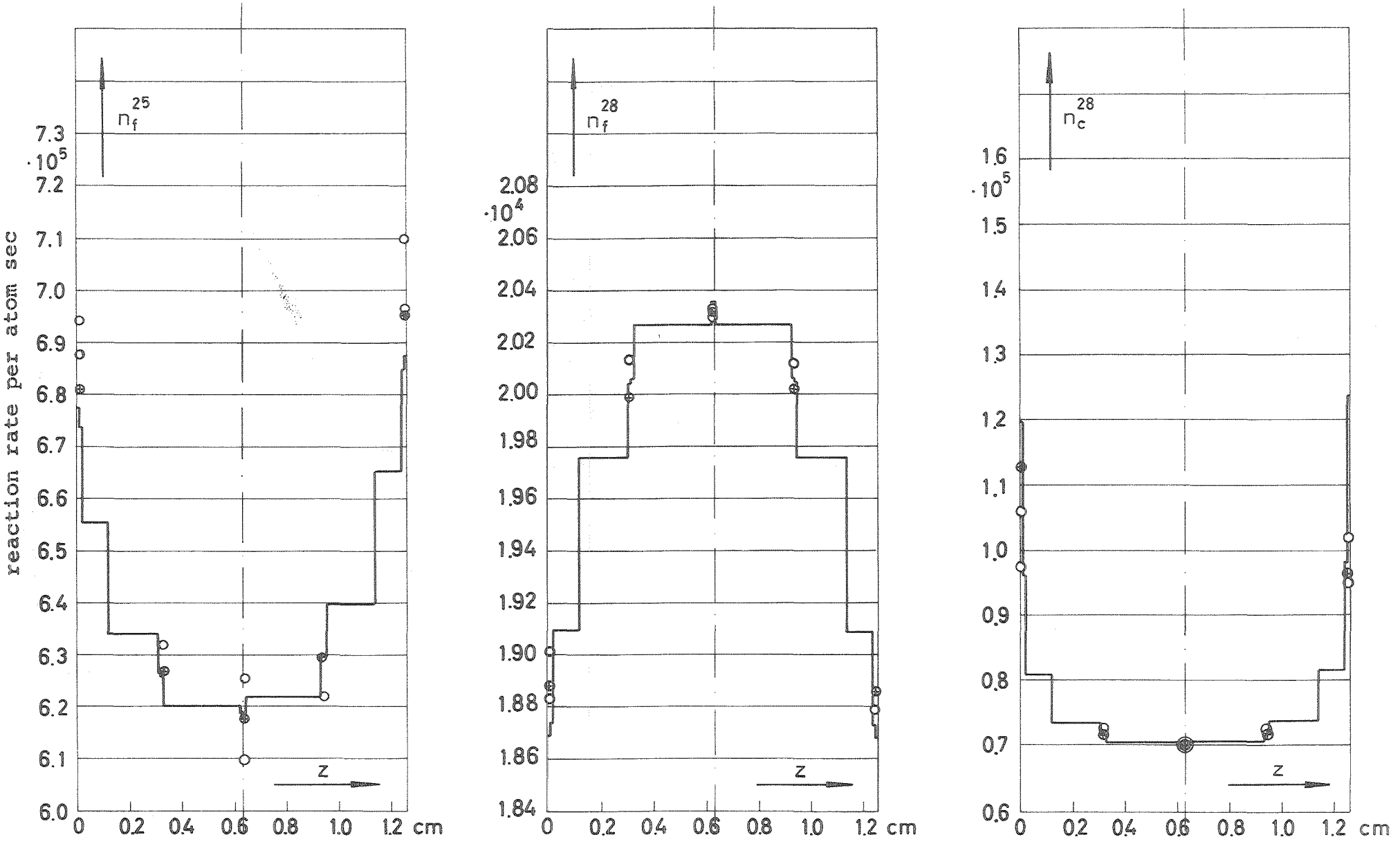

Fig. 28: Fine structure of reaction rates within the U(20%) platelets (double bunched cell, l = 5.028 cm)

⊛ foil measurement in STARK 6 o foil measurement in SNEAK 3A-2 (normalized)
—— ZERA calculation with SNEAK set (case III), normalized to STARK 6 experiment

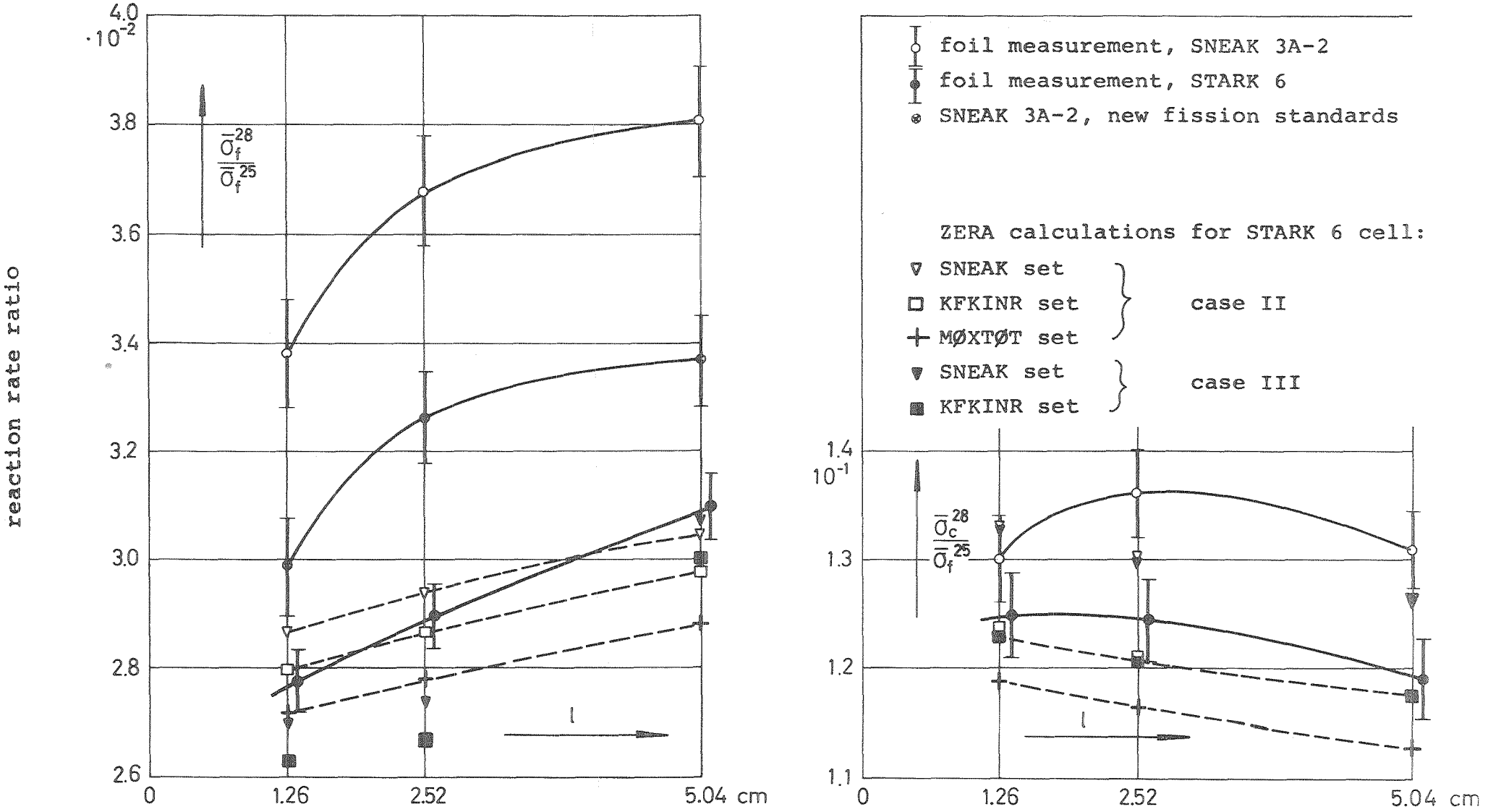

Fig. 29: Ratios of fuel-averaged reaction rates for U^{235} and U^{238} in the normal cell of STARK 6 and two bunched configurations (l = repetition length of the lattice)

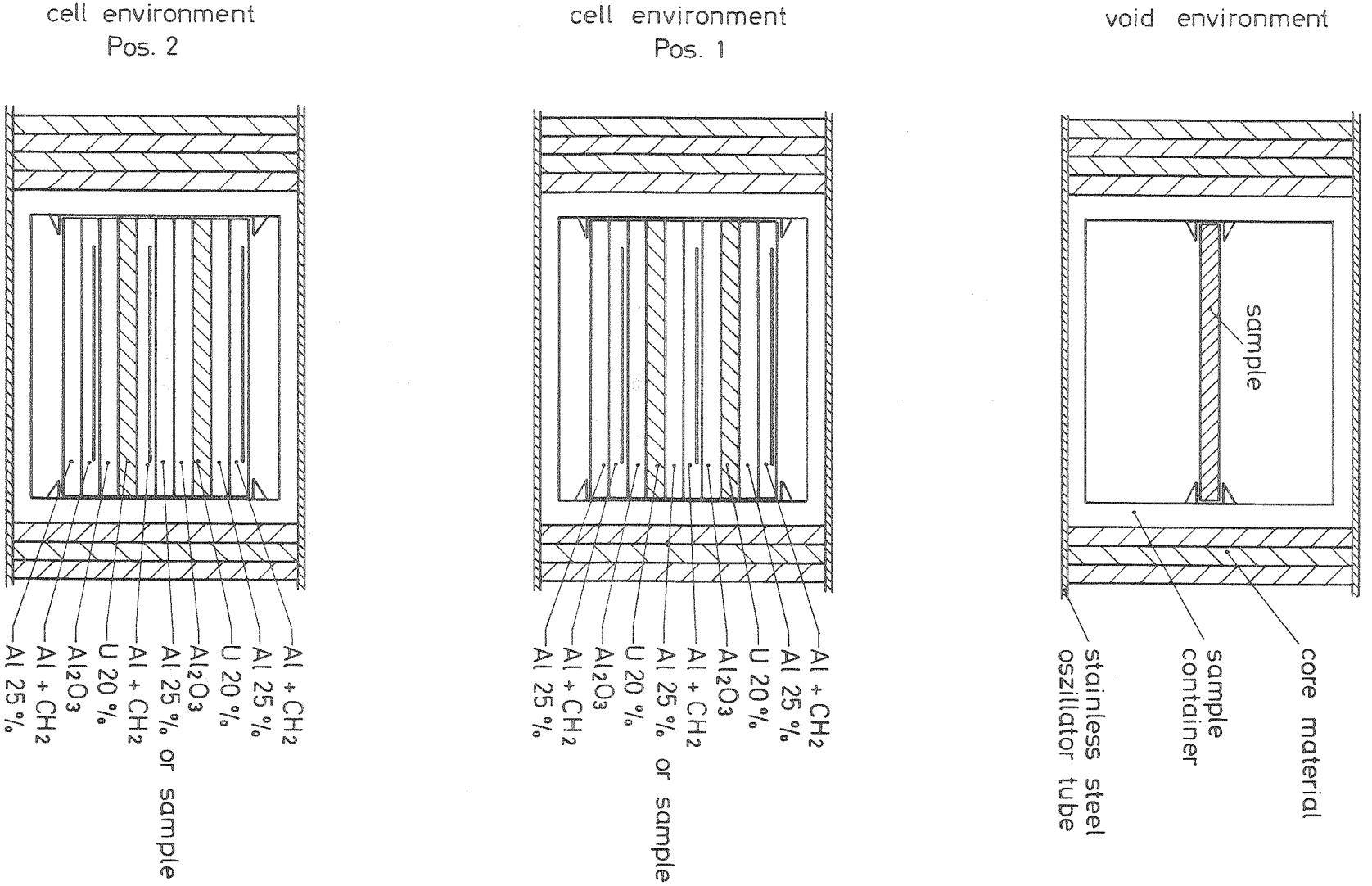

Fig. 30: Sample arrangement for material worth measurement

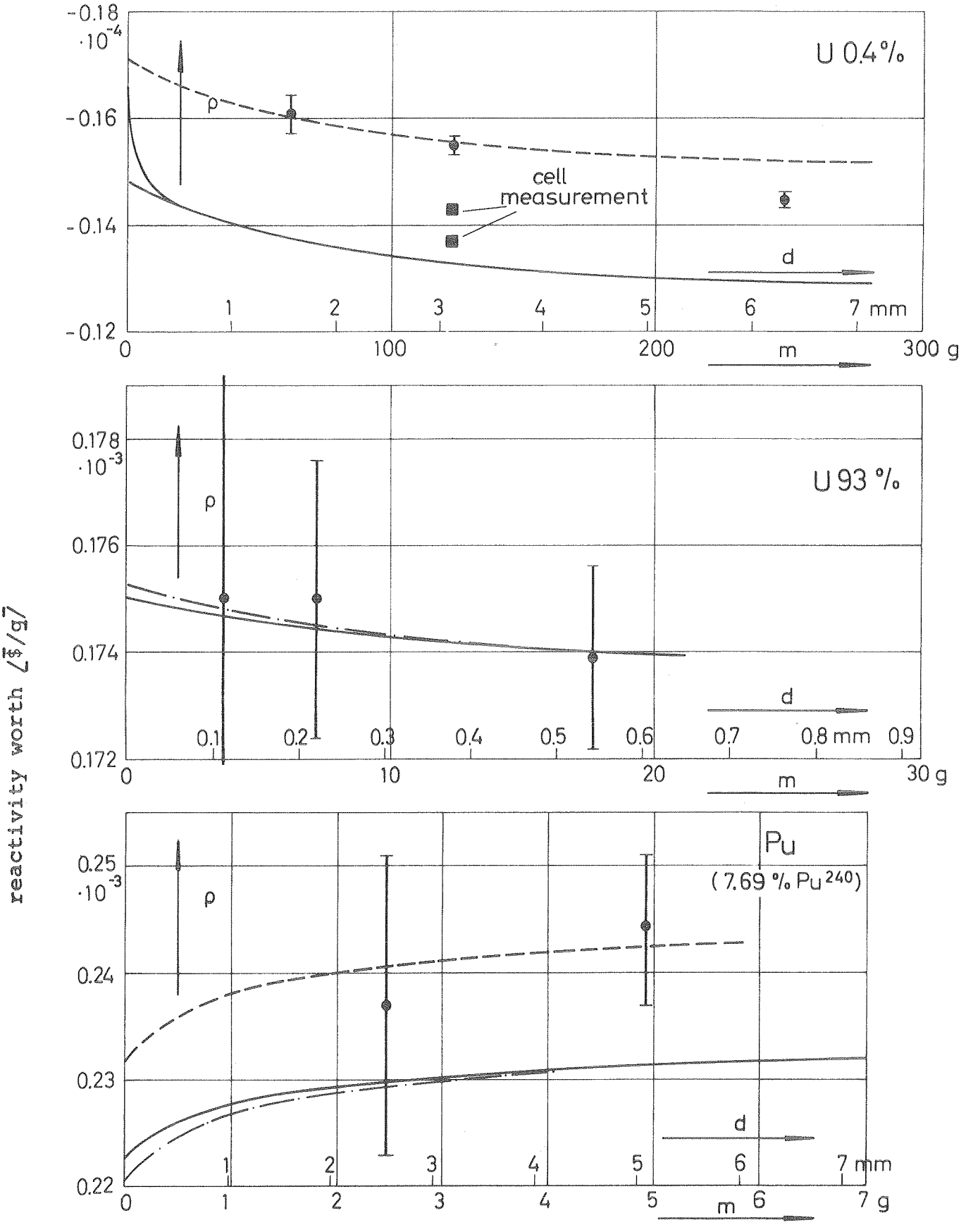

Fig. 31: Reactivity worth vs. sample mass m
pile oscillator data (void region)
integral transport calculation, KFKINR {homogeneous / heterogeneous}
calculation, fitted to experiment

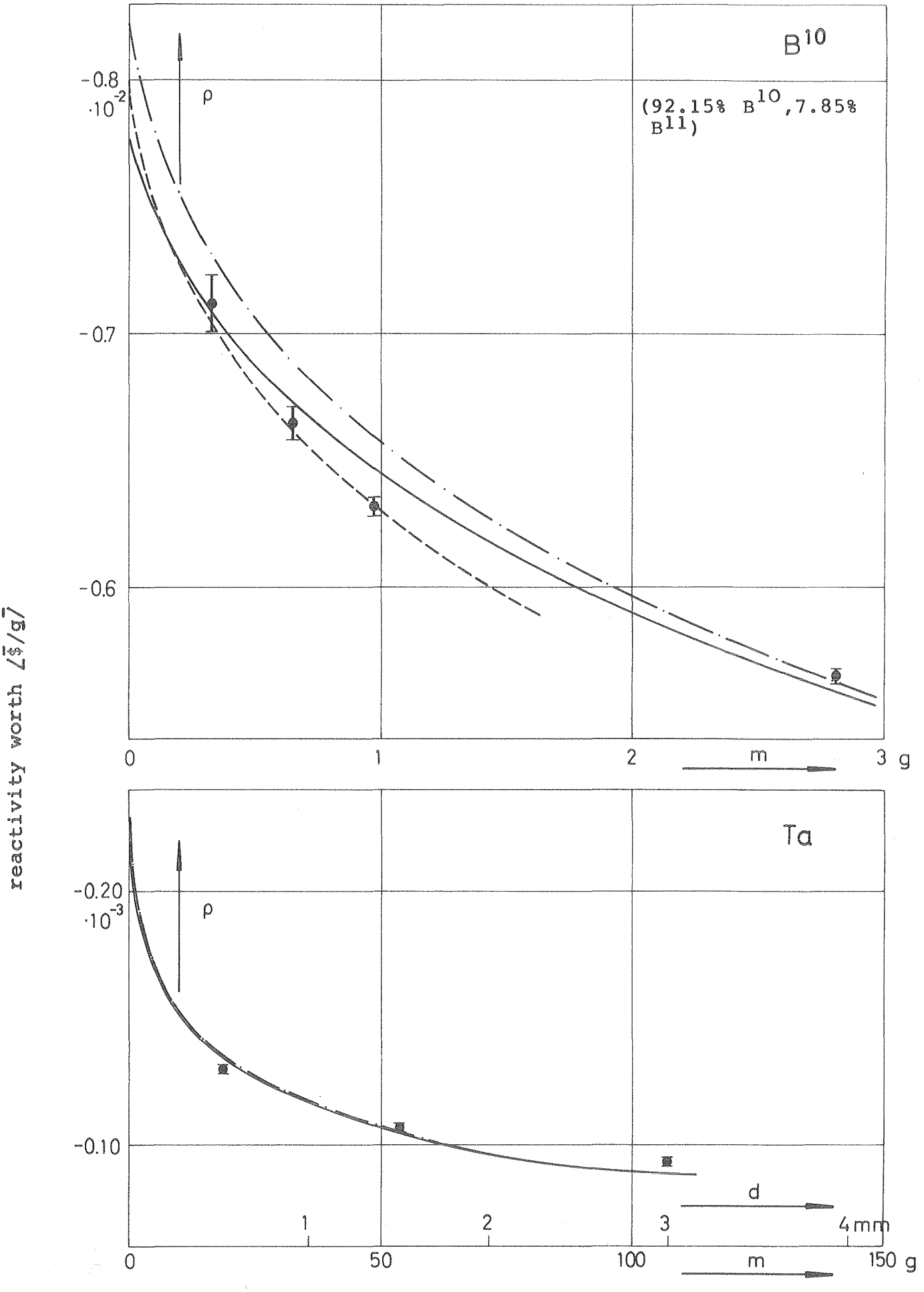

Fig. 32: Reactivity worth vs. sample mass m
● pile oscillator data (void region)
——— } integral transport calculation, KFKINR { homogeneous / heterogeneous
– – – – calculation, fitted to experiment

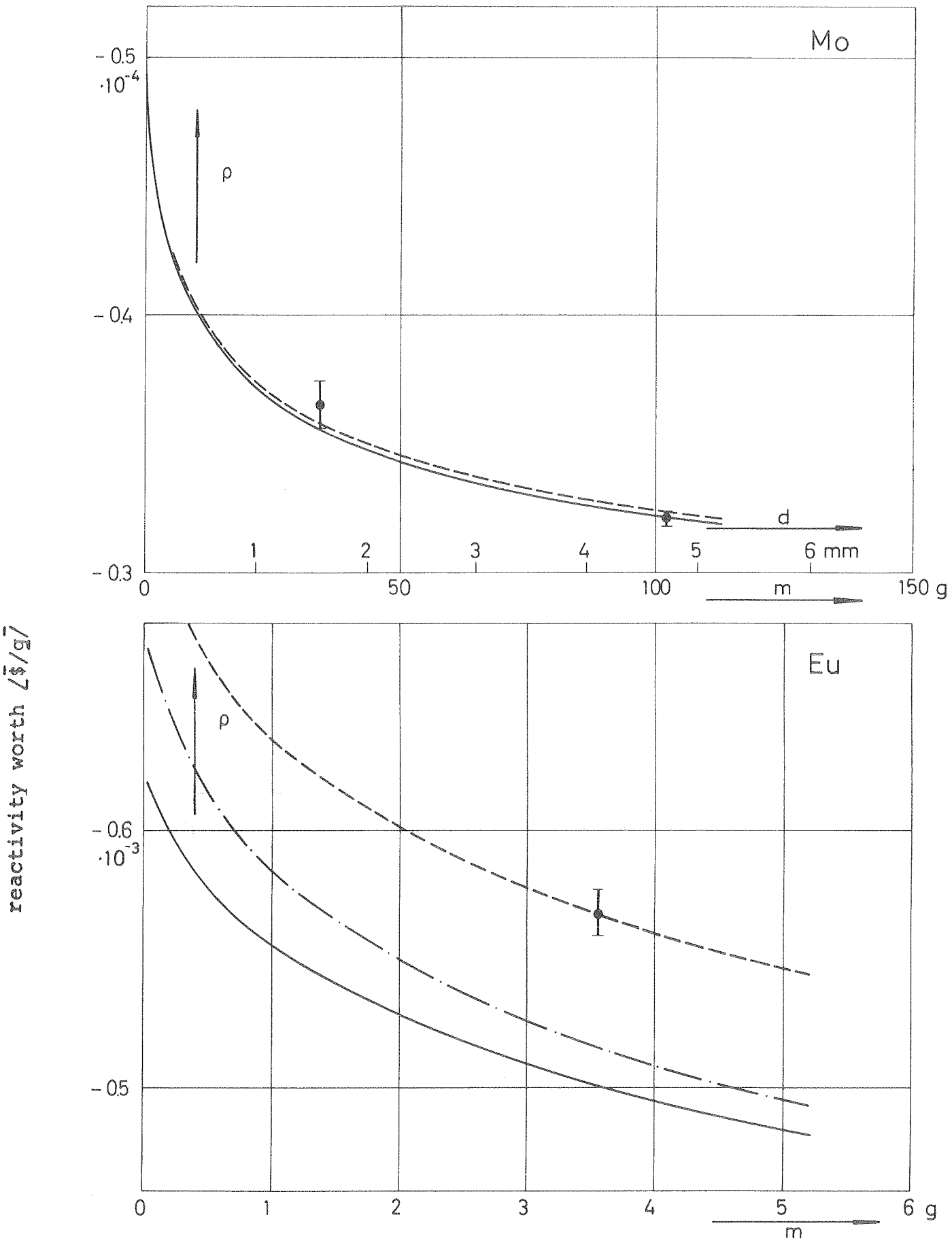

Fig. 33: Reactivity worth vs. sample mass m

pile oscillator data (void region)

integral transport calculation, KFKINR {homogeneous / heterogeneous

calculation, fitted to experiment

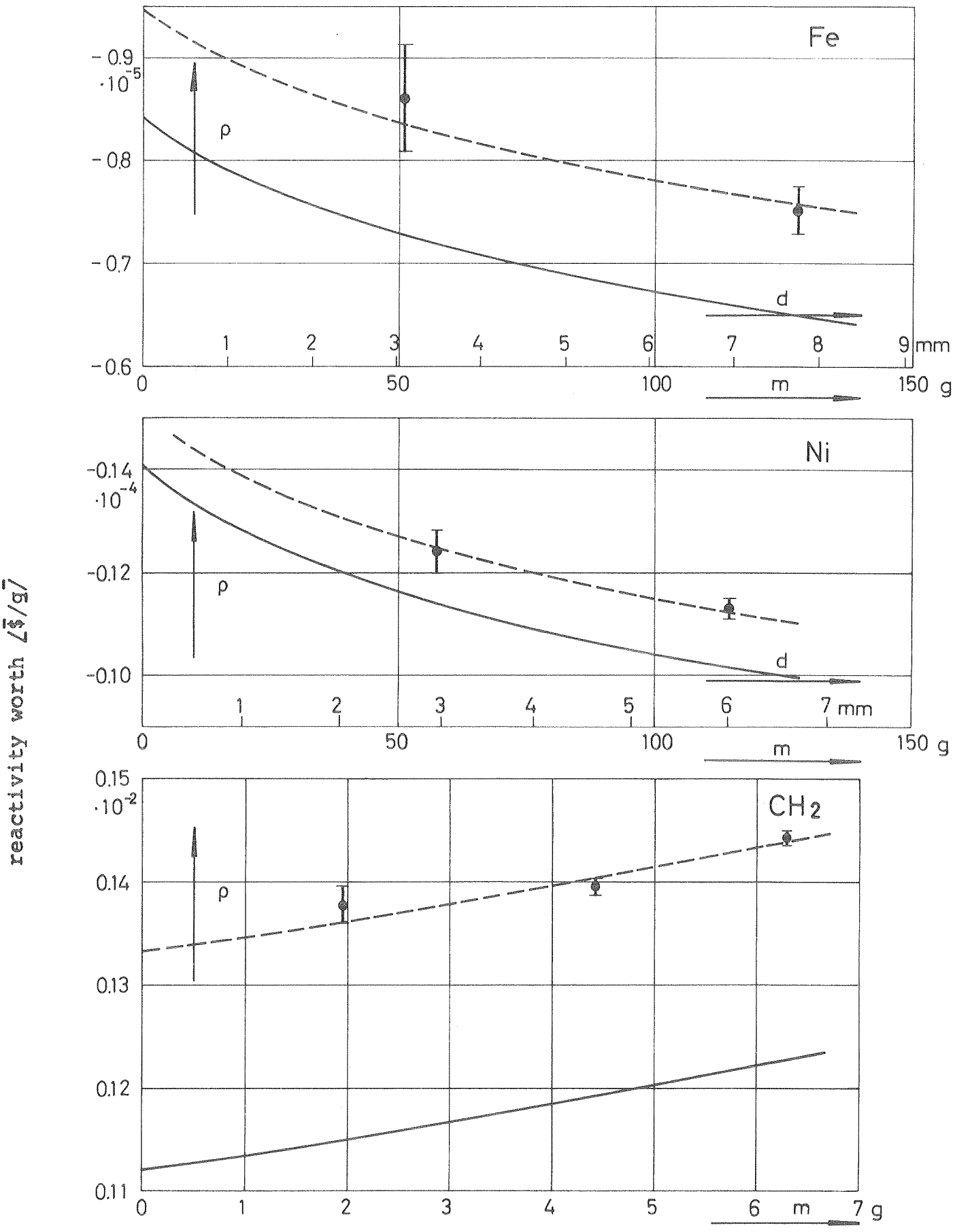

Fig. 34: Reactivity worth vs. sample mass m

pile oscillator data (void region)

——— integral transport calculation, KFKINR, homogeneous

– – – – calculation, fitted to experiment

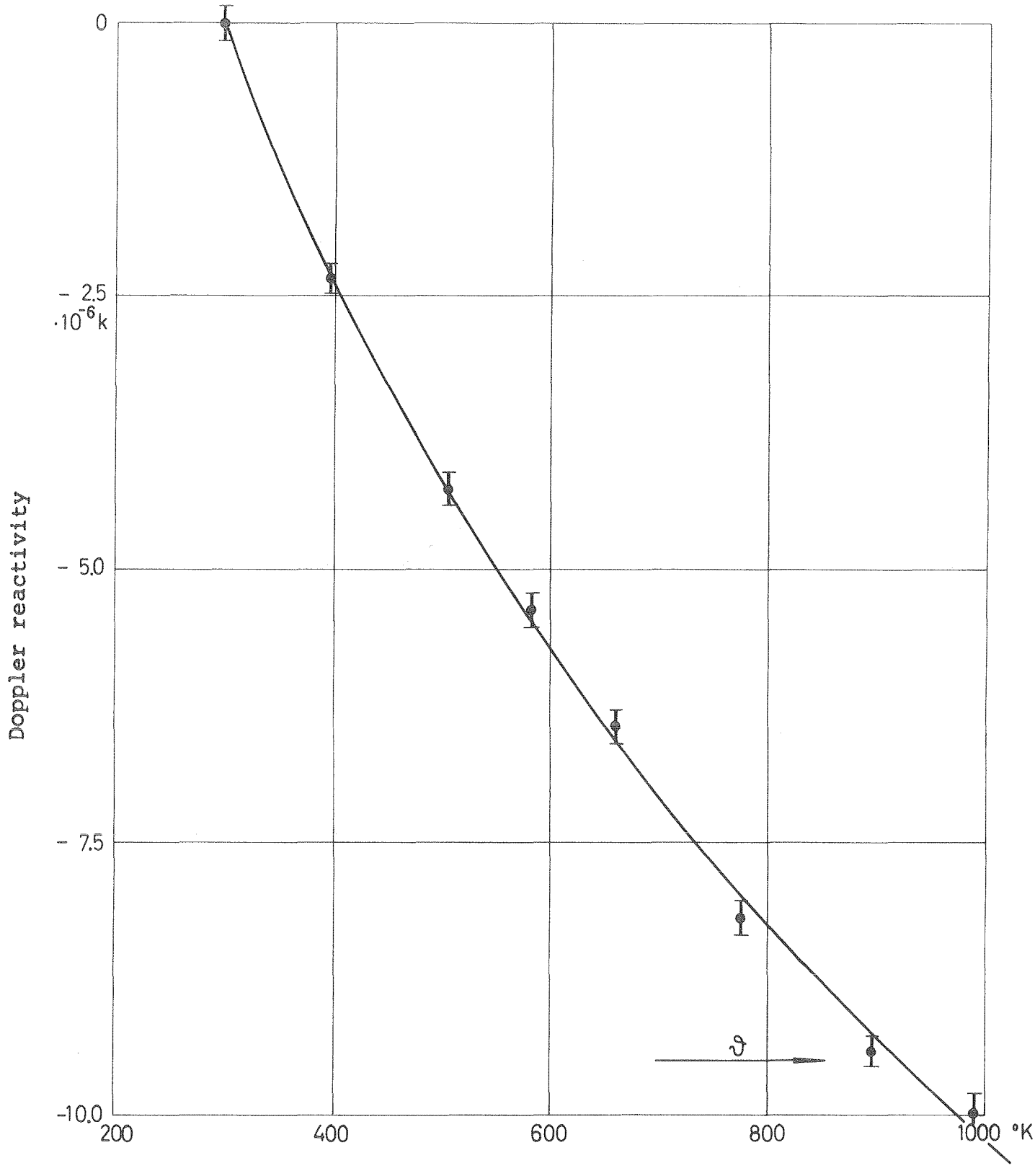

Fig. 35: Doppler reactivity vs. temperature for a 0.2% depl. UO_2 sample

oscillator measurement

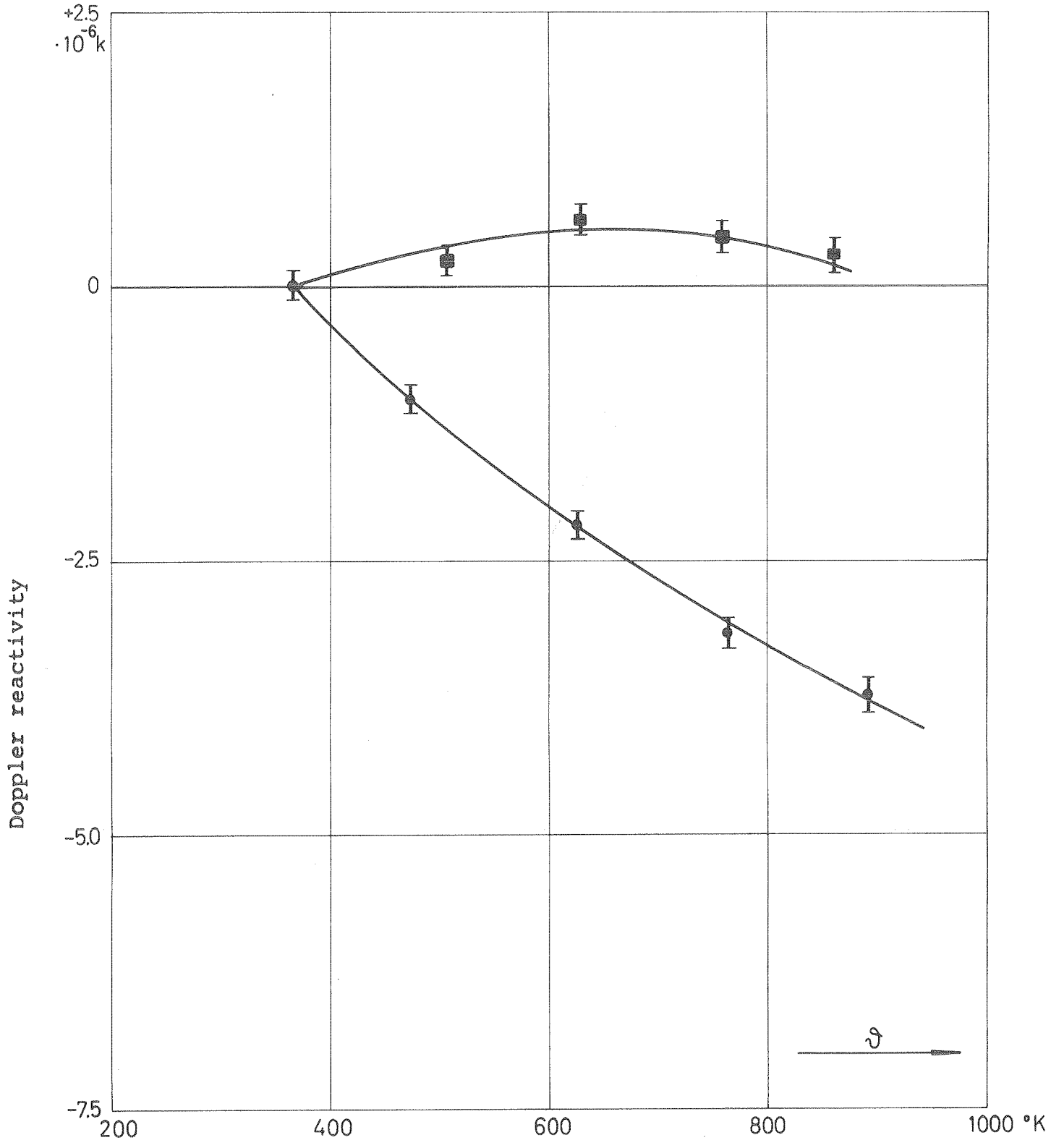

Fig. 36: Doppler reactivity vs. temperature for a PuO_2 sample
oscillator measurement (normal environment)
oscillator measurement (boron environment)